# References

Abbundi, R., Clark, A.E., & Koon, N.C., "Temperature dependence of the magnetostriction and magnetization in single crystal $HoFe_2$," Journal of Applied Physics, Volume 50, Number 3, pp. 1671-1673, March 1979.

Adly, A.A., Mayergoyz, I.D., & Bergqvist, A., "Preisach modelling of magnetostrictive hysteresis," Journal of Applied Physics, Volume 69, Number 8, pp. 5777-5779, 15 April 1991.

Anderson, B.D.O., & Moore, J.B., "Optimal Control - Linear Quadratic Methods," Prentice-Hall, Englewood Cliffs, NJ, 1989.

Ashley, S., "Magnetostrictive actuators," Mechanical Engineering, pp. 68 – 70, June 1998.

Atalik, T.S., & Utku, S., "Stochastic Linearization of Multi-Degree-of-Freedom Non-Linear Systems," Earthquake Engineering and Structural Dynamics, Volume 4, pp. 411-420, 1976.

Bartkowiak, R.A., "Electric Circuits," Intext Educational Publishers, New York, 1973.

Bathe, K-J., "Finite Element Procedures in Engineering Analysis," Prentice-Hall, Englewood Cliffs, NJ, 1982.

Bednarck, S., "The giant magnetostriction in ferromagnetic composites within an elastomer matrix," Applied Physics A - Materials Science & Processing, Volume 68, Number 1, pp. 63 – 67, January, 1999.

Béliveau, J.-G., & Soucy, Y., "Damping Synthesis Using Complex Substructure Modes and a Hermitian System Representation," AIAA Journal, Vol. 23, No. 12, pp. 1952-1956, December 1985.

Benfield, W.A., & Hruda, R.F., "Vibration Analysis of Structures by Component Mode Substitution, AIAA Journal, Vol. 9, No. 7, pp. 1255-1261, July 1971.

Bergqvist, A., & Engdahl, G., "A Stress-dependent Magnetic Preisach Hysteresis Model," IEEE Transactions on Magnetics, Volume 27, Number 6, pp. 4796-4798, November 1991.

Billings, S.A., Tsang, K.M., & Tomlinson, G.R., "Application of the NARMAX Method to Nonlinear Frequency Response Estimation," Proceedings of the 6th International Modal Analysis Conference, Kissimmee, FL, pp. 1433-1438, 1988.

Bishop, R.H., "Modern Control Systems Analysis and Design Using MATLAB," Addison Wesley, Reading, MA, 1993.

Bittanti, S., Campi, M., & Lorito, F., "ICSS: A program for the identification and control of time varying systems," Proceedings of the European Simulation Multiconference, pp. 588-592, 1992.

Bozic, S.M., "Digital and Kalman Filtering," Edward Arnold, London, 1990.

Braun, S.G., & Ram, Y.M., "Structural Parameter Identification in the Frequency Domain: The Use of Overdetermined Systems," Transactions of the American Society of Mechanical Engineers, Journal of Dynamic Systems, Measurement and Control, Volume 109, pp. 120-123, June 1987.

Besbes, M., Ren, Z., & Razek, A., "Finite Element Analysis of Magneto-Mechanical Coupled Phenomena in Magnetostrictive Materials," IEEE Transactions on Magnetics, Volume 32, Number 3, pp. 1058-1061, May 1996.

Broch, J.T., "Mechanical Vibration and Shock Measurements," Bruel & Kjær, Glostrup, Denmark, April 1984.

Brogan, W.L., "Modern Control Theory," Second edition, Prentice-Hall, Englewood Cliffs, NJ, 1985.

Bryant, M.D., "Bond Graph Models for Linear Motion Magnetostrictive Actuators," Transactions of the American Society of Mechanical Engineers, Journal of Dynamic Systems, Measurement, and Control, Volume 118, pp. 161-167, March 1996.

Bryant, M.D., Fernández, B., Wang, N., Murty, V.V., Vadlamani, V., and West, T.S., "Active Vibration Control in Structures Using Magnetostrictive Terfenol with Feedback and/or Neural Network Controllers," Journal of Intelligent Material Systems and Structures, Volume 4, pp. 484-489, 1993.

Budgor, A.B., Lindenberg, K., & Shuler, K.E., "Studies in Nonlinear Stochastic Processes. II. The Duffing Oscillator Revisited," Journal of Statistical Physics, Volume 15, Number 5, pp. 375-391, 1976.

Burden, R.L., & Faires, J.D., "Numerical analysis," Third edition, Prindle, Weber & Schmidt, Boston, MA, 1985.

Butler, J.L., "Application Manual for the Design of Etrema Terfenol-D Magnetostrictive Transducers," Edge Technologies Inc., Ames, Iowa, February 1988.

Butler, J.L., Butler, A.L., & Butler, C.L., "Hybrid magnetostrictive / piezoelectric Tonpilz transducer," Journal of the Acoustical Society of America, Volume 94, Number 2, Part 1, pp. 636-641, August 1993.

Butler, J.L., & Lizza, N.L., "Eddy current loss factor series for magnetostrictive rods," Journal of the Acoustical Society of America, Volume 82, Number 1, p. 378, July 1987.

Chapra, S.C., & Canale, R.P., "Numerical Methods for Engineers - with Personal Computer Applications," McGraw-Hill, New York, 1985.

Chen, S., Billings, S.A., & Luo, W., "Orthogonal least squares methods and their application to non-linear system identification," International Journal of Control, Volume 50, Number 5, pp. 1873-1896, 1989.

Clark, A.E., "High Power Rare Earth Magnetostrictive Materials," Journal of Intelligent Material Systems and Structures, Volume 4, Number 1, pp. 70-75, January 1993.

Clark, A.E., & Savage, H.T., "Magnetostriction of Rare Earth-$Fe_2$ Compounds under Compressive Stress," Journal of Magnetism and Magnetic Materials 31-34, pp. 849-851, 1983.

Clark, A.E., Spano, M.L., & Savage, H.T., "Effect of Stress on the Magnetostriction and Magnetization of Rare Earth-$Re_{1.95}$ Alloys," IEEE Transactions on Magnetics, Volume MAG-19, Number 5, pp. 1964-1966, September 1983.

Clark, A.E., Teter, J.P., Wun-Fogle, M., Moffett, M., & Lindberg, J., "Magnetomechanical coupling in Bridgman-grown $Tb_{0.3}Dy_{0.7}Fe_{1.9}$ at high drive levels," Journal of Applied Physics, Volume 67, Number 9, pp. 5007-5009, 1 May 1990.

Clough, R.W., & Penzien, J., "Dynamics of Structures," McGraw-Hill Kogakusha, Tokyo, 1982.

Conte, S.D., & de Boor, C., "Elementary Numerical Analysis," Second edition, McGraw-Hill Kogakusha, Tokyo, 1972.

Cooper, J.E., "Comparison of Some Time-Domain-System Identification Techniques Using Approximate Data Correlations," Journal of Modal Analysis, pp. 51-57, April 1989.

Cooper, W.D., & Helfrick, A.D., "Electronic Instrumentation and Measurement Techniques," Third edition, Prentice-Hall, Englewood Cliffs, NJ, 1985.

Cowan, C.F.N., & Grant, P.M., "Adaptive Filters," Prentice-Hall Signal Processing Series, Englewood Cliffs, NJ, 1985.

Craig, R.R. (jr.), "Structural Dynamics - An Introduction to Computer Methods," John Wiley & Sons, New York, 1981.

Craig, R.R. (jr.), & Bampton, M.C.C., "Coupling of Substructures for Dynamic Analyses," AIAA Journal, Vol. 6, No. 7, pp. 1313-1319, July 1968.

Crawley, E.F., & Hall, S.R., "The Dynamics of Controlled Structures, 1991 Notes," Massachusetts Institute of Technology Space Engineering Research Center, Cambridge, MA, July 1991.

D'Azzo, J.J., & Houpis, C.H., "Linear Control System Analysis and Design – Conventional and Modern," Second edition, McGraw-Hill, Singapore, 1986.

Dimas, D.J., & Pardoen, G.C., "Extrapolation of Modal-Analysis Techniques to Nonlinear Damped Systems," The International Journal of Analytical and Experimental Modal Analysis, Volume 3, Number 3, pp. 81-88, July 1988.

Doong, T., & Mayergoyz, I.D., "On Numerical Implementation of Hysteresis Models," IEEE Transactions on Magnetics, Volume MAG-21, Number 5, pp. 1853-1855, September 1985.

Doyle, J.C., Glover, K., Khargonekar, P.P., & Francis, B.A., "State-Space Solutions to Standard $H_2$ and $H_\infty$ Control Problems," IEEE Transactions on Automatic Control, Volume 34, Number 8, pp. 831-847, August 1989.

Dyberg, J., "Magnetostrictive Rods in Mechanical Applications," Presented at The First Conference on Giant Magnetostrictive Alloys and Their Impact on Actuator and Sensor Technology, Marbella, Spain, 7-9 March 1986.

ElMadany, M.M., & Dokainish, M.A., "Articulated Vehicle Dynamic Analyses Using Equivalent Linearization Technique," SAE Paper 801421, SAE/SP-80/475, pp. 75-86, 1980.

Ewins, D.J., "Modal Testing: Theory and Practice," Research Studies Press Ltd, Taunton, Somerset, England, 1991.

Franklin, G.F., Powell, J.D., & Workman, M.L., "Digital Control of Dynamic Systems," Second edition, Addison Wesley, Reading, MA, 1990.

Füllekrug, U., "Structural-Dynamics Identification in the Time-Domain, Estimation of Modal Parameters Based on Forced Vibrations," Journal of Modal Analysis, pp. 58-67, April 1989.

Gerald, C.F., & Wheatley, P.O., "Applied Numerical Analysis," Third edition, Addison-Wesley, Reading, MA, 1984.

Gelb, A., & Vander Velde, W.E., "Multiple-Input Describing Functions and Nonlinear System Design," McGraw-Hill, 1968.

Goodwin, G.C., & Sin, K.S., "Adaptive Filtering Prediction and Control," Prentice Hall, Englewood Cliffs, NJ, 1984.

Hall, D.L., & Flatau, A.B., "Non-linearities, Harmonics and Trends in Dynamic Applications of Terfenol-D," Proceedings of the North American Conference on Smart Structures and Materials, SPIE, volume 1917-86, 1993.

Harris, C.M., "Shock and Vibration Handbook," Third edition, McGraw-Hill, New York, 1988.

Hayes, J.G., "Numerical Approximation to Functions and Data," The Athlone Press, University of London, 1970.

Hiller, M.W., Bryant, M.D., & Umegaki, J., "Attenuation and Transformation of Vibration Through Active Control of Magnetostrictive Terfenol," Journal of Sound and Vibration, Volume 134, Number 3, pp. 507-519, 1989.

Hintz, R.M., "Analytical Methods in Component Modal Synthesis," AIAA Journal, Vol. 13, No. 8, pp. 1007-1016, August 1975.

Hyde, T.T., "Active Vibration Isolation for Precision Space Structures," PhD Thesis, Department of Aeronautics and Astronautics, Massachusetts Institute of Technology, January 1996.

Ibrahim, R.A., "Response Analysis of Nonlinear Systems using Functional-Perturbation Type Approach," Proceedings of the 6th International Modal Analysis Conference, Kissimmee, FL, pp. 1480-1488, 1988.

Jacobson, D.H., "Extensions of Linear-Quadratic Control, Optimization and Matrix Theory," Academic Press, London, 1977.

Jacquot, R.G., "Modern Digital Control Systems," Dekker, New York, 1981.

Jiles, D.C., "Introduction to Magnetism and Magnetic Materials," Chapman & Hall, 1991.

Joshi, C.H., "Compact Magnetostrictive Actuators and Linear Motors," Paper presented at Actuator 2000 Conference, Bremen, Germany, June 2000.

Karnopp, D.C., & Trikha, A.K., "Comparative Study of Optimization Techniques for Shock and Vibration Isolation, Transactions of the American Society of Mechanical Engineers, Journal of Engineering for Industry, pp. 1128-1132, November 1969.

Kashyap, R.L., & Rao, A.R., "Dynamic Stochastic Models from Empirical Data," Academic Press, New York, 1976.

Khargonekar, P.P., Petersen, I.R., & Rotea, M.A., "$H_\infty$ Optimal Control with State-Feedback, IEEE Transactions on Automatic Control, Volume 33, Number 8, pp. 786-788, August 1988.

Kim, B., "Dual-Loop DPLL Gear-Shifting Algorithm for Fast Synchronization," IEEE Transactions on Circuits and Systems – II: Analog and Digital Signal Processing, Volume 44, Number 7, pp. 577-586, July 1997.

Kirk, D.E., "Optimal Control Theory - An introduction," Prentice-Hall, Englewood Cliffs, NJ, 1970.

Klein, L.R., & Dowell, E.H., "Analysis of Modal Damping by Component Modes Using Lagrange Multipliers," Transactions of the American Society of Mechanical Engineers, Journal of Applied Mechanics, pp. 527-528, June 1974.

Kubomura, K., "Component Mode Synthesis for Damped Structures," AIAA Journal, Vol. 25, No. 5, pp. 740-745, May 1987.

Kubomura, K., "A Theory of Substructure Modal Synthesis," Transactions of the American Society of Mechanical Engineers, Journal of Applied Mechanics, Volume 49, pp. 903-909, December 1982.

Kuo, B.C., "Automatic Control Systems," Fourth edition, Prentice-Hall, Englewood Cliffs, NJ, 1982.

Kvarnsjö, L., "On Characterization, Modelling and Application of Highly Magnetostrictive Materials," PhD Thesis, Royal Institute of Technology, Electric Power Research Centre, Department of Electrical Plant Engineering, Stockholm, Sweden, 1993.

Kwakernaak, H., & Sivan, R., "Linear Optimal Control Systems," Wiley-Interscience, New York, 1972.

Leonard, P.J., Rodger, D., Karagular, T., & Coles, P.C., "Finite Element Modelling of Hysteresis," IEEE Transactions on Magnetics, Volume 31, Number 3, pp. 1801-1804, May 1995.

Likhachev, A.A., & Ullakko, K., "Quantitative model of large magnetostrain effect in ferromagnetic shape memory alloys," The European Physical Journal B, Volume 14, Number 2, pp. 263 – 257, March 2000.

Liu, K., & Miller, D.W., "Time Domain State-Space Identification of Structural Systems," Transactions of the American Society of Mechanical Engineers, Journal of Dynamic Systems, Measurement, and Control, Volume 117, pp. 608-618, December 1995.

Liu, K., Jacques, R.N., & Miller, D.W., "Frequency Domain Structural System Identification by Observability Range Space Extraction, Transactions of the American Society of Mechanical Engineers, Journal of Dynamic Systems, Measurement, and Control, Volume 118, pp. 211-220, June 1996.

Machine Design, "Cabin Noise Squelched with Antivibes," p.25, April 4, 1994.

Maciejowski, J.M., "Multivariable Feedback Design," Addison Wesley, Wokingham, England, 1989.

Masri, S.F., Chassiakos, A.G., & Caughey, T.K., "Identification of Nonlinear Dynamic Systems Using Neural Networks," Transactions of the American Society of Mechanical Engineers, Journal of Applied Mechanics, Volume 60, pp. 123-133, March 1993.

Masri, S.F., Chassiakos, A.G., & Caughey, T.K., "Structure-unknown non-linear dynamic systems: identification through neural networks," Smart Materials and Structures, Volume 1, pp. 45-56, 1992.

Masters, B.P., & Crawley, E.F., & van Schoor, M.C., "Global Structure Modeling Using Force-State Component Identification," AIAA Journal of Guidance, Control and Dynamics, Volume 19, Number 1, pp. 198-206, January/February 1996.

Mathews, J.H, & Fink, K.D., "Numerical Methods Using Matlab," Third edition, Prentice-Hall, Upper Saddle River, NJ, 1999.

McCaig, M., & Clegg, A.G., "Permanent Magnets in Theory and Practice," Second edition, Pentech, London, 1987.

Meeks, S.W., & Timme, R.W., "Rare earth iron magnetostrictive underwater sound transducer," Journal of the Acoustical Society of America, Volume 62, Number 5, pp. 1158-1164, November 1977.

Meirovitch, L., "Dynamics and Control of Structures," John Wiley & Sons, New York, 1990.

Ossart, F., Davidson, R., & Charap, S.H., "A 3D Moving Vector Preisach Hysteresis Model," IEEE Transactions on Magnetics, Volume 31, Number 3, pp. 1785-1788, May 1995.

Petersen, I.R., "Disturbance Attenuation and $H^{\infty}$ Optimization: A Design Method Based on the Algebraic Riccati Equation," IEEE Transactions on Automatic Control, Volume AC-32, Number 5, pp. 427-429, May 1987.

Petersen, I.R., "Complete Results for a Class of State Feedback Disturbance Attenuation Problems," IEEE Transactions on Automatic Control, Volume 34, Number 11, pp. 1196-1199, November 1989.

Pinches, M.J., & Ashby, J.G., "Power Hydraulics," Prentice Hall International, UK, 1989.

Pratt, J., "Design and analysis of a self-sensing Terfenol-D magnetostrictive actuator," MS Thesis, Department of Aerospace Engineering and Engineering Mechanics, Iowa State University, Ames, Iowa, 1993.

Press, W.H., Teukolsky, S.A., Vetterling, W.T., & Flannery, B.P., "Numerical Recipes in FORTRAN - The Art of Scientific Computing," Second edition, Cambridge University Press, New York, 1992.

Raath, A.D., "Dynamic System Identification," Project Report VLG\90\050, Centre for Structural Mechanics, Laboratory for Advanced Engineering, 5 April 1990.

Randall, R.B., "Frequency Analysis," Third edition, Bruel & Kjær, Glostrup, Denmark, September 1987.

Rao, S.S., "The Finite Element Method in Engineering," Second edition, Pergamon Press, Elmsford, NY, 1989.

Reed, R.S., "Shock isolation using an active magnetostrictive element," Proceedings from 59th Shock and Vibration Symposium, Volume 4, Sandia National Laboratories, Albuquerque, NM, October 1988.

Reed, R.S., "Active Vibration Isolation Using a Magnetostrictive Actuator," Technical Paper, System Engineering Department, U.S. Naval Academy at Annapolis, 1989.

Restorff, J.B., Savage, H.T., Clark, A.E., & Wun-Fogle, M., "Preisach modelling of hysteresis in Terfenol," Journal of Applied Physics, Volume 67, Number 9, pp. 5016-5018, 1 May 1990.

Rizzoli, V., & Masotti, D., "General-Purpose Analysis of Nonlinear Circuits Containing Saturating / Hysteretic Inductors by the Harmonic-Balance Technique," IEEE Transactions on Magnetics, Volume 31, Number 3, pp. 2290-2303, May 1995.

Roark, R.J., & Young, W.C., "Formulas for Stress and Strain," Fifth edition, McGraw-Hill, Tokyo, 1983.

Rubin, S., "Improved Component-Mode Representation for Structural Dynamic Analysis," AIAA Journal, Vol. 13, No. 8, pp. 995-1006, August 1975.

Sablik, M.J., & Jiles, D.C., "A model for hysteresis in magnetostriction," Journal of Applied Physics, Volume 64, Number 10, pp. 5402-5404, 15 November 1988.

Schoukens, J. & Pintelon, R., "Identification of Linear Systems – A Practical Guideline to Accurate Modelling," Pergamon Press, Oxford, 1991.

Schulze, M.P., Greenough, R.D., & Galloway, R.D., "The Stress Dependence of $k_{33}$, $d_{33}$, $\lambda$ and $\mu$ in $Tb_{0.3}Dy_{0.7}Fe_{1.95}$," IEEE Transactions on Magnetics, Volume 28, Number 5, pp. 3159-3161, September 1992.

Schwarzenbach, J. & Gill, K.F., "System Modelling and Control," Second edition, Edward Arnold, London, 1986.

Sears, F.W., & Zemansky, M.W., "University Physics," Fourth edition, Addison Wesley, Reading, MA, 1975.

Sewell, J, & Kuhn, P., "Comparison of Magnetic Biasing Techniques for Terfenol D," in Proceedings of Second International Conference on Giant Magnetostrictive and Amorphous Alloys for Actuators and Sensors, C. Tyrén, Ed., Marbella, Spain, October 1988.

Shigley, J.E., "Mechanical Engineering Design," Third edition, McGraw-Hill Kogakusha, Tokyo, 1977.

Sievers, L.A., & von Flotow, A.H., "Comparison and Extensions of Control Methods for Narrow-Band Disturbance Rejection," IEEE Transactions on Signal Processing, Volume 40, Number 10, pp. 2377-2391, October 1992.

Simon, M., & Tomlinson, G.R., "Use of Hilbert Transform in Modal Analysis of Linear and Nonlinear Structures," Journal of Sound and Vibration, Volume 96, Number 4, pp. 421-436, 1984.

Singer, N.C., & Seering, W.P., "Preshaping Command Inputs to Reduce System Vibration," Transactions of the American Society of Mechanical Engineers, Journal of Dynamic Systems, Measurement, and Control, Volume 112, pp. 76-82, March 1990.

Sinha, N.K., & Kuszta, B., "Modelling and Identification of Dynamic Systems," Van Nostrand Reinhold Electrical / Computer Science and Engineering Series, New York, 1983.

Skogestad, S., & Postlethwaite, I., Multivariable Feedback Control – Analysis and Design, John Wiley & Sons, Chichester, England, November 1997.

Slotine, J-J.E., & Li, W., "Applied Nonlinear Control," Prentice Hall, Englewood Cliffs, NJ, 1991.

Spiegel, M.R., "Mathematical Handbook of Formulas and Tables," Schaum's Outline Series in Mathematics, McGraw-Hill, New York, 1968.

Spring Design Manual, Part 2, "Design and Application of Helical and Spiral Springs," Society of Automotive Engineers, SAE HS 795, 1990.

Stockum, L.A., & Carroll, G.R., "Precision stabilized platforms for shipboard electro-optical systems," SPIE Volume 493, The National Symposium and Workshop on Optical Platforms, pp. 414-425, 1984.

Thomson, W.T., "Theory of Vibration with Applications," Fourth edition, Chapman & Hall, Englewood Cliffs, NJ, 1993.

Tomlinson, G.R., "Detection, Identification and Quantification of Nonlinearity in Modal Analysis – A Review," Proceedings of the 4th International Modal Analysis Conference, Los Angeles, CA, Volume 2, pp. 837-843, 1986.

Tse, F.S., Morse, I.E., & Hinkle, R.T., "Mechanical Vibrations - Theory and Applications," Second edition, Allyn & Bacon, Boston, MA, 1978.

Tsui, C-C., "Robust Control System Design – Advanced State-space Techniques," Marcel Dekker, New York, 1996.

Vajda, F., & Della Torre, E., "Modelling $\Delta m$ Curves Using the Complete-Moving-Hysteresis Model," IEEE Transactions on Magnetics, Volume 31, Number 3, pp. 1809-1812, May 1995.

Van Schoor, M.C., "The Coupled Nonlinear Dynamics of Spacecraft with Fluids in Tanks of Arbitrary Geometry," PhD Thesis, Department of Aeronautics and Astronautics, Massachusetts Institute of Technology, March 1989.

Van Schoor, M.C., & Bester, C.R., "The Development of a Magnetostrictive-Hydraulically Gained Actuator," Project Report, Laboratory for Advanced Engineering, Department of Mechanical Engineering, Universtiy of Pretoria, Pretoria, RSA, 1992.

Van Schoor, M.C., Masters, B.P., & Rodgers, J., "Smart Materials: Opportunities for Competitive Products," Course presented at the University of Pretoria, South Africa, 28 – 30 June, 1999.

Vidyasagar, M., "Nonlinear System Analysis," Prentice-Hall, Englewood Cliffs, NJ, 1978.

Vinh, T., Haoui, A., & Chevalier, Y., "Extension of Modal Analysis to Nonlinear Structure," Proceedings of the 2nd International Modal Analysis Conference, Orlando, FL, pp. 852-857, 1984.

Wakiwaka, H., Umezawa, T., Yamada, H., Kobayashi, K., & Yoshikawa, T., "Improvement of Flux Density Uniformity in Giant Magnetostrictive Material for Acoustic Vibration Element," IEEE Transactions on Magnetics, Volume 29, Number 6, pp. 2443-2445, November 1993.

Weaver, W., & Johnston, P.R., "Finite Elements for Structural Analysis," Prentice-Hall, Englewood Cliffs, NJ, 1984.

Widrow, B., & Stearns, S.D., "Adaptive Signal Processing," Prentice-Hall, Englewood Cliffs, NJ, 1985.

Wen, Y.K., "Equivalent Linearization for Hysteretic Systems Under Random Excitation," Transactions of the ASME, Journal of Applied Mechanics, Volume 47, pp. 150-154, March 1980.

Worden, K., Stansby, P.K., & Tomlinson, G.R., "Identification of Nonlinear Wave Forces," Journal of Fluids and Structures, Volume 8, pp. 19-71, 1994.

Worden, K., & Tomlinson, G.R., "Developments in Force-State Mapping for Nonlinear Systems," Proceedings of the 6th International Modal Analysis Conference, Kissimmee, FL, pp. 1471-1479, 1988.

Wright, J.R., & Al-Haddid, M.A., "Sensitivity of the Force-State Mapping Approach to Measurement Errors," The International Journal of Analytical and Experimental Modal Analysis, Volume 6, Number 2, pp. 89-103, April 1991.

Zienkiewicz, O.C., "The Finite Element Method," Third edition, McGraw-Hill, London, 1977.

# APPENDICES

# Appendix A
# Complex Laplace-domain transfer functions from state-space equations

Consider the state and output equations of an LTI system (equations 2.5.1.19):

$$\dot{x} = Ax + Bu \quad \textbf{(A.1a)}$$
$$y = Cx + Du \quad \textbf{(A.1b)}$$

The Laplace-transform of equation A.1a is:

$$sX(s) - x(0) = AX(s) + BU(s) \quad \textbf{(A.2)}$$

For $x(0) = 0$, equation A.2 becomes:

$$sX(s) = AX(s) + BU(s) \quad \textbf{(A.3)}$$

Solving equation A.3 for $X(s)$ gives:

$$X(s) = [sI - A]^{-1} BU(s) \quad \textbf{(A.4)}$$

The Laplace-transform of equation A.1b is:

$$Y(s) = CX(s) + DU(s) \quad \textbf{(A.5)}$$

Substitution of equation A.4 into equation A.5 gives:

$$Y(s) = \left(C[sI - A]^{-1} B + D\right)U(s) \quad \textbf{(A.6)}$$

The transfer function $G(s)$ is the ratio of the output $Y(s)$ to the input $U(s)$:

$$G(s) = \frac{Y(s)}{U(s)} = C[sI - A]^{-1} B + D \quad \textbf{(A.7)}$$

# Appendix B
# Exact solution methods for equations of motion of nonlinear systems

Consider the equation of motion for natural behaviour of an undamped SDOF system with a general, nonlinear restoring force $g(y)$, as governed by the DE:

$$m\ddot{y} + \kappa g(y) = 0 \tag{B.1}$$

where $m$ is the mass, $\kappa$ is a constant, $y$ and $\ddot{y}$ are the mass displacement and acceleration respectively.

Equation B.1 can be written as:

$$\frac{d(\dot{y}^2)}{dy} + 2\frac{\kappa}{m} g(y) = 0 \tag{B.2}$$

The *time versus displacement* relationship is obtained by integrating equation B.2 twice:

$$t - t_0 = \frac{1}{\sqrt{2\frac{\kappa}{m}}} \int_0^y \frac{d\chi_2}{\sqrt{\int_{\chi_2}^{Y} g(\chi_1) d\chi_1}} \tag{B.3}$$

where $t$ is time, $t_0$ corresponds to the time when $y = 0$, $Y$ is the displacement when $\dot{y} = 0$ and $\chi_1$ and $\chi_2$ are integration variables. The *displacement versus time* relationship may be obtained by inverting equation B.3.

For an odd nonlinear restoring force, i.e. $g(-y) = -g(y)$, the natural period of vibration $\tau_n$ is given by:

$$\tau_n = \frac{4}{\sqrt{2\frac{\kappa}{m}}} \int_0^Y \frac{d\chi_2}{\sqrt{\int_{\chi_2}^{Y} g(\chi_1) d\chi_1}} \tag{B.4}$$

Exact solutions can be obtained in all cases where the integrals in equation B.4 can be explicitly expressed in terms of $Y$. For pure powers of displacement $g(y) = y^n$, $\tau_n$ is given by:

$$\tau_n = \frac{4}{\sqrt{\frac{\kappa}{m} Y^{n-1}}} \psi(n) \tag{B.5}$$

where $\psi(n)$ is a function whose values are given in table B.1, for $n$ ranging from 0 to 7.

**Table B.1: Values of the function $\psi(n)$ [Harris, 1988]**

| $n$ | $\psi(n)$ |
|---|---|
| 0 | 1,4142 |
| 1 | 1,5708 |
| 2 | 1,7157 |
| 3 | 1,8541 |
| 4 | 1,9818 |
| 5 | 2,1035 |
| 6 | 2,2186 |
| 7 | 2,3282 |

Solutions for polynomials of displacement and velocity-squared damping are given by Harris [1988]. Exact solutions for forced vibration of nonlinear systems are virtually nonexistent, except if the system can be represented in a stepwise linear manner [Harris, 1988].

# Appendix C
# The perturbation method

Consider the following equation of motion for natural behaviour of a weakly nonlinear SDOF system:

$$\underbrace{\ddot{y}+\omega_0^2 y}_{linear}+\underbrace{\frac{\kappa}{m}g(\dot{y},y)}_{nonlinear}=0 \qquad \textbf{(C.1)}$$

where $\omega_0$ is the linear system natural frequency, $\kappa$ is a small parameter and $g$ is a nonlinear function of speed $\dot{y}$ and displacement $y$. The first two terms on the left hand side of equation C.1 describe the behaviour of the linear part of the system, while the third, or perturbation term, accounts for the effects of the weak nonlinearity.

A solution of the following form is assumed for $y$ [Gelb & VanderVelde, 1968]:

$$y(t)=y_0(t)+\frac{\kappa}{m}y_1(t)+\left(\frac{\kappa}{m}\right)^2 y_2(t)+\cdots+ \qquad \textbf{(C.2)}$$

where $y_0$, $y_1$, $y_2$, $\cdots$, are displacement functions of time. These functions are obtained by solving the following system of linear, non-homogeneous, 2nd order DE's:

$$\ddot{y}_0+\omega_0^2 y_0=0 \qquad \textbf{(C.3a)}$$

$$\ddot{y}_1+\omega_0^2 y_1=-g(\dot{y}_0,y_0) \qquad \textbf{(C.3b)}$$

$$\ddot{y}_2+\omega_0^2 y_2=-\frac{\partial g}{\partial y}(\dot{y}_0,y_0)y_1-\frac{\partial g}{\partial \dot{y}}(\dot{y}_0,y_0)\dot{y}_1 \qquad \textbf{(C.3c)}$$

$$\vdots \qquad \vdots \qquad \vdots \qquad \vdots$$

Equations C.3a to C.3b are solved recursively. The first equation (C.3a) is solved for $y_0$ and $\dot{y}_0$. With $y_0$ and $\dot{y}_0$ known, $g$, $\partial g/\partial y$ and $\partial g/\partial \dot{y}$ are obtained. Equation C.3b is subsequently solved for $y_1$ and $\dot{y}_1$, whereafter equation C.3c is solved for $y_2$ and $\dot{y}_2$. The solutions of $y_0$, $y_1$ and $y_2$ are substituted into equation C.2 to obtain $y(t)$. The procedure can be repeated as many times as the number of terms required in the series expansion in equation C.2.

# Appendix D
# The method of slowly varying amplitude and phase

Consider the following equation of motion for natural behaviour of a weakly nonlinear SDOF system:

$$\underbrace{\ddot{y}+\omega_0^2 y}_{linear}+\underbrace{\frac{\kappa}{m}g(\dot{y},y)}_{nonlinear}=0 \qquad \textbf{(D.1)}$$

where $\omega_0$ is the linear system natural frequency, $\kappa$ is a small parameter and $g$ is a nonlinear function of speed $\dot{y}$ displacement $y$.

A solution of the following form is assumed for $y$ [Gelb & VanderVelde, 1968]:

$$y(t)=A\sin\psi \qquad \textbf{(D.2)}$$

where $A$ and $\psi$ are functions of time, given by:

$$A=A(t) \qquad \textbf{(D.3a)}$$
$$\psi=\omega_0 t+\theta(t) \qquad \textbf{(D.3b)}$$

The following set of approximate DE's in $A$ and $\theta$ can be derived [Gelb & VanderVelde, 1968]:

$$\dot{A}\approx-\frac{1}{2\pi\omega_0}\int_0^{2\pi}\mu g(A\sin\psi,A\omega_0\cos\psi)\cos\psi d\psi \qquad \textbf{(D.4a)}$$

$$\dot{\theta}\approx\frac{1}{2\pi\omega_0}\int_0^{2\pi}\frac{1}{A}\mu g(A\sin\psi,A\omega_0\cos\psi)\cos\psi d\psi \qquad \textbf{(D.4b)}$$

Equations D.4 are solved as follows: The right hand side of equation D.4 a is integrated with respect to $\psi$, resulting in a 1st order separable DE in $A$. This DE is solved and its solution $A=\underline{A}$ is obtained. Subsequently, the right hand side of equation D.4b is integrated with respect to $\psi$ and another 1st order DE is obtained. Replacing A by $\underline{A}$, the latter DE is solved to obtain its solution $\theta=\underline{\theta}$.

The solution of equation D.1 is then:

$$y(t)=\underline{A}(t)\sin[\omega_0 t+\underline{\theta}(t)] \qquad \textbf{(D.5)}$$

# Appendix E
# Statistical linearization

Consider a general nonlinear SDOF system with an equation of motion of the form

$$g(\ddot{y},\dot{y},y)=f(t) \tag{E.1}$$

where $g$ is the total internal force and $f$ is the stationary gaussian random excitation force with zero mean. It is assumed that a stationary solution to equation E.1 exists.

The linear equivalent of equation E.1 is:

$$m\ddot{y}+c\dot{y}+ky=f(t) \tag{E.2}$$

where $m$, $c$ and $k$ are the mass, damping coefficient and spring stiffness to be determined, such that the solution of equation E.2 will give an approximate solution to equation E.1.

In approximating a nonlinear system by a linear system, an error will be made. The error may be defined as the difference between the solutions of the two systems, an can be written as:

$$e=g(\ddot{y},\dot{y},y)-m\ddot{y}-c\dot{y}-ky \tag{E.3}$$

The mass, damping coefficient and stiffness are determined by setting the mean square (MS) error equal to zero, resulting in:

$$m=E\left[\frac{\partial g(\ddot{y},\dot{y},y)}{\partial \ddot{y}}\right] \tag{E.4a}$$

$$c=E\left[\frac{\partial g(\ddot{y},\dot{y},y)}{\partial \dot{y}}\right] \tag{E.4b}$$

$$k=E\left[\frac{\partial g(\ddot{y},\dot{y},y)}{\partial y}\right] \tag{E.4c}$$

where $E[\ ]$ is the expected value of the term in brackets.

The method of equivalent linearization can be applied to a large variety of nonlinear system types. Examples are systems with cubic stiffening characteristics [Atalik & Utku, 1976], nonlinear damping characteristics [Atalik & Utku, 1976], hysteretic restoring forces [Wen, 1980], the Duffing oscillator [Budgor et al, 1976] and equations of motion of articulated vehicles [ElMadany & Dokainish , 1980]. Application of the method to a system with hysteretic restoring forces, as described by Wen [1980], is discussed next.

## Statistical linearization applied to a system with hysteretic restoring forces

Consider a system whose equation of motion is of the form

$$m\ddot{\bar{y}} + g(\dot{\bar{y}}, \bar{y}) + z(\bar{y}) = \bar{f}(t) \qquad \textbf{(E.5)}$$

where $\bar{y}$ is the dimensionless displacement and $\bar{f}$ is the dimensionless force:

$$\bar{y} = \frac{y}{Y} \qquad \textbf{(E.6a)}$$

$$\bar{f} = \frac{f}{F_y} \qquad \textbf{(E.6b)}$$

In equation E.5, $g$ is the nonhysteretic component of the restoring force, while $z$ is the hysteretic component.

The relationship between $z$ and $y$ is given by the following 1st order nonlinear DE:

$$\dot{z} = -\gamma|\dot{y}|.z.|z|^{n-1} - \beta\dot{y}|z|^{n} + G\dot{y} \qquad \textbf{(E.7)}$$

where $\gamma$ and $\beta$ are parameters which control the shape of the hysteresis loop, $G$ is the restoring force amplitude and $n$ is an exponent which describes the smoothness of transition from elastic to plastic response.

From Wen [1980], equations E.5 and E.7 can be written in linear state-space form as

$$\dot{x} = Ax + Bu \qquad \textbf{(E.8)}$$

where $x$ and $u$ are the state vector and input respectively:

$$x = \{\bar{y}, \quad z, \quad \dot{\bar{y}}\}^T \qquad \textbf{(E.9a)}$$

$$u = \bar{f}(t) \qquad \textbf{(E.9b)}$$

$A$ and $B$ are the coefficient and driving matrices respectively, given by:

$$A = \begin{bmatrix} 0 & 0 & 0 \\ 0 & -k_h & -c_h \\ -\alpha\omega_0^2 & -(1-\alpha)\omega_0^2 & -2\zeta_0\omega_0 \end{bmatrix} \qquad \textbf{(E.10a)}$$

$$B = [0, \quad 0, \quad 1/m]^T \qquad \textbf{(E.10b)}$$

In equation E.10a, $\alpha$ is the post-to pre-yielding stiffness ratio, $\zeta_0$ is the viscous damping ratio

and $\omega_0$ is the pre-yielding natural frequency:

$$\omega_0 = \sqrt{\frac{F_Y}{mY}} \tag{E.11}$$

$k_h$ and $c_h$ are the linearized hysteresis stiffness and damping coefficient. Both $k_h$ and $c_h$ depend on $n$. For the special case of $n = 1$, $k_h$ and $c_h$ are given by:

$$k_h = \gamma E\left[|\dot{y}|\right] + \beta E\left[\dot{y}\frac{\partial |z|}{\partial z}\right] \tag{E.12a}$$

$$c_h = \gamma E\left[z\frac{\partial |\dot{y}|}{\partial y}\right] + \beta E\left[|z|\right] - G \tag{E.12b}$$

It can be seen that the highly nonlinear system, as described by equations E.5 and E.7, is replaced by the equivalent linear system, as represented by equations E.8 to E.12. By comparison, the linear equations are considerably easier to solve than the nonlinear equations. Linear solutions of the above hysteretic system to gaussian inputs are given by Wen [1980].

# Appendix F
# The Describing Function (DF) method

Consider a nonlinear system driven by a harmonic input of the form

$$u(t) = U \sin \omega t \tag{F.1}$$

where $u$ is the input as a function of time and $U$ is the input amplitude.

The output $y(t)$, which is generally non-sinusoidal, can be expressed as follows by means of a Fourier series:

$$y(t) = \frac{a_0}{2} + \sum_{i=1}^{\infty} [a_i \cos(i\omega t) + b_i \sin(i\omega t)] \tag{F.2}$$

where the Fourier coefficients are $a_i$ and $b_i$ are functions of $U$ and $\omega$, determined by:

$$a_0 = \frac{1}{\pi} \int_{-\pi}^{\pi} y(t) d(\omega t) \tag{F.3a}$$

$$a_i = \frac{1}{\pi} \int_{-\pi}^{\pi} y(t) \cos(i\omega t) d(\omega t) \tag{F.3b}$$

$$b_i = \frac{1}{\pi} \int_{-\pi}^{\pi} y(t) \sin(i\omega t) d(\omega t) \tag{F.3c}$$

For an odd nonlinearity, the coefficient $a_0$ is zero:

$$a_0 = 0 \tag{F.4}$$

In harmonic DF analysis, only the fundamental frequency is considered. Therefore, *y(t)* can be approximated by:

$$y(t) \approx y_1(t) = a_1 \cos \omega t + b_1 \sin \omega t \tag{F.5}$$

The output *y(t)* is written in terms of the output amplitude and phase of the fundamental frequency as:

$$y_1(t) = Y \sin(\omega t + \phi) \tag{F.6}$$

where $Y$ are the output amplitude and phase respectively, as functions of input amplitude and frequency:

$$Y = Y(U, \omega) \tag{F.7a}$$

$$\phi = \phi(U, \omega) \tag{F.7b}$$

In terms of the fundamental Fourier coefficients, $Y$ and $\phi$ are:

$$Y = \sqrt{a_1^2 + b_1^2} \tag{F.8a}$$

$$\phi = \tan^{-1}\left(\frac{a_1}{b_1}\right) \tag{F.8b}$$

In complex representation, $y_1$ can be written as:

$$y_1 = Ye^{j(\omega t+\phi)} \tag{F.9}$$

The describing function $N$ of a nonlinear system is the ratio of the fundamental component of the output, to the input:

$$N = \frac{Ye^{j(\omega t+\phi)}}{Ue^{j\omega t}} \tag{F.10}$$

where $N$ is a function of the input amplitude and frequency:

$$N = N(U,\omega) \tag{F.11}$$

In rectangular coordinates, $N$ can be written as:

$$N(U,\omega) = \frac{1}{U}(b_1 + ja_1) \tag{F.12}$$

The above derivation is only applicable to harmonically excited nonlinear systems. The DF method can also be extended to analyze nonlinear system behaviour to non-harmonic inputs, like two-sinusoid inputs, dual-inputs (e.g. DC plus sinusoid), transient and random inputs. $N$ is tabled for a vast range of nonlinearities, for each of the above input types, by Gelb & Vander Velde [1968]. Examples of nonlinearities applicable to the analysis of Terfenol-D characteristics, are saturation and hysteresis. The DF's of these nonlinearities can be found in Gelb & Vander Velde [1968].

# Appendix G
# Fifth order Runge-Kutta (R-K) method

In the R-K methods, the states and outputs are obtained in the time domain by direct integration of the state equations. The solution of each state equation is approximated by a polynomial. The order of the polynomial can vary from 1st order to 5th order and higher. The higher the order, the more accurate the solution for the same computational effort [Chapra & Canale, 1985]. For this reason, higher order methods are often preferred to lower order methods.

The R-K methods are discussed in detail by Burden & Faires [1985], Chapra & Canale [1985], Conte & de Boor [1972], Gerald & Wheatley [1984] and Press et al [1992]. A short description of the 5th order method, also known as Butcher's method, is given below.

Consider a nonlinear time-invariant system, whose state and output equations are of the following form (see equations 2.5.1.2a and 2.5.1.2b):

$$\dot{x} = f(x,u) \qquad \textbf{(G.1a)}$$
$$y = g(x,u) \qquad \textbf{(G.1b)}$$

Equations G.1a and G.1b are solved by dividing time into finite intervals, and by recursively calculating the states and outputs for successive intervals using simple algebra.

Time at the beginning of the $i$-th time step is denoted by $t_i$. The state and output equations corresponding to $t_i$ are:

$$\dot{x}_i = f(x_i,u_i) \qquad \textbf{(G.2a)}$$
$$y_i = g(x_i,u_i) \qquad \textbf{(G.2b)}$$

where $x_i$, $u_i$ and $y_i$ respectively represent the state vector, input and output at the beginning of the $i$-th time step.

The state vector $x_{i+1}$, at the beginning of the $i$+1-th time step, is obtained by the following equation:

$$x_{i+1} = x_i + \frac{\Delta t}{90}(7k_1 + 32k_3 + 12k_4 + 32k_5 + 7k_6) \qquad \textbf{(G.3)}$$

where $\Delta t$ is the time step, given by:

$$\Delta t = t_{i+1} - t_i \qquad \textbf{(G.4)}$$

$\Delta t$ may be constant, or may be adjusted during simulation to accommodate changing stiffness of the system. Generally, the smaller $\Delta t$, the more accurate the solutions.

Variables $k_1$ to $k_6$ in equation G.3 represent the derivatives of the state vector at intermediate

intervals between $t_i$ and $t_{i+1}$. Note that $k_2$ does not appear in equation G.3. It is a "dummy" variable, which is only used to determine $k_3$, $k_4$ and $k_6$.

Variables $k_1$ to $k_6$ are determined recursively by means of the following equations:

$$k_1 = f(t_i, \quad x_i) \tag{G.5a}$$

$$k_2 = f\left(t_i + \frac{\Delta t}{4}, \quad x_i + \frac{\Delta t}{4}k_1\right) \tag{G.5b}$$

$$k_3 = f\left(t_i + \frac{\Delta t}{4}, \quad x_i + \frac{\Delta t}{8}k_1 + \frac{\Delta t}{8}k_2\right) \tag{G.5c}$$

$$k_4 = f\left(t_i + \frac{\Delta t}{2}, \quad x_i - \frac{\Delta t}{2}k_2 + (\Delta t)k_3\right) \tag{G.5d}$$

$$k_5 = f\left(t_i + \frac{3\Delta t}{4}, \quad x_i + \frac{3\Delta t}{16}k_1 + \frac{9\Delta t}{16}k_4\right) \tag{G.5e}$$

$$k_6 = f\left(t_i + \Delta t, \quad x_i - \frac{3\Delta t}{7}k_1 + \frac{2\Delta t}{7}k_2 + \frac{12\Delta t}{7}k_3 - \frac{12\Delta t}{7}k_4 + \frac{8\Delta t}{7}k_5\right) \tag{G.5f}$$

The output $y_{i+1}$ for the $i$+1-th time step is given by:

$$y_{i+1} = g(x_{i+1}, u_{i+1}) \tag{G.6}$$

# Appendix H
# Actuator nonlinear dehysterized transfer functions

In order to obtain the nonlinear, dehysterized *TF's*, three sets of simulations are done, one for each of the input RMS values, i.e. 2,18 V, 1,63 V and 1,09 V. The nonlinear state equations (equations 2.5.1.11 and 2.5.1.12) are solved in the time-domain by means of the 5$^{th}$ order Runge-Kutta method. The states are the actuator displacement $x_a$, speed $\dot{x}_a$ and coil current $I$ (see equation 2.5.1.4). The input is the coil voltage $V$. The input with the highest RMS value, i.e. 2,18 V, is applied first. The initial values of the states are set equal to zero.

For each time-step, stress and field are calculated from the states, using equations 2.4.4 and 2.4.10. The magnetostrictive and magnetization parameters, i.e. permeability $\mu^\sigma$, Young's modulus $E$, piezomagnetic cross-coupling constant $d^\sigma$ and strain constant $d^H$, are calculated from stress and field, using equations 2.5.1.10a to 2.5.1.10d. The state equations are integrated using equations G.3 and G.5a to G.5f (see appendix G), thereby obtaining the state vector at the end of each time step. The outputs are calculated in terms of the states at the end of each time step, using equation G.6. At the beginning of a new time-step, input voltage is updated and the procedure as set out in this paragraph, is repeated. At the end of the simulation, outputs for all the time steps are stored. The procedure is repeated for the 1,63 V and 1,09 V RMS inputs.

The nonlinear dehysterized transfer functions for the three coil input voltages, in terms of the inputs and outputs, are obtained by means of the following equation:

$$G(j\omega)=\frac{P_{xy}}{P_{xx}} \qquad \textbf{(H.1)}$$

where $G(j\omega)$ is the transfer function between the coil input voltage and actuator displacement output, $P_{xy}$ is the cross-spectral density (CSD) between the input and output and $P_{xx}$ is the power spectral density (PSD) of the input. Since the displacement signal is a simulation output, no measurement noise is present, resulting in high coherence.

$G(j\omega)$ in equation H.1 is complex, with a frequency-dependent magnitude and phase angle. The transfer function magnitude and phase, for a 2,18 V RMS coil input voltage, are shown in figure H.1.

The DC magnitude is 13,57 $\mu$m/V. The resonance frequency is 375 Hz. The maximum magnitude, at resonance, is 21,88 $\mu$m/V. The ratio between the maximum and DC magnitudes is 1,61. The -3dB bandwidth, i.e. where the magnitude is 70,7% of the DC value, is 482 Hz. The *TF* phase decreases linearly from 0 Hz to approximately 300 Hz. This reduction in phase can be attributed to coil inductance. At 375 Hz, phase decreases more rapidly with frequency. This phase decrease is due to resonance. Above 482 Hz, the actuator is operated in its filtering range, where the slope of the phase is approximately equal to that for frequencies below 300 Hz.

Similar *TF* spectra to figure H.1, exist for the 1,63 V and 1,09 V RMS coil input voltages. These spectra will however not be shown because they correspond almost exactly with the *TF* shown in figure H.1. Instead, the maximum and static magnitudes and their ratio, resonance frequency and -3 dB bandwidth for the three input voltages, are given in table H.1.

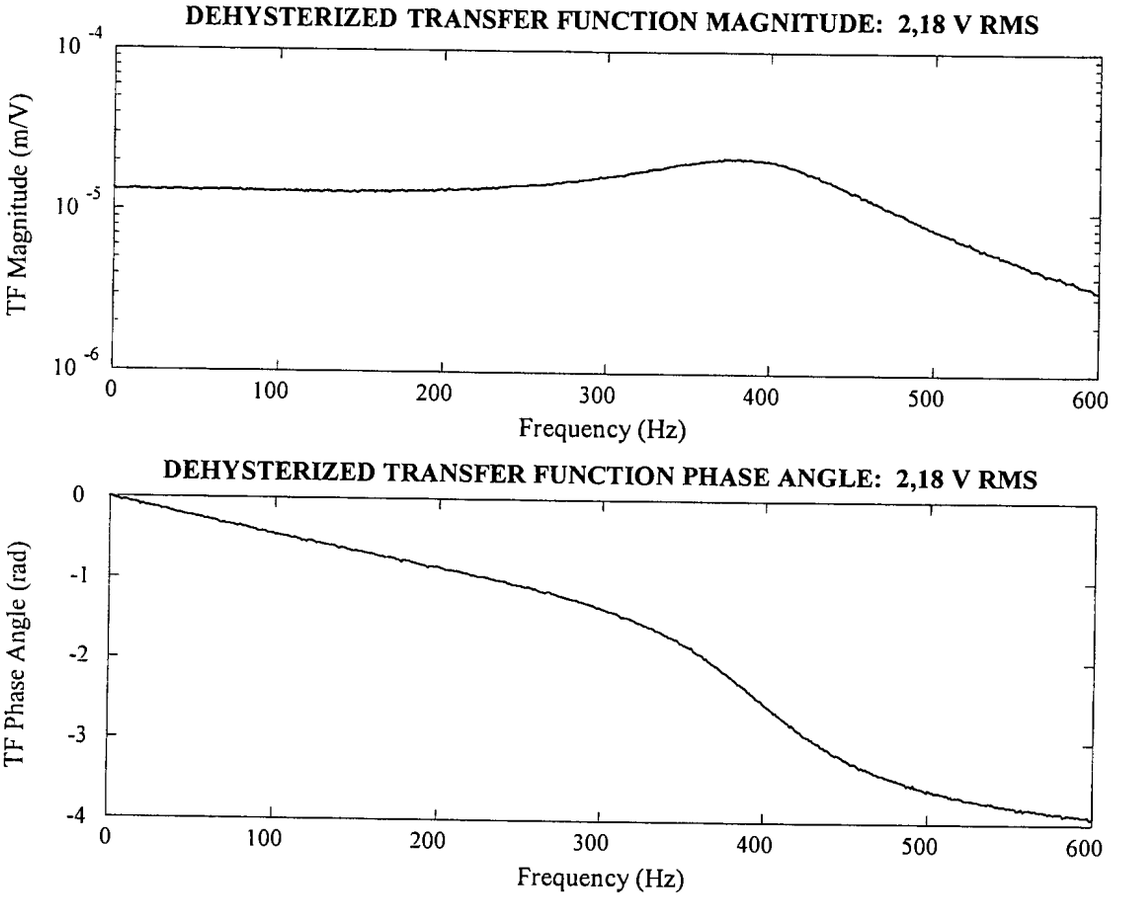


**Figure H.1: Dehysterized transfer function for a 2,18 V RMS coil input voltage**

**Table H.1: Nonlinear dehysterized static & dynamic transfer function parameters**

| Parameter | 2,18 V | 1,63 V | 1,09 V |
|---|---|---|---|
| **Static magnitude ($TF_S$):** | 13,57 $\mu$m/V | 13,68 $\mu$m/V | 13,76 $\mu$m/V |
| **Maximum magnitude ($TF_R$):** | 21,88 $\mu$m/V | 21,95 $\mu$m/V | 21,99 $\mu$m/V |
| **$TF_R/TF_S$:** | 1,61 | 1,60 | 1,60 |
| **Resonance frequency:** | 375 Hz | 375 Hz | 375 Hz |
| **-3 dB bandwidth:** | 483 Hz | 482 Hz | 481 Hz |

It can be seen from table H.1 that the static and dynamic parameters are, for all practical purposes, independent of input voltage. The dehysterized characteristics can therefore be considered linear and can be expressed in terms of constant magnetostrictive and magnetization parameters, i.e. $\mu^\sigma$, $E$, $d^\sigma$ and $d^H$. The conclusion can be drawn that, for the

voltage inputs used in the simulations, the actuator is excited inside its linear range, i.e. outside its saturation range (see figure 2.2.1.6). The linear parameters are calculated in appendix J and their effects on the linear *TF* are discussed.

# Appendix J
# Actuator linear dehysterized characteristics

An equivalent linear *TF* of the actuator, using constant magnetostrictive and magnetization parameters, is obtained in this section. The linear *TF* magnitude and phase are calculated from the average parameters and compared with the nonlinear *TF* magnitude and phase. It is shown that the linear phase spectra closely match the nonlinear spectra, but that the magnitude spectra differ, especially for frequencies above the resonance frequency.

The average values of $\mu^\sigma$, $E$, $d^\sigma$ and $d^H$ are calculated as follows from the nonlinear time-domain simulation outputs:

$$\mu^\sigma = \mu_m^\sigma = \frac{1}{T}\int_{t=0}^{t=T} \mu^\sigma(t)dt \qquad \textbf{(J.1a)}$$

$$E = E_m = \frac{1}{T}\int_{t=0}^{t=T} E(t)dt \qquad \textbf{(J.1b)}$$

$$d^\sigma = d_m^\sigma = \frac{1}{T}\int_{t=0}^{t=T} d^\sigma(t)dt \qquad \textbf{(J.1c)}$$

$$d^H = d_m^H = \frac{1}{T}\int_{t=0}^{t=T} d^H(t)dt \qquad \textbf{(J.1d)}$$

where $t$ is time, $T$ is the maximum time and the subscript $m$ denotes the average value of the particular parameter.

The average parameters for the three coil input voltages, using equations J.1a to J.1d, with $T = 40$ s, are given in table J.1.

**Table J.1: Average linear dehysterized magnetostrictive & magnetization parameters**

| Parameter | 2,18 V RMS | 1,63 V RMS | 1,09 V RMS |
|---|---|---|---|
| Permeability $\mu^\sigma$: | 6,962 $\mu$Tm/A | 6,969 $\mu$Tm/A | 6,977 $\mu$Tm/A |
| Young's modulus $E$: | 23,46 GPa | 23,36 GPa | 23,28 GPa |
| Piezomagnetic cross-coupling constant $d^\sigma$: | 1,088.$10^{-8}$ m/A | 1,089.$10^{-8}$ m/A | 1,09.$10^{-8}$ m/A |
| Strain constant $d^H$: | 1,204.$10^{-8}$ m/A | 1,208.$10^{-8}$ m/A | 1,21.$10^{-8}$ m/A |

The parameters tabled above and the actuator parameters ($m_a$, $G$, $R_c$, $N$, $l_T$ and $A_T$, from table 2.7.3.1), are used to calculate $k_a$ and $\omega_n$ (equations 2.4.22 and 2.4.23) and $L_f$, $cf$ and $L_0$ (equations 2.4.45 to 2.4.47). For the dehysterized characteristics, zero damping is used. The Laplace-domain transfer functions are calculated from equations 2.5.2.1 to 2.5.2.3. The frequency-domain transfer function magnitude and phase angle are calculated from equation 2.5.3.6a and 2.5.3.6b respectively.

The linear dehysterized *TF* magnitude and phase, for a 2,18 V RMS coil input voltage, are shown in figure J.1. For comparison purposes, the nonlinear *TF* magnitude and phase are also shown. It can be seen from figure J.1 that the *TF* phase obtained from the linear average parameters is virtually identical to that obtained from the nonlinear simulations. The linear and nonlinear *TF* magnitudes compare well for frequencies below approximately 300 Hz. However, for frequencies above 300 Hz, the magnitudes differ. The difference increases with an increase in frequency.

The difference in magnitudes can be attributed to the fact that the *TF* calculated from average parameters does not include the effects of superharmonics. The result would be the same if the harmonic balance technique were used. The nonlinear *TF*, on the other hand, was obtained using the 5$^{th}$ order Runge-Kutta method. Using this method, at least one superharmonic for all frequencies, up to 50% of the Nyquist frequency, is included in the output (see section 2.7.1).

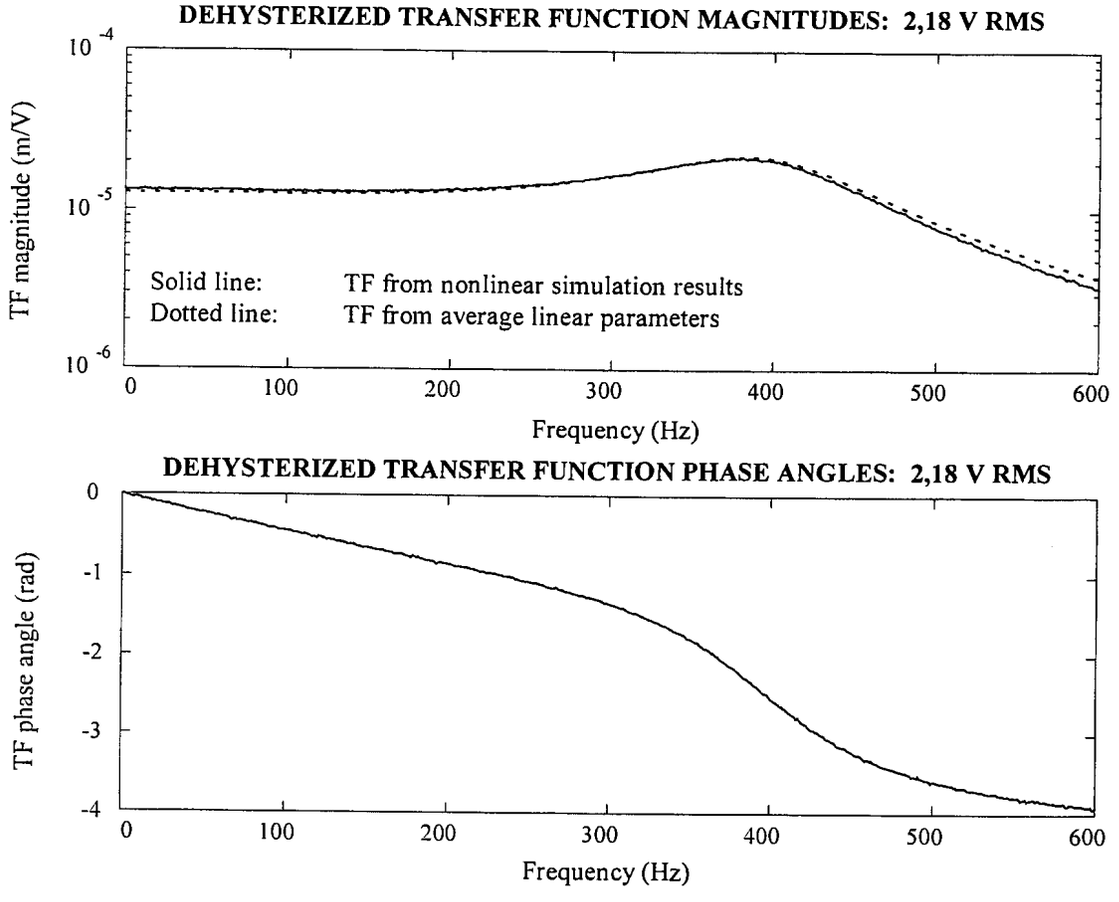


**Figure J.1: Linear and nonlinear dehysterized *TF*'s for a 2,18 V RMS input**

The linear, dehysterized *TF* parameters for an input voltage of 2,18 V RMS, using the average values of $\mu^{\sigma}$, $E$, $d^{\sigma}$ and $d^{H}$ in table J.1, are given in table J.2. For comparison purposes, the nonlinear *TF* parameters, from table H.1, are also given.

**Table J.2: Linear and nonlinear *TF* characteristics for a 2,18 V RMS input**

| Parameter | Nonlinear | Linear |
|---|---|---|
| **Static magnitude ($TF_S$):** | 13,57 $\mu$m/V | 13,00 $\mu$m/V |
| **Maximum magnitude ($TF_R$):** | 21,88 $\mu$m/V | 23,52 $\mu$m/V |
| **$TF_R/TF_S$:** | 1,61 | 1,81 |
| **Resonance frequency:** | 375 Hz | 385 Hz |
| **-3 dB bandwidth:** | 483 Hz | 500 Hz |

A comprehensive list of the linear characteristics, for each input voltage, is given in table J.3.

**Table J.3: Linear characteristics for 2,18 V, 1,63 V and 1,09 V RMS input voltages**

| Parameter | 2,18 V RMS | 1,63 V RMS | 1,09 V RMS |
|---|---|---|---|
| $p_0$ | $1{,}400.10^5$ | $1{,}397.10^5$ | $1{,}392.10^5$ |
| $q_0$ | $1{,}077.10^{10}$ | $1{,}071.10^{10}$ | $1{,}065.10^{10}$ |
| $q_1$ | $7{,}754.10^6$ | $7{,}715.10^6$ | $7{,}683.10^6$ |
| $q_2$ | 2486 | 2482 | 2476 |
| $q_3$ | 1 | 1 | 1 |
| $\mu^\sigma$ | $6{,}962.10^{-6}$ Tm/A | $6{,}969.10^{-6}$ Tm/A | $6{,}977.10^{-6}$ Tm/A |
| $E$ | 23,46 GPa | 23,36 GPa | 23,28 GPa |
| $d^\sigma$ | $1{,}088.10^{-8}$ A/m | $1{,}089.10^{-8}$ A/m | $1{,}090.10^{-8}$ A/m |
| $d^H$ | $1{,}204.10^{-8}$ A/m | $1{,}208.10^{-8}$ A/m | $1{,}210.10^{-8}$ A/m |
| $f_n$ | 331,3 Hz | 330,6 Hz | 330,0 Hz |
| $f_{deff}$ | 397,6 Hz | 396,6 Hz | 395,8 Hz |
| $\zeta_{eff}$ | 15,9% | 15,9% | 15,8% |
| $L_f$ | 2,304 mH | 2,306 mH | 2,309 mH |
| $cf$ | 0,6643 | 0,6640 | 0,6635 |
| $L_o$ | 1,287 mH | 1,289 mH | 1,292 mH |
| $R_c/L_o$ | 395,7 Hz | 395,0 Hz | 394,12 Hz |
| $F_I$ | 27,03 N/A | 27,01 N/A | 26,98 N/A |

Note that the effective damped natural frequency of the actuator *exceeds* the undamped natural frequency. The reason is that $f_n$ is the uncoupled (mechanical) natural frequency of the actuator, as given by equation 2.4.22, while $f_{deff}$ is the imaginary part of the complex pole of the coupled *TF* (see equations 2.6.11 and 2.6.12a).

Table J.3 shows that the dehysterized parameters vary slightly for different RMS inputs. This is however not the case if hysteresis effects are taken into account (see appendix K).

# Appendix K
# Actuator linear characteristics, including hysteresis effects

Actuator linear characteristics, including hysteresis effects, are calculated using the iterative harmonic balance technique. The technique is explained in more detail in section 2.7.2. The permeability $\mu^\sigma$, strain constant $d^H$ and damping coefficient $c$, as well as the static and dynamic parameters, are input voltage- and frequency-dependent. The effects of hysteresis on $E$ and $d^\sigma$ are insignificant in comparison with its effect on $\mu^\sigma$ and $d^H$ (see section 2.3) and are therefore neglected.

Harmonic voltages, whose RMS-values correspond with those of the random voltage inputs used in the time-domain simulations, are used as inputs. This is done to allow a direct comparison between the dehysterized and hysteresis characteristics. For each voltage amplitude and frequency, the field amplitude $H_A$, permeability $\mu^\sigma$, strain constant $d^H$ and damping coefficient $c$, are calculated. The values of $E$ and $d^\sigma$, for the appropriate voltage input, are obtained from table J.3 (see appendix J).

The frequency band is 0,01 Hz to 600 Hz. Frequency resolution varies according to the slope of the magnitude curve with respect to frequency. At low frequency, where the slope is low, a low resolution is used. As the slope increases, resolution is increased.

$\mu^\sigma$, $E$, $d^\sigma$ and $d^H$, together with $m_a$, $G$, $R_c$, $N$, $l_T$ and $A_T$ (from table 2.7.3.1), are used to calculate $k_a$ and $\omega_n$ (equations 2.4.22 and 2.4.23), $L_f$, $cf$ and $L_0$ (equations 2.4.45 to 2.4.47). The dimensionless damping factor $\zeta$ is obtained from equation 2.4.25. The $TF$ numerator and denominator polynomial coefficients are calculated by means of equation 2.5.2.4, table 2.5.2.1 and equations 2.5.2.5. The transfer function magnitude and phase for each frequency are calculated from equation 2.5.3.6a and 2.5.3.6b respectively.

The field strength frequency spectrum for a 2,18 V RMS input is shown in figure K.1. The field amplitude at 0,01 Hz is 17,62 kA/m. From 0,01 Hz to 328 Hz, field amplitude decreases. At 328 Hz, a gap appears in the spectrum, where the iterative harmonic balance technique fails to give convergence. The frequency range of non-convergence is 328 Hz to 332 Hz. The gap is situated at the minimum field amplitude (4156 A/m). For frequencies above 332 Hz, field increases until a local peak is reached at 440 Hz. From 440 Hz to 600 Hz, field amplitude decreases with an increase in frequency.

Similar spectra can be shown for the 1,63 V RMS and 1,09 V RMS inputs. The ranges of non-convergence for these inputs are 327 Hz to 331 Hz and 324 Hz to 331 Hz respectively.

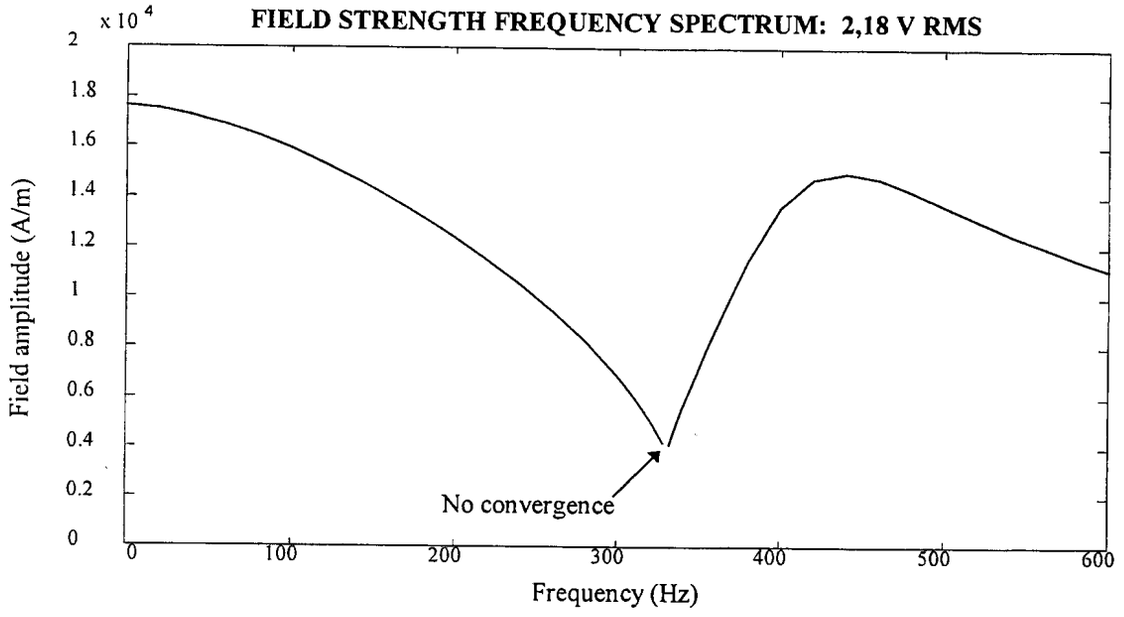


**Figure K.1: Field strength frequency spectrum, including hysteresis: 2,18 V RMS**

The frequency spectrum of permeability, including hysteresis, for a 2,18 V RMS input voltage, is shown in figure K.2. The permeability at 0,01 Hz is 5,57 $\mu$Tm/A. Permeability decreases from 0,01 Hz to 328 Hz, where $\mu^{\sigma}$ is 0,62 $\mu$Tm/A. For frequencies from 328 Hz to 332 Hz, permeability cannot be calculated, due to the convergence problem explained above. Above 332 Hz, permeability increases with frequency until a local peak is reached at 440 Hz. For frequencies above 440 Hz, permeability decreases with an increase in frequency.

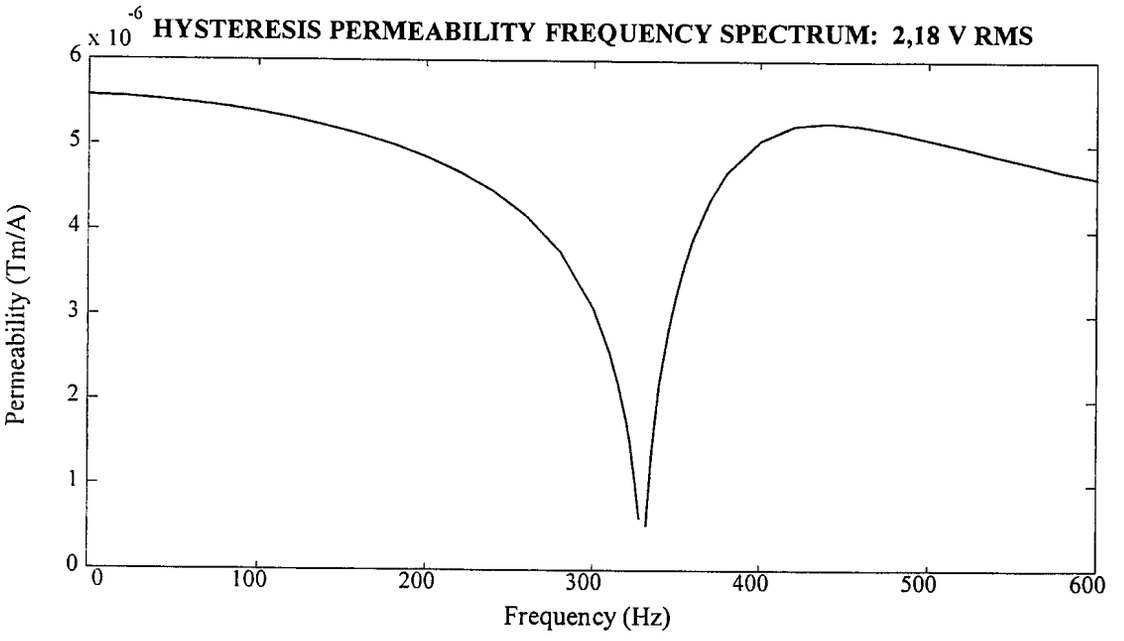


**Figure K.2: Permeability frequency spectrum, including hysteresis: 2,18 V RMS**

The frequency spectrum of the strain constant, including hysteresis, for a 2,18 V RMS input voltage, is shown in figure K.3. The strain constant at 0,01 Hz is $9{,}52.10^{-9}$ m/A. Strain constant decreases from 0,01 Hz to 328 Hz, where $d^H$ is $1{,}27.10^{-9}$ m/A. Above 332 Hz, strain constant increases until a local peak is reached at 440 Hz. For frequencies above 440 Hz, strain constant decreases with an increase in frequency.

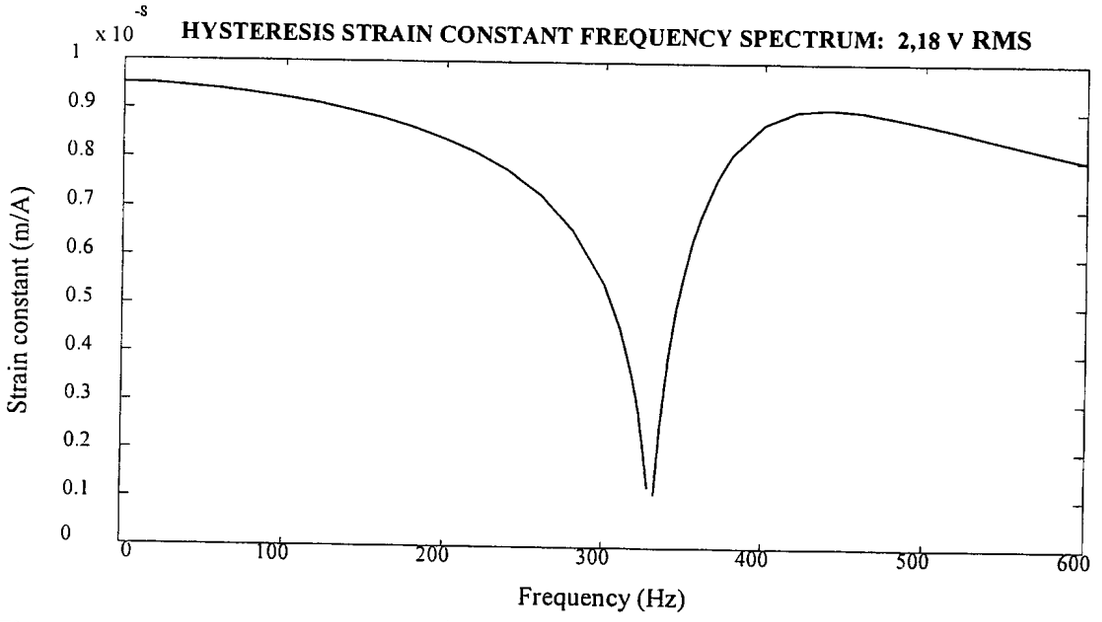


**Figure K.3: Strain constant frequency spectrum, including hysteresis: 2,18 V RMS**

For comparison purposes, the spectra of the strain constants for 1,63 V RMS and 1,09 V RMS inputs are shown together with that of the 2,18 V RMS input (see figure K.4). It can be seen that strain constant increases with an increase in input voltage.

The frequency spectrum of the damping coefficient, for a 2,18 V RMS input voltage, is shown in figure K.5. The damping coefficient at 0,01 Hz is $1{,}31.10^{6}$ Ns/m. A sharp notch appears between 328 Hz and 332 Hz. At the latter frequency, the damping coefficient is 4,59 Ns/m. For a frequency range of 0,01 Hz to approximately 200 Hz, damping coefficient varies hyperbolically with frequency. In this range, the mathematical relationship between frequency and damping coefficient is:

$$c(f) = \frac{13076}{f} \qquad \textbf{(K.1)}$$

where $f$ is frequency and $c$ is damping coefficient.

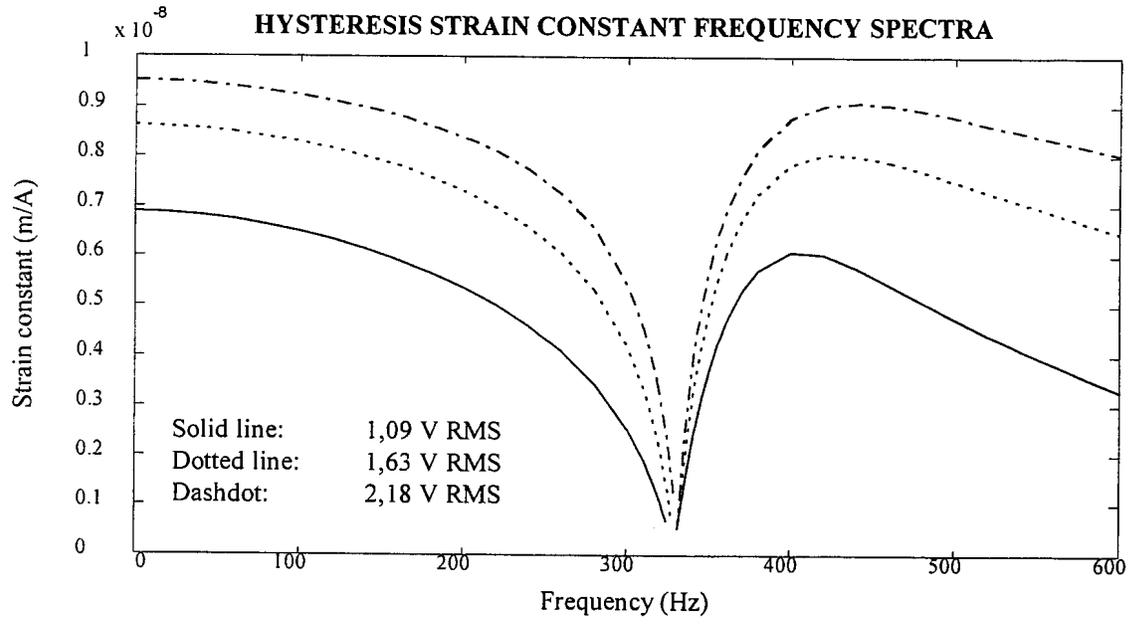


**Figure K.4:** **Strain constant frequency spectra, including hysteresis, for 2,18 V, 1,63 V and 1,09 V RMS coil input voltages**

The hyperbolic relationship between damping coefficient and frequency was discussed in section 2.3, where hysteresis models of Terfenol-D were derived (see also equation 2.3.15). On a logarithmic scale, the damping coefficient characteristic between 0,01 Hz and 200 Hz is a straight line, as shown in figure K.5.

The magnitude and phase of the transfer function for a 2,18 V RMS input, including hysteresis, are shown in figure K.6, together with the dehysterized magnitude and phase.

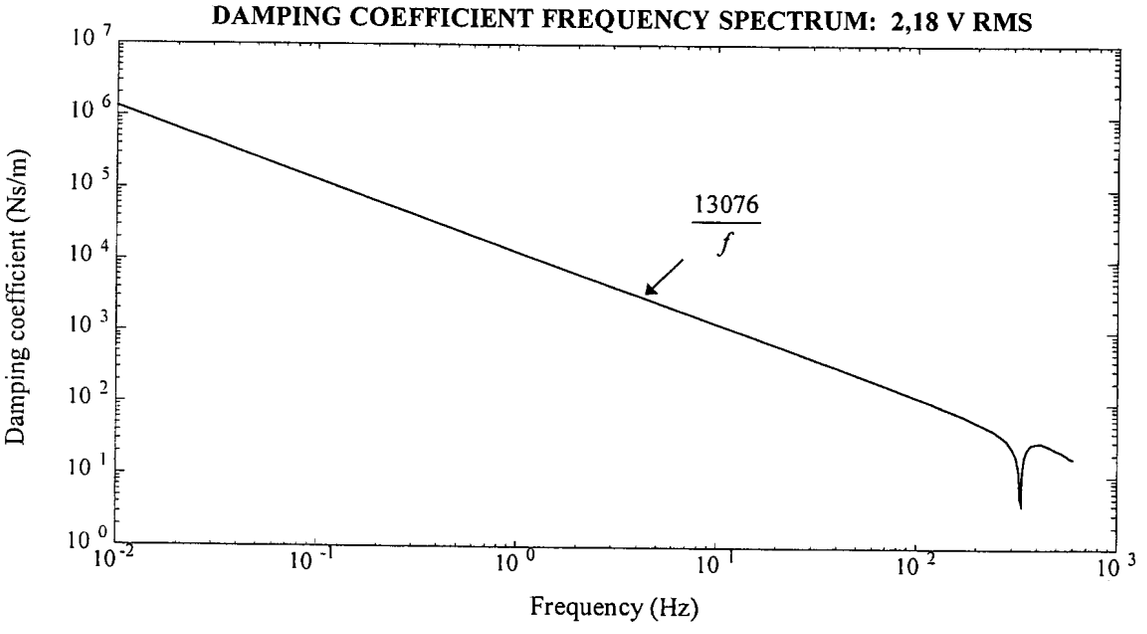


**Figure K.5:** **Damping coefficient frequency spectrum for 2,18 V RMS input**

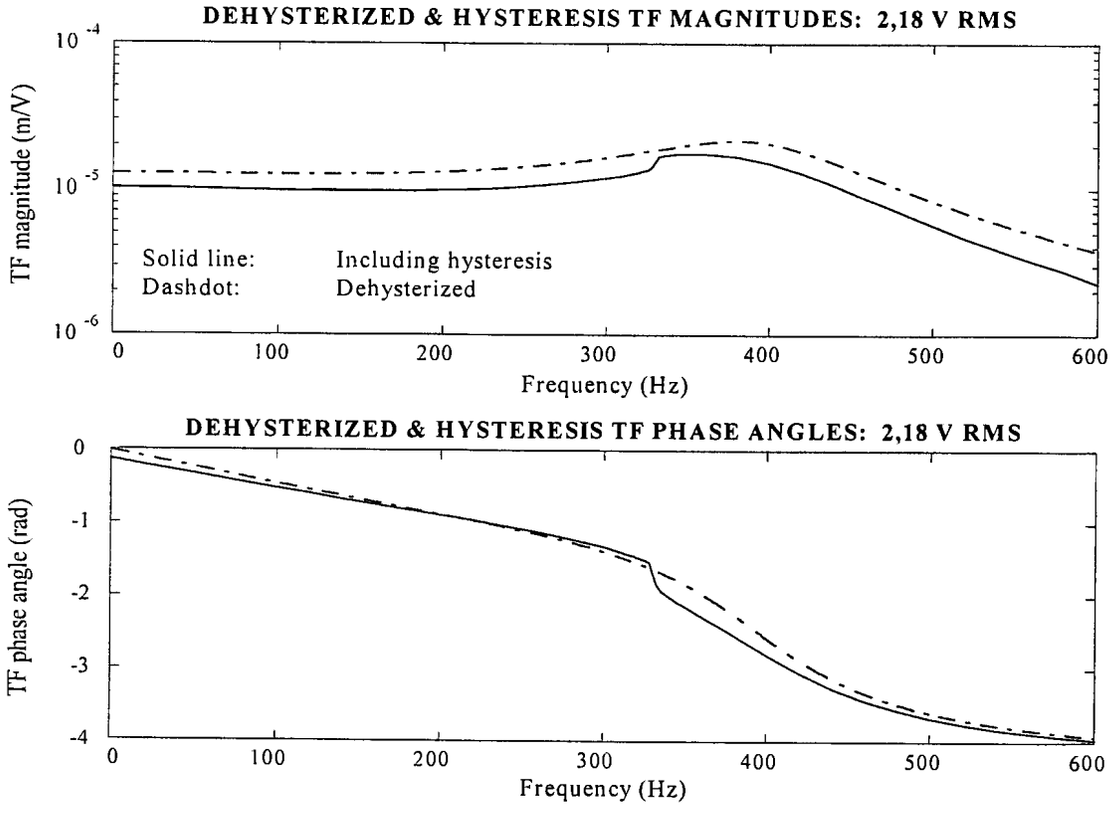


**Figure K.6: Dehysterized and hysteresis transfer functions for a 2,18 V RMS input**

At 0,01 Hz, the magnitude for hysteresis behaviour is 10,2 $\mu$m/V, compared with 13,57 $\mu$m/V for dehysterized behaviour (see table H.1). The resonance frequency and maximum magnitude for the hysteresis *TF* are 355 Hz and 17,7 $\mu$m/V respectively, compared with 375 Hz and 21,88 $\mu$m/V for the dehysterized *TF*. The inclusion of hysteresis effects therefore reduces magnitude at 0,01 Hz by 24,8%, resonance frequency by 5,3% and maximum magnitude by 19,1%.

Magnitude decreases slightly from 0,01 Hz to approximately 190 Hz, which can be attributed to coil inductance. At approximately 250 Hz, magnitude gradually increases with frequency. Between 328 Hz and 332 Hz, magnitude rises sharply with frequency. From 328 Hz to 370 Hz, magnitude is almost constant. Above 370 Hz, a gradual reduction in magnitude sets in. The -3 dB bandwidth is 475 Hz, which is 1,5% lower than in the dehysterized case.

The phase angle displays a peculiar characteristic, especially at low frequencies. At 0,01 Hz, phase is considerably lower that in the dehysterized case. The reason is the extremely high damping coefficient, i.e. $1{,}31.10^6$ Ns/m, at 0,01 Hz (see also figure K.5). This phase characteristic is typical of hysteretic systems.

For frequencies from 0,01 Hz to 328 Hz, the slope of the phase, with respect to frequency, is lower than in the dehysterized case. Between 328 Hz and 332 Hz, phase decreases sharply. At 332 Hz, the phase is considerably lower than in the dehysterized case. Above 332 Hz, a

gradual phase reduction sets in, until 600 Hz, where the phases of the dehysterized and hysteresis *TF's* are approximately equal.

A summary of the most important hysteresis characteristics at 0,01 Hz and resonance, for a 2,18 V RMS input, is given in table K.1.

**Table K.1: Hysteresis characteristics at 0,01 Hz and resonance for a 2,18 V RMS input**

| Parameter | 0,01 Hz | Resonance (355 Hz) |
|---|---|---|
| Field amplitude $H_A$ | 17618 A/m | 7946 A/m |
| Permeability $\mu^\sigma$ | $5{,}57.10^{-6}$ Tm/A | $3{,}63.10^{-6}$ Tm/A |
| Young's modulus $E$ | 23,46 GPa | 23,46 GPa |
| Piezomagnetic cross-coupling constant $d^\sigma$ | $1{,}088.10^{-8}$ m/A | $1{,}088.10^{-8}$ m/A |
| Strain constant $d^H$ | $9{,}522.10^{-9}$ m/A | $6{,}338.10^{-9}$ m/A |
| Damping coefficient $c$ | $1{,}31.10^{6}$ Ns/m | 24,31 Ns/m |
| $TF$ magnitude | 10,2 $\mu$m/V | 17,7 $\mu$m/V |
| $TF$ phase | -0,1263 rad | -2,205 rad |
| Stroke length (17,5 V p-p) | 178,5 $\mu$m | 309,8 $\mu$m |

The transfer function spectra for 1,63 V and 1,09 V RMS inputs are shown in figures K.7 and K.8 respectively. For a 1,63 V RMS input, the magnitude at 0,01 Hz is 9,27 $\mu$m/V, which is 32,2% lower than in the dehysterized case. The maximum magnitude of 17,9 $\mu$m/V occurs at 345 Hz, a reduction of 18,5% in maximum magnitude and 8% in resonance frequency, in comparison with the dehysterized case. The -3 dB bandwidth is 470 Hz, which is 2,5% lower than in the dehysterized case.

For a 1,09 V RMS input, the magnitude at 0,01 Hz is 7,42 $\mu$m/V, which is 46% lower than in the dehysterized case. The maximum magnitude of 18,1 $\mu$m/V occurs at 340 Hz, a reduction of 17,7% in maximum magnitude and 9,3% in resonance frequency, in comparison with the dehysterized case. The -3 dB bandwidth is 445 Hz, which is 7,5% lower than in the dehysterized case.

A graphical comparison between the hysteresis transfer functions for the 2,18 V, 1,63 V and 1,09 V RMS inputs, is shown in figure K.9. The effect of input voltage on the *TF* spectra, as discussed above, is clearly visible. Furthermore, a typical nonlinear softening characteristic is displayed. This is due to the voltage dependence of the strain constant, as shown in figure K.4.

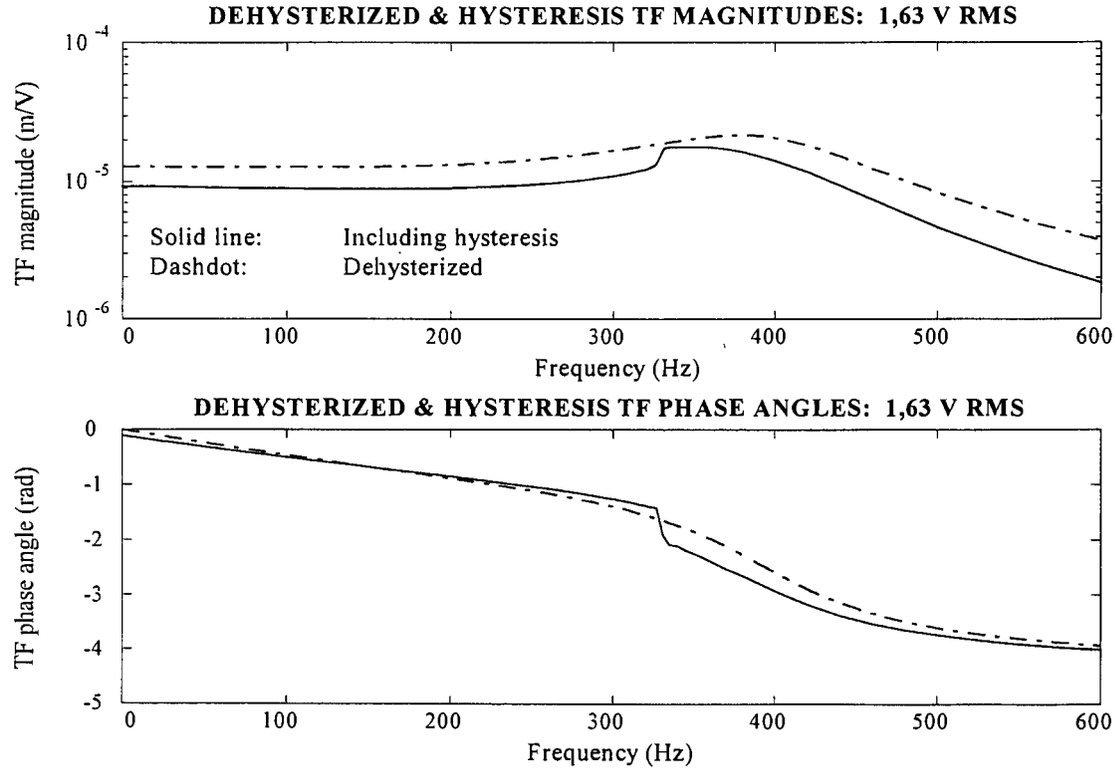


**Figure K.7: Dehysterized and hysteresis transfer functions for a 1,63 V RMS input**

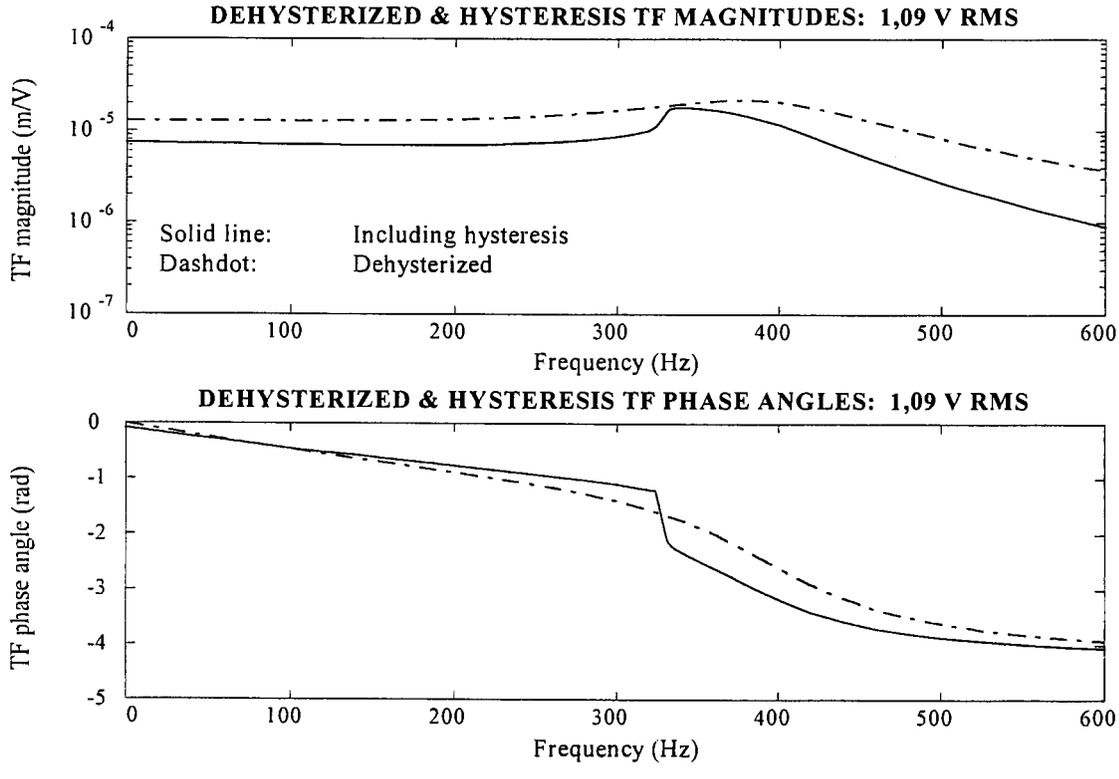


**Figure K.8: Dehysterized and hysteresis transfer functions for a 1,09 V RMS input**

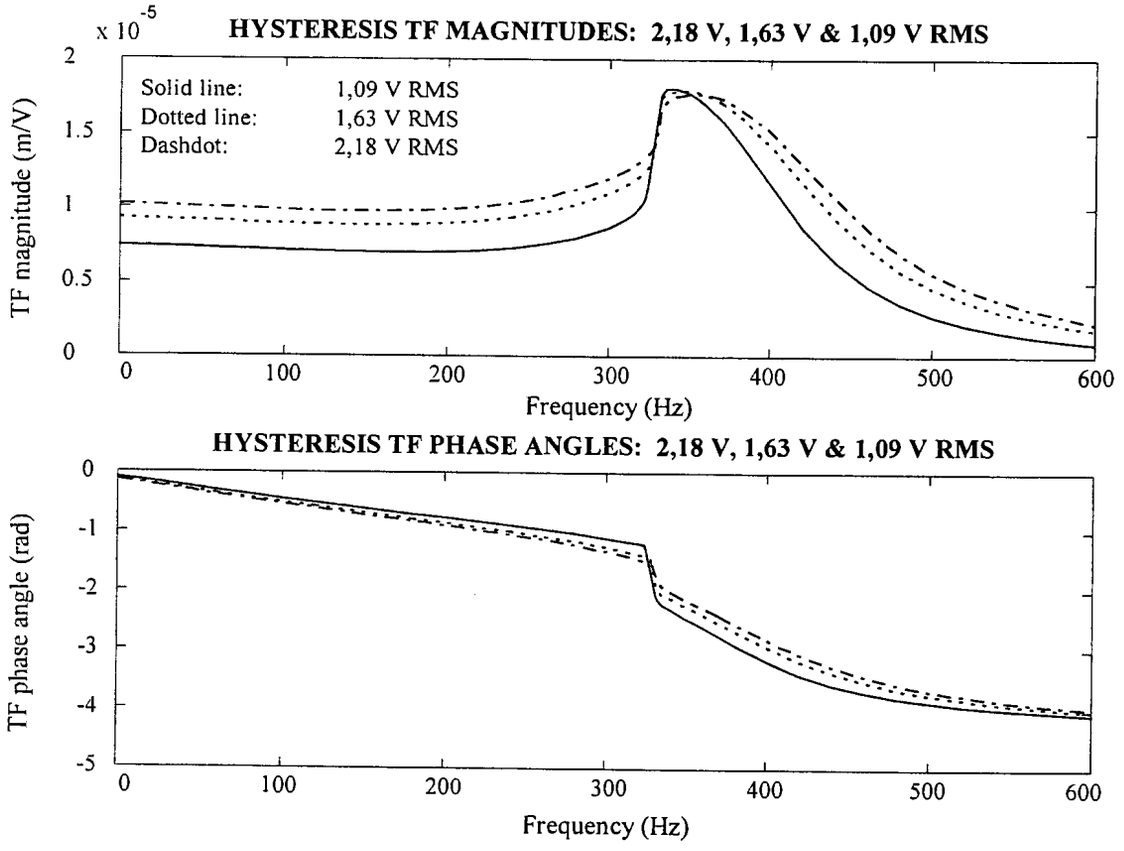


**Figure K.9: Hysteresis transfer functions for 2,18 V, 1,63 V and 1,09 V RMS inputs**

# Appendix L
# Exact separation of variables method

Consider equation 2.8.2.1:

$$\underbrace{\rho_s A_s \frac{\partial^2 w}{\partial t^2}}_{mass\ \ term} + \underbrace{E_s I_s \frac{\partial^4 w}{\partial x^4}}_{stiffness\ \ term} = P \qquad \textbf{(L.1)}$$

Using separation of variables, the exact solution to equation L.1 is expressed as:

$$w(x,t) = \sum_{i=1}^{\infty} \phi_i(x) q_i(t) \qquad \textbf{(L.2)}$$

where $\phi_i(x)$ is the $i$-th normal mode shape of the beam at a position $x$ on the beam and $q_i(t)$ is the $i$-th modal amplitude at time $t$.

The equation of motion for natural behaviour of the beam, from equation L.1, is:

$$\underbrace{\rho_s A_s \frac{\partial^2 w}{\partial t^2}}_{mass\ \ term} + \underbrace{E_s I_s \frac{\partial^4 w}{\partial x^4}}_{stiffness\ \ term} = 0 \qquad \textbf{(L.3)}$$

For natural behaviour, $q_i$ is a harmonic function of time:

$$q_i = \sin \omega_i t \qquad \textbf{(L.4)}$$

where $\omega_i$ is the $i$-th angular natural frequency. The differential equation describing the $i$-th normal mode shape, is

$$\frac{d^4 \Phi_i}{dx^4} - \beta_i^4 \Phi_i = 0 \qquad \textbf{(L.5)}$$

where $\beta_i$ is the $i$-th eigenvalue, given by:

$$\beta_i = \left( \frac{\rho_s A_s}{E_s I_s} \omega_i^2 \right)^{\frac{1}{4}} \qquad \textbf{(L.6)}$$

The general solution of equation L.5 is:

$$\Phi_i(x) = A_i \cos \beta_i x + B_i \sin \beta_i x + C_i \cosh \beta_i x + D_i \sinh \beta_i x \qquad \textbf{(L.7)}$$

The values of $\beta_i$ depend on the beam supports. Tabulated values of $\beta_i$ for cantilever, simply-supported, clamped-clamped and clamped-free beams, are given by Harris [1988], Thomson [1993] and Tse et al [1978]. In most of these references, only the first four to six eigenvalues are given.

# Appendix M
# Derivation of system state-space model

The forced modal equation of motion of the system (equation 2.8.5.1) is:

$$M^*\ddot{q} + C^*\dot{q} + K^*q = Q \tag{M.1}$$

where $M^*$, $C^*$ and $K^*$ are normal mode mass, damping and stiffness matrices respectively and $Q$ is the modal excitation force vector, given by:

$$Q = \int_{x=0}^{x=l} \Phi^T(x) F(x,t)\,dx \tag{M.2}$$

$F$ is the excitation force at any point $x$, at time $t$:

$$F = F(x,t) \tag{M.3}$$

In a more concise matrix form, equation M.2 can be written as:

$$Q = \Phi^T F \tag{M.4}$$

The coordinates $x_{a1}$ and $x_{a2}$ of the actuator attachment points are:

$$x_{a1} = 0 \tag{M.5a}$$
$$x_{a2} = l \tag{M.5b}$$

Substitution of equations M.5 into equation M.2 and writing the resulting equation in the form of equation M.4, gives:

$$Q = \left[\Phi^T(0) \quad \Phi^T(l)\right] \begin{Bmatrix} F_{a1} \\ F_{a2} \end{Bmatrix} \tag{M.6}$$

$F_{a1}$ and $F_{a2}$ are the actuator excitation forces, which (from section 2.4) can be expressed as:

$$F_{a1} = \frac{A_T E N d^H}{G l_T} I_1 \tag{M.7a}$$

$$F_{a2} = \frac{A_T E N d^H}{G l_T} I_2 \tag{M.7b}$$

where $I_1$ and $I_2$ are the two actuator coil currents.

The modal equation of motion is obtained by substitution of equations M.7a and M.7b into

equation M.6 and by subsequent substitution of the resulting equation into equation M.1:

$$\ddot{q} + 2Z\Omega\dot{q} + \Omega^2 q = \frac{A_T E N d^H}{G l_T} M^{*-1}\left[\Phi^T(0) \quad \Phi^T(l)\right]\begin{Bmatrix} I_1 \\ I_2 \end{Bmatrix} \tag{M.8}$$

where Z is the diagonal modal damping matrix, whose elements are given as follows in terms of the damping coefficient $C_{ii}^*$, mass $M_{ii}^*$ and natural frequency $\Omega_{ii}$ of the *i*-th normal mode:

$$Z_{ii} = \frac{C_{ii}^*}{2M_{ii}^*\Omega_{ii}} \tag{M.9}$$

The coil current equations are:

$$\dot{I}_1 = -\frac{A_T E N d^\sigma}{G l_T L_0}\dot{w}(0,t) - \frac{R_c}{L_0} I_1 + \frac{1}{L_0} V_1 \tag{M.10a}$$

$$\dot{I}_2 = -\frac{A_T E N d^\sigma}{G l_T L_0}\dot{w}(l,t) - \frac{R_c}{L_0} I_2 + \frac{1}{L_0} V_2 \tag{M.10b}$$

where $V_1$ and $V_2$ are the coil input voltages and $\dot{w}(0,t)$ and $\dot{w}(l,t)$ are the vertical translational speeds at the actuator attachment points, given by:

$$\dot{w}(0,t) = \Phi(0)\dot{q}(t) \tag{M.11a}$$

$$\dot{w}(l,t) = \Phi(l)\dot{q}(t) \tag{M.11b}$$

Substitution of equations M.11 into equations M.10 gives:

$$\begin{Bmatrix} \dot{I}_1 \\ \dot{I}_2 \end{Bmatrix} = -\frac{A_T E N d^\sigma}{G l_T L_0}\begin{bmatrix} \Phi(0) \\ \Phi(l) \end{bmatrix}\dot{q} - \frac{R_c}{L_0}\begin{bmatrix} 1 & 0 \\ 0 & 1 \end{bmatrix}\begin{Bmatrix} I_1 \\ I_2 \end{Bmatrix} + \frac{1}{L_0}\begin{bmatrix} 1 & 0 \\ 0 & 1 \end{bmatrix}\begin{Bmatrix} V_1 \\ V_2 \end{Bmatrix} \tag{M.12}$$

Combining equations M.8 and M.12 and writing the resulting system of equations in state-space form, gives:

$$\begin{Bmatrix} \{\dot{q}\} \\ \{\ddot{q}\} \\ \begin{Bmatrix} \dot{I}_1 \\ \dot{I}_2 \end{Bmatrix} \end{Bmatrix} = \begin{bmatrix} 0 & I & 0 \\ -\Omega^2 & -2Z\Omega & \frac{A_T E N d^H}{G l_T} M^{*-1}\left[\Phi^T(0) \quad \Phi^T(l)\right] \\ 0 & -\frac{A_T E N d^\sigma}{G l_T L_0}\begin{bmatrix} \Phi(0) \\ \Phi(l) \end{bmatrix} & -\frac{R_c}{L_0}\begin{bmatrix} 1 & 0 \\ 0 & 1 \end{bmatrix} \end{bmatrix}\begin{Bmatrix} \{q\} \\ \{\dot{q}\} \\ \begin{Bmatrix} I_1 \\ I_2 \end{Bmatrix} \end{Bmatrix} + \begin{bmatrix} 0 & 0 \\ 0 & 0 \\ \frac{1}{L_0}\begin{bmatrix} 1 & 0 \\ 0 & 1 \end{bmatrix} \end{bmatrix}\begin{Bmatrix} V_1 \\ V_2 \end{Bmatrix} \tag{M.13}$$

The outputs can be chosen to be the translational and rotational displacements of the instrument. The rotational displacement, which is equal to the LOS angle $\theta$, is of prime importance. The translational displacement is not required, since it does not determine LOS accuracy. Two other outputs, which are of importance, are the vertical displacements $w_1$ and $w_2$ at the instrument attachment points $x_1$ and $x_2$ on the support structure. The difference between these two outputs, divided by the instrument length, gives the LOS angle $\theta$.

Displacement $w_1$ is given by:

$$w_1 = w(x_1, t) = \Phi(x_1) q(t) \tag{M.14}$$

Displacement $w_2$ is given by:

$$w_2 = w(x_2, t) = \Phi(x_2) q(t) \tag{M.15}$$

The angular displacement $\theta$ of the optical instrument is:

$$\theta(t) = \frac{1}{l}(w_2 - w_1) \tag{M.16}$$

Substitution of equations M.14 and M.15 into equation M.16 gives:

$$\theta(t) = \frac{1}{l}\left(\Phi(x_2) - \Phi(x_1)\right) q(t) \tag{M.17}$$

Equations M.14, M.15 and M.17 are combined as follows in one output equation:

$$\begin{Bmatrix} w_1 \\ w_2 \\ \theta \end{Bmatrix} = \begin{bmatrix} \{\Phi(x_1)\} & \{0\} & \{0 \quad 0\} \\ \{\Phi(x_2)\} & \{0\} & \{0 \quad 0\} \\ \left\{\frac{1}{l}\left(\Phi(x_2) - \Phi(x_1)\right)\right\} & \{0\} & \{0 \quad 0\} \end{bmatrix} \begin{Bmatrix} \{q\} \\ \{\dot{q}\} \\ \begin{Bmatrix} I_1 \\ I_2 \end{Bmatrix} \end{Bmatrix} \tag{M.18}$$

# Appendix N
# Derivation of the complex Laplace-domain transfer function of a hydraulically-gained magnetostrictive actuator

A hydraulically-gained Terfenol-D actuator is schematically shown in figure N.1. Its equivalent mechanical model is shown in figure N.2.

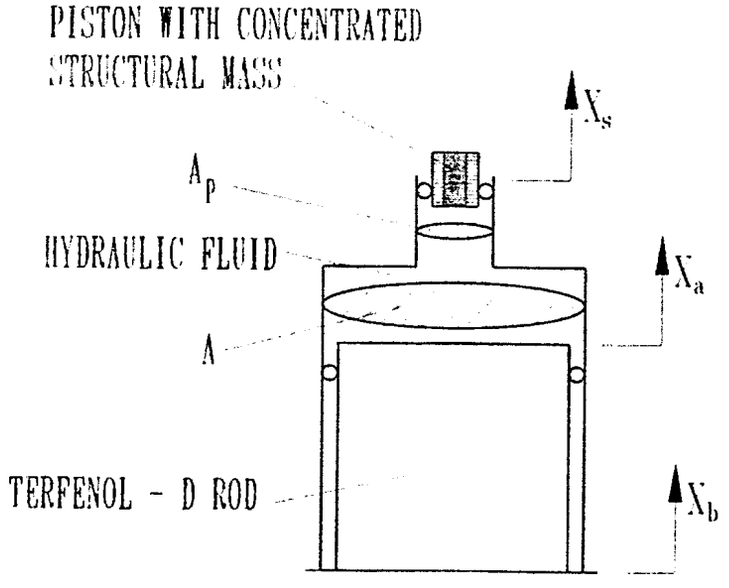


**Figure N.1: Hydraulically-gained magnetostrictive actuator**

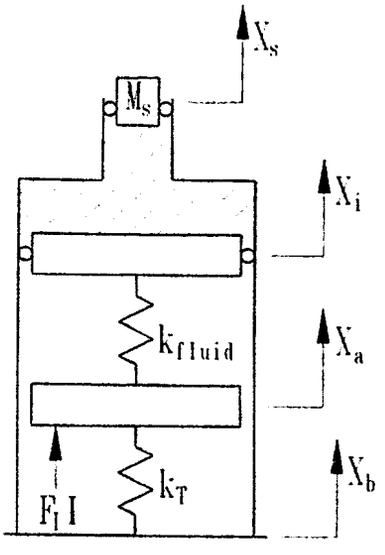


**Figure N2: Equivalent mechanical model of the hydraulically-gained actuator**

The derivation that follows, will be done for a static base, i.e. $x_b = 0$.

## Bulk modulus and equivalent linear liquid stiffness

The bulk modulus $K_B$ of a fluid is defined as the ratio of the change in pressure $dP$, to the change in volume $dV$ per unit volume $V$:

$$K_B = \frac{dP}{\left(\frac{dV}{V}\right)} \tag{N.1}$$

which gives:

$$dP = \frac{K_B}{V} dV \tag{N.2}$$

Multiplication of equation N.2 with the Terfenol-D rod cross-sectional area $A$ gives:

$$AdP = \frac{AK_B}{V} dV \tag{N.3}$$

The infinitesimal change in the force transmitted by the fluid $dF_{fluid}$ is given by:

$$dF_{fluid} = AdP \tag{N.4}$$

The infinitesimal change in fluid volume is given by:

$$dV = Ad\left(x_a - x_i\right) \tag{N.5}$$

Substitution of equations N.4 and N.5 into equation N.3 and rewriting the resulting equation gives:

$$\frac{dF_{fluid}}{d\left(x_a - x_i\right)} = \frac{A^2 K_B}{V} \tag{N.6}$$

It can be seen from equation N.6 that the rate of change of the force transmitted by the fluid, with respect to the deflection of the rod, is directly proportional to the rod area squared, directly proportional to the fluid bulk modulus and inversely proportional to the fluid volume. $A$ and $K_B$ are constant, while $V$ is not. Equation N.6 is therefore nonlinear. In order to obtain a linear force-deflection characteristic, equation N.6 must be linearized. This is done below.

During excitation of the actuator, the fluid volume will contain a DC, or reference component $V_{ref}$ and a fluctuating component $\Delta V$:

$$V = V_{ref} + \Delta V \tag{N.7}$$

Substitution of equation N.7 into equation N.6 gives:

$$\frac{dF_{fluid}}{d(x_a - x_i)} = \frac{A^2 K_\beta}{V_{ref} + \Delta V} \tag{N.8}$$

Dividing both the numerator and denominator of the right hand side of equation N.8 by $V_{ref}$ gives:

$$\frac{dF_{fluid}}{d(x_a - x_i)} = \frac{\frac{A^2 K_\beta}{V_{ref}}}{1 + \frac{\Delta V}{V_{ref}}} \tag{N.9}$$

Most hydraulic fluids have high bulk moduli. $\Delta V/V_{ref}$ is therefore relatively small for most hydraulic fluids, so that the numerator on the right hand side of equation N.9 can be approximated by:

$$1 + \frac{\Delta V}{V_{ref}} \approx 1 \tag{N.10}$$

Substitution of equation N.10 into equation N.9 gives:

$$\frac{dF_{fluid}}{d(x_a - x_i)} = \frac{A^2 K_\beta}{V_{ref}} \tag{N.11}$$

It can be seen from equation N.11 that the equivalent linear liquid stiffness $k_{fluid}$ is given by:

$$k_{fluid} = \frac{A^2 K_\beta}{V_{ref}} \tag{N.12}$$

## Deflection of the Terfenol-D rod

Consider figure N.2. The deflection $x_a$ of the rod is determined by the force balance equation:

$$k_{fluid}(x_i - x_a) - k_T x_a + F_I I = 0 \tag{N.13}$$

where $I$ is the coil current, $F_I$ is the force per unit current and $k_T$ is the rod stiffness. $F_I$ and $k_T$ are respectively given by:

$$F_I = \frac{AENd^H}{l_T} \tag{N.14a}$$

$$k_T = \frac{AE}{l_T} \tag{N.14b}$$

Rewriting equation N.13 gives:

$$x_a = \frac{k_{fluid}}{k_{fluid} + k_T} x_i + \frac{F_l}{k_{fluid} + k_T} I \qquad \textbf{(N.15)}$$

The displacement gain is given as follows in terms of $x_s$ and $x_i$:

$$G = \frac{x_s}{x_i} \qquad \textbf{(N.16)}$$

Substitution of equation N.16 into equation N.15 gives the deflection of the rod as follows in terms of $x_s$ and $I$:

$$x_a = \frac{k_{fluid}}{k_{fluid} + k_T} \frac{x_s}{G} + \frac{F_l}{k_{fluid} + k_T} I \qquad \textbf{(N.17)}$$

## Equation of motion

The equation of motion of the piston is:

$$\ddot{x}_s = \frac{PA_p}{m_s} + \ddot{x}_i \qquad \textbf{(N.18)}$$

where $P$ is the fluid pressure and $A_p$ is the piston cross-sectional area.

The displacement gain factor, in terms of the piston and rod areas, is given by:

$$G = \frac{A}{A_p} \qquad \textbf{(N.19)}$$

Substitution of equation N.19 into equation N.18 gives:

$$\ddot{x}_s = \frac{PA}{m_s G} + \ddot{x}_i \qquad \textbf{(N.20)}$$

Substitution of equation N.16 into equation N.20 and simplification of the resulting equation gives:

$$\ddot{x}_s = \frac{PA}{m_s (G - 1)} \qquad \textbf{(N.21)}$$

The force exerted by the rod on the fluid, is given by:

$$PA = k_{fluid} (x_a - x_i) \qquad \textbf{(N.22)}$$

Substitution of equation N.22 into equation N.21 gives:

$$\ddot{x}_s = \frac{k_{fluid}}{m_s(G-1)}(x_a - x_i) \tag{N.23}$$

Substitution of equation N.16 into equation N.23 and simplification of the resulting equation gives:

$$\ddot{x}_s + \frac{k_{fluid}}{m_s G(G-1)} x_s = \frac{k_{fluid}}{m_s(G-1)} x_a \tag{N.24}$$

Substitution of equation N.17 into equation N.24 gives:

$$\ddot{x}_s + \frac{k_{fluid}}{m_s G(G-1)} x_s = \frac{k_{fluid}}{m_s(G-1)}\left(\frac{k_{fluid}}{k_{fluid}+k_T}\frac{x_s}{G} + \frac{F_l}{k_{fluid}+k_T} I\right) \tag{N.25}$$

Collecting terms containing $x_s$ on the left hand side gives:

$$\ddot{x}_s + \frac{k_{fluid}}{m_s G(G-1)}\left(1 - \frac{k_{fluid}}{k_{fluid}+k_T}\right) x_s = \frac{F_l}{m_s(G-1)}\left(\frac{k_{fluid}}{k_{fluid}+k_T}\right) I \tag{N.26}$$

Simplification of equation N.26 gives the equation of motion as follows in terms of $x_s$ and $I$:

$$\ddot{x}_s + \frac{k_T}{m_s G(G-1)}\left(\frac{k_{fluid}}{k_{fluid}+k_T}\right) x_s = \frac{F_l}{m_s(G-1)}\left(\frac{k_{fluid}}{k_{fluid}+k_T}\right) I \tag{N.27}$$

## Coil current equation

The coil current equation of an ungained magnetostrictive actuator is given by:

$$\dot{I} = -\frac{AENd^{\sigma}}{l_T L_0}\dot{x}_a - \frac{R_c}{L_0} I + \frac{1}{L_0} V \tag{N.28}$$

Substitution of equation N.17 into equation N.28 gives:

$$\dot{I} = -\frac{AENd^{\sigma}}{l_T L_0}\left(\frac{k_{fluid}}{k_{fluid}+k_T}\frac{\dot{x}_s}{G} + \frac{F_l}{k_{fluid}+k_T}\dot{I}\right) - \frac{R_c}{L_0} I + \frac{1}{L_0} V \tag{N.29}$$

Collecting terms containing $\dot{I}$ on the left hand side gives:

$$\left[1+\left(\frac{k_T}{k_{fluid}+k_T}\right)\frac{F_I N d^\sigma}{L_0}\right]\dot{I}=-\left(\frac{k_{fluid}}{k_{fluid}+k_T}\right)\frac{k_T N d^\sigma}{G L_0}\dot{x}_s-\frac{R_c}{L_0}I+\frac{1}{L_0}V \qquad \textbf{(N.30)}$$

The term $k_T/\left(k_{fluid}+k_T\right)$ is expressed as:

$$\frac{k_T}{k_{fluid}+k_T}=1-\frac{k_{fluid}}{k_{fluid}+k_T} \qquad \textbf{(N.31)}$$

Substitution of equation N.31 into equation N.30 gives the coil current equation as follows in terms of $x_s$ and $I$:

$$\left[1+\left(1-\frac{k_{fluid}}{k_{fluid}+k_T}\right)\frac{F_I N d^\sigma}{L_0}\right]\dot{I}=-\left(\frac{k_{fluid}}{k_{fluid}+k_T}\right)\frac{k_T N d^\sigma}{G L_0}\dot{x}_s-\frac{R_c}{L_0}I+\frac{1}{L_0}V \qquad \textbf{(N.32)}$$

## State-space equations

The equation of motion (N.27) and coil current equation (N.32) are simplified by defining the following two constant parameters $\alpha$ and $\beta$:

$$\alpha=\frac{k_{fluid}}{k_{fluid}+k_T} \qquad \textbf{(N.33a)}$$

$$\beta=1+(1-\alpha)\frac{F_I N d^\sigma}{L_0} \qquad \textbf{(N.33b)}$$

Substitution of equation N.33a into equation N.27 gives the equation of motion as:

$$\ddot{x}_s+\alpha\frac{k_T}{m_s G(G-1)}x_s=\alpha\frac{F_I}{m_s(G-1)}I \qquad \textbf{(N.34)}$$

Substitution of equations N.33 into equation N.32 and dividing both sides of the resulting equation by $\beta$ gives the coil current equation as:

$$\dot{I}=-\frac{\alpha}{\beta}\frac{k_T N d^\sigma}{G L_0}\dot{x}_s-\frac{R_c}{\beta L_0}I+\frac{1}{\beta L_0}V \qquad \textbf{(N.35)}$$

The equation of motion (N.34) and coil current equation (N.35) are combined into a single set of state-space equations, in the following familiar form:

$$\dot{x} = Ax + Bu \tag{N.36a}$$
$$y = Cx + Du \tag{N.36b}$$

where

$$x = \left\{x_s, \quad \dot{x}_s, \quad I\right\}^T \tag{N.37}$$

is the state vector,

$$u = V \tag{N.38}$$

is the coil voltage input,

$$y = x_s \tag{N.39}$$

is the actuator displacement output,

$$A = \begin{bmatrix} 0 & 1 & 0 \\ -\alpha \dfrac{k_T}{m_s G(G-1)} & 0 & \alpha \dfrac{F_l}{m_s(G-1)} \\ 0 & -\dfrac{\alpha}{\beta}\dfrac{k_T N d^{\sigma}}{G L_0} & -\dfrac{1}{\beta}\dfrac{R_c}{L_0} \end{bmatrix} \tag{N.40}$$

is the coefficient matrix,

$$B = \begin{bmatrix} 0 \\ 0 \\ \dfrac{1}{\beta L_0} \end{bmatrix}^T \tag{N.41}$$

is the driving matrix,

$$C = \begin{bmatrix} 1 & 0 & 0 \end{bmatrix} \tag{N.42}$$

is the output matrix and

$$D = 0 \tag{N.43}$$

is the transmission matrix.

### Coil voltage to displacement *TF*

The coil voltage input to displacement output *TF* is obtained from:

$$\frac{X_s(s)}{U(s)} = C[sI - A]^{-1} B + D \qquad \textbf{(N.44)}$$

Substitution of equations N.40 to N.43 into equation N.44, and using the relationships for $k_T$ and $F_l$ in equations N.14, gives the *TF* as:

$$\frac{X_s(s)}{V(s)} = \frac{\dfrac{\alpha}{\beta}\dfrac{AENd^H}{m_s(G-1)l_T L_0}}{s^3 + \dfrac{1}{\beta}\dfrac{R_c}{L_0}s^2 + \left[\alpha\dfrac{AE}{m_s G(G-1)l_T} + \dfrac{\alpha^2}{\beta}\left(\dfrac{AEN}{l_T}\right)^2 \dfrac{d^\sigma d^H}{m_s G(G-1)L_0}\right]s + \dfrac{\alpha}{\beta}\dfrac{AE}{m_s G(G-1)l_T}\dfrac{R_c}{L_0}} \qquad \textbf{(N.45)}$$

# Appendix P
# Displacement gain factor for elliptical gain mechanism

Consider figure 3.4.1.4. The undeformed lengths of the major and minor axes of the ellipse are given by $b$ and $a$, respectively. The displacement gain factor $G$ is the ratio of the change in length $\Delta a$ of the minor axis, to the change in length $\Delta b$ of the major axis:

$$G = \frac{\Delta a}{\Delta b} \tag{P.1}$$

It is however more convenient to obtain an equation for the gain factor in terms of the change in length of the major axis only, since this will make it possible to obtain the output displacement of the gain mechanism for a given input displacement. The derivation of this equation is done as follows. Exact and approximate equations for the perimeter of an ellipse are given and compared. It will be shown that the approximate equation is reasonably accurate for $a/b$ ratios ranging from 0,1 to 1. The approximate equation is then used to derive an expression for $\Delta a$ in terms of $a$, $b$ and $\Delta b$. The latter equation is substituted into equation P.1 to give the gain factor.

The exact equation for the perimeter of an ellipse, from Spiegel [1968], is:

$$P_e = 4b \int_0^{\pi/2} \sqrt{1 - k^2 \sin^2 \theta}\, d\theta \tag{P.2}$$

where $P_e$ is the perimeter, $\theta$ is a dummy variable, which ranges from zero to the included angle between the major and minor axes, i.e. $\pi/2$, and $k$ is a dimensionless constant, which depends on the lengths of the major and minor axes:

$$k = \frac{\sqrt{b^2 - a^2}}{b} \tag{P.3}$$

Division of equation P.2 by $b$, gives the ratio of the exact perimeter, to the length of the major axis:

$$\frac{P_e}{b} = 4 \int_0^{\pi/2} \sqrt{1 - k^2 \sin^2 \theta}\, d\theta \tag{P.4}$$

The integral in equation P.4 is an incomplete elliptical integral of the second kind and does not have a closed-form solution. The solution can be obtained numerically.

As an alternative, the following approximate equation can be used [Spiegel, 1968]:

$$P_e \approx 2\pi \sqrt{\frac{1}{2}\left(a^2 + b^2\right)} \tag{P.5}$$

From equation P.5, the ratio of the approximate perimeter to the length of the major axis, is obtained as:

$$\frac{P_e}{b} \approx 2\pi\sqrt{\frac{1}{2}\left[\left(\frac{a}{b}\right)^2 + 1\right]} \qquad \textbf{(P.6)}$$

The approximate and exact $P_e/b$ ratios, for $a/b$ ratios from 0,1 to 1, together with the percentage error of the approximate $P_e/b$ ratio, are given in table P.1.

**Table P.1: Approximate and exact $P_e/b$ ratios for different $a/b$ ratios**

| $a/b$ | Approximate $P_e/b$ (Equation P.6) | Exact $P_e/b$ (Equation P.4) | % Error |
|---|---|---|---|
| 0,10 | 4,4650 | 4,0574 | 10,05 |
| 0,20 | 4,5309 | 4,2052 | 7,74 |
| 0,30 | 4,6385 | 4,3910 | 5,64 |
| 0,40 | 4,7851 | 4,5993 | 4,04 |
| 0,50 | 4,9673 | 4,8444 | 2,54 |
| 0,60 | 5,1812 | 5,1065 | 1,46 |
| 0,70 | 5,4232 | 5,3817 | 0,77 |
| 0,80 | 5,6897 | 5,6725 | 0,30 |
| 0,90 | 5,9773 | 5,9732 | 0,07 |
| 1,00 (circle) | 6,2832 | 6,2832 | 0,00 |

It can be seen from table P.1 that the aproximate $P_e/b$ ratio, as obtained from equation P.6, is acceptably accurate for the given range of $a/b$ ratios.

Equation P.6 is subsequently used to derive an equation for $G$ in terms of $a$, $b$ and $\Delta b$. It is assumed that the perimeter $P_e$ stays constant, irrepective of $\Delta b$.

Replacing the approximate equation P.6 with an equation, squaring both sides, and rewriting gives:

$$\frac{P_e^2}{2\pi^2} = a^2 + b^2 \qquad \textbf{(P.7)}$$

For a constant perimeter, $b$ can be increased to $b+\Delta b$, and $a$ can be simultaneously decreased to $a-\Delta a$, without affecting the left hand side of equation P.7. Replacing $a$ with $a-\Delta a$ and $b$ with $b+\Delta b$ in equation P.7, gives:

$$\frac{P_e^2}{2\pi^2} = (a - \Delta a)^2 + (b + \Delta b)^2 \qquad \textbf{(P.8)}$$

Equations P.7 and P.8 are equal, therefore:

$$(a-\Delta a)^2+(b+\Delta b)^2=a^2+b^2 \qquad \textbf{(P.9)}$$

Simplification of equation P.9 gives the following quadratic equation in $\Delta a$:

$$(\Delta a)^2-2a(\Delta a)+\left[2b\Delta b+(\Delta b)^2\right]=0 \qquad \textbf{(P.10)}$$

The roots of equation P.10 are:

$$\Delta a=a\pm\sqrt{a^2-2b\Delta b+(\Delta b)^2} \qquad \textbf{(P.11)}$$

Rejection of the largest root in equation P.11 gives $\Delta a$ as follows in terms of $a$, $b$ and $\Delta b$:

$$\Delta a=a-\sqrt{a^2-2b\Delta b+(\Delta b)^2} \qquad \textbf{(P.12)}$$

Substitution of equation P.12 into equation P.1, gives the following expression for $G$ in terms of $a$, $b$ and $\Delta b$:

$$G=\frac{a-\sqrt{a^2-2b\Delta b+(\Delta b)^2}}{\Delta b} \qquad \textbf{(P.13)}$$

# Appendix Q
## Exact and approximate gain factors for octagonal flexural gain mechanism

Consider figure 3.4.1.5. The displacement gain factor is the ratio of the change in height of the octagonal gain mechanism to the elongation of the rod:

$$G = \frac{x_s}{x_a} \tag{Q.1}$$

where $x_a$ is the product of the strain $\varepsilon$ in the rod and the rod length $l_T$:

$$x_a = \varepsilon l_T \tag{Q.2}$$

and $x_s$ is given by:

$$x_s = 2(h_0 - h) \tag{Q.3}$$

The initial height $h_0$ of the slanted beam is given by:

$$h_0 = r\sin\theta_0 \tag{Q.4}$$

and the final height $h$ is given by:

$$h = \sqrt{r^2 - \left(r\cos\theta_0 + \frac{x_a}{2}\right)^2} \tag{Q.5}$$

The final height is obtained in terms of the rod strain and length, by substitution of equation Q.2 into equation Q.5:

$$h = \sqrt{r^2 - \left(r\cos\theta_0 + \frac{\varepsilon l_T}{2}\right)^2} \tag{Q.6}$$

Substitution of equations Q.4 and Q.6 into equation Q.3 gives $x_s$ as follows:

$$x_s = 2\left(r\sin\theta_0 - \sqrt{r^2 - \left(r\cos\theta_0 + \frac{\varepsilon l_T}{2}\right)^2}\right) \tag{Q.7}$$

The exact gain factor is obtained by substitution of equations Q.7 and Q.2 into equation Q.1:

$$G = 2\frac{r\sin\theta_0 - \sqrt{r^2 - \left(r\cos\theta_0 + \frac{\varepsilon l_T}{2}\right)^2}}{\varepsilon l_T} \tag{Q.8}$$

## Approximate gain factor

An approximate equation for the displacement gain, in terms of $\theta_0$, is subsequently derived.

From equation Q.8:

$$\frac{G\varepsilon l_T}{2} - r\sin\theta_0 = -\sqrt{r^2 - \left(r\cos\theta_0 + \frac{\varepsilon l_T}{2}\right)^2} \qquad \textbf{(Q.9)}$$

Squaring both sides of equation Q.9 gives:

$$\left(\frac{G\varepsilon l_T}{2} - r\sin\theta_0\right)^2 = r^2 - \left(r\cos\theta_0 + \frac{\varepsilon l_T}{2}\right)^2 \qquad \textbf{(Q.10)}$$

Expanding terms on both sides of equation Q.10 gives:

$$\left(\frac{G\varepsilon l_T}{2}\right)^2 - G\varepsilon l_T r\sin\theta_0 + r^2\sin^2\theta_0 = r^2 - r^2\cos^2\theta_0 - \varepsilon l_T r\cos\theta_0 - \left(\frac{\varepsilon l_T}{2}\right)^2 \qquad \textbf{(Q.11)}$$

Neglecting 2nd order terms and noting that $\sin^2\theta_0 + \cos^2\theta_0 \equiv 1$, equation Q.11 reduces to:

$$-G\varepsilon l_T r\sin\theta_0 \approx -\varepsilon l_T r\cos\theta_0 \qquad \textbf{(Q.12)}$$

From equation Q.12, the following approximate equation for $G$, in terms of $\theta_0$, results:

$$G \approx \cot\theta_0 \qquad \textbf{(Q.13)}$$

A graphical comparison between the gain factors calculated with equations Q.8 and Q.13, for initial angles ranging from 5° to 30°, an active rod length of 35 mm, strain of 1000 $\mu\varepsilon$ and slanted beam radius of 19 mm, is shown in figure Q.1.

The error of the approximate gain factor, relative to the exact gain factor, is shown in figure Q.2. It can be seen that the approximate gain factor is sufficiently accurate for initial angles ranging from 5° to 30°, i.e. for gains ranging from 1,7 to 11,4. The error is less than 5% for angles larger than 5,8° and less than 1° for angles larger than 12,8°.

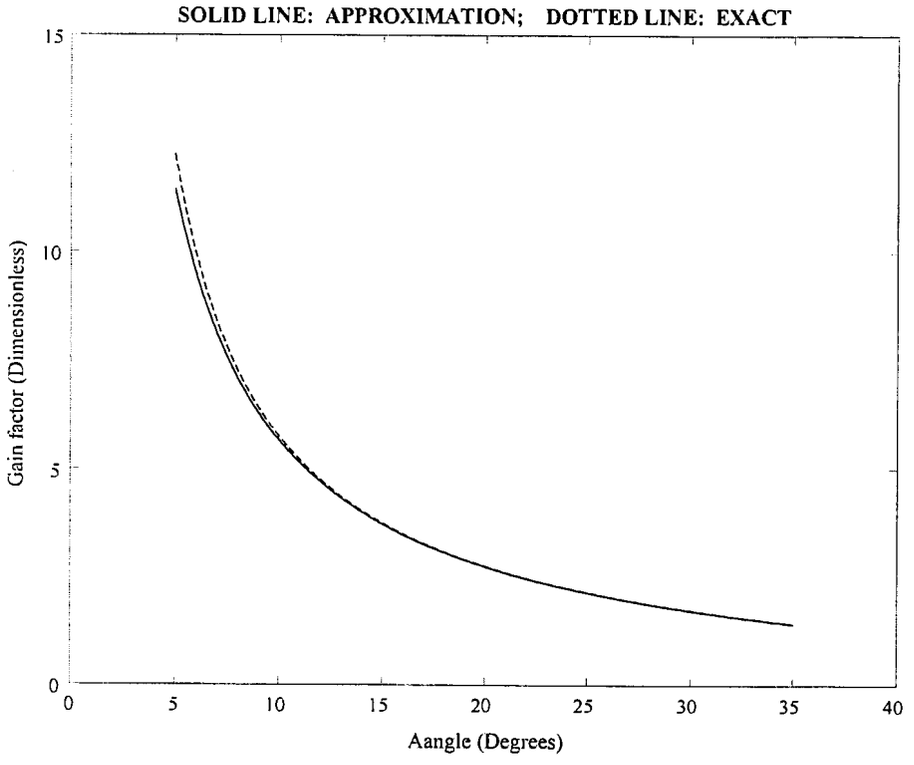


**Figure Q.1: Approximate and exact gain factors versus initial angle of slanted beam**

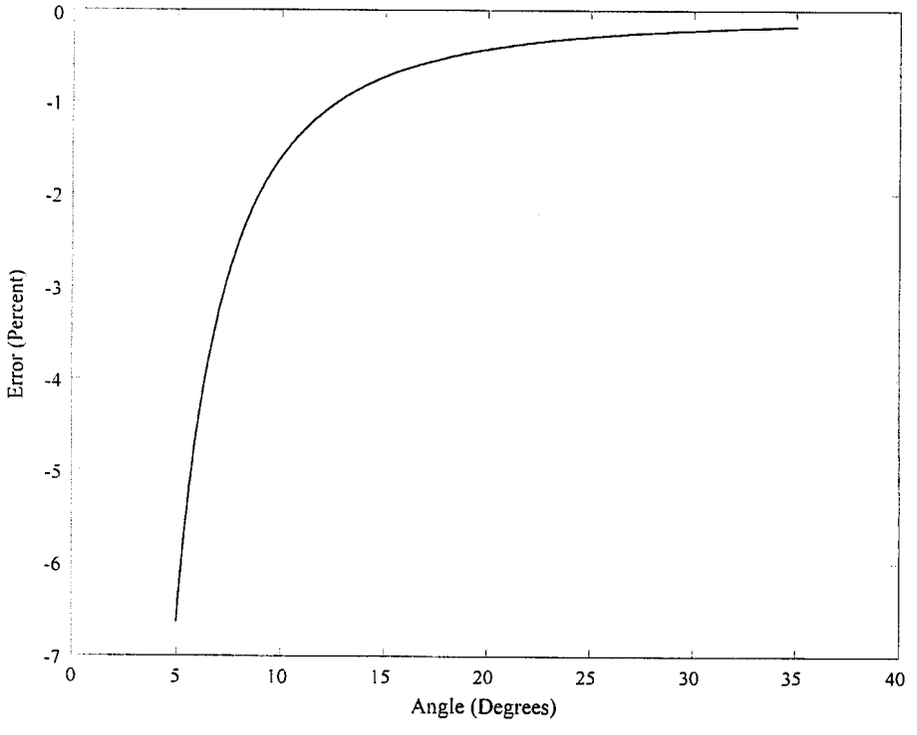


**Figure Q.2: Error of approximate gain factor versus initial angle of slanted beam**

# Appendix R
# Volume of a permanent magnet

Consider figure 3.4.2.1. The fluxes in the magnet, Terfenol-D rod and air gap between the end caps and magnet, are respectively given by:

$$\phi_m = B_m A_m \quad \textbf{(R.1a)}$$
$$\phi_T = B_T A_T \quad \textbf{(R.1b)}$$
$$\phi_g = B_g A_g \quad \textbf{(R.1c)}$$

where $\phi_m$, $\phi_T$ and $\phi_g$ are the fluxes in the magnet, rod and air gap respectively. $B_m$, $B_T$ and $B_g$ are the flux densities in the magnet, rod and air gap respectively. $A_m$, $A_T$ and $A_g$ are the cross-sectional areas of the magnet, rod and air gap respectively.

The flux in the magnet is equal to the flux in the rod and the flux in the air gap:

$$\phi_m = \phi_T = \phi_g \quad \textbf{(R.2)}$$

Substitution of equations R.1a to R.1c into equation R.2 gives:

$$B_g = \frac{B_T A_T}{A_g} \quad \textbf{(R.3a)}$$

$$B_m = \frac{B_T A_T}{A_m} \quad \textbf{(R.3b)}$$

The total magnetomotive force in the loop is zero:

$$H_m l_m + H_T l_T + H_g l_g = 0 \quad \textbf{(R.4)}$$

where $H_m$ is the demagnetizing force in the magnet and $H_T$ and $H_g$ are the field in the rod and the field in the gap respectively. $l_m$, $l_T$ and $l_g$ are the magnet, rod and gap lengths respectively.

In equation R.4, it is assumed that the permeability of the end caps is infinite. The assumption is justifiable, for two reasons. In the first place, the end caps are made of steel, which has a relatively high permeability. Secondly, the end caps are relatively thin in comparison with the rod length.

Equation R.4 can be written as:

$$H_m l_m = -H_T l_T - H_g l_g \quad \textbf{(R.5)}$$

The field in the gap is given by:

$$H_g = \frac{B_g}{\mu_0} \tag{R.6}$$

where $\mu_0 = 4\pi.10^{-7}\ Tm/A$ is the permeability of free space.

Substitution of equation R.6 into equation R.3a gives:

$$H_g = \frac{B_T A_T}{\mu_0 A_g} \tag{R.7}$$

Subsequent substitution of equation R.7 into equation R.5 gives:

$$H_m l_m = -\frac{B_T A_T l_g}{\mu_0 A_g} - H_T l_T \tag{R.8}$$

$H_m$ is obtained as follows from equation R.8:

$$H_m = -\frac{1}{l_m}\left(\frac{B_T A_T l_g}{\mu_0 A_g} - H_T l_T\right) \tag{R.9}$$

Multiplying equation R.3b with equation R.9 gives:

$$B_m H_m = -\frac{B_T A_T}{A_m l_m}\left(\frac{B_T A_T l_g}{\mu_0 A_g} - H_T l_T\right) \tag{R.10}$$

The magnet volume $V_m$ is given by:

$$V_m = A_m l_m \tag{R.11}$$

Substitution of equation R.11 into equation R.10 gives:

$$B_m H_m = -\frac{B_T A_T}{V_m}\left(\frac{B_T A_T l_g}{\mu_0 A_g} - H_T l_T\right) \tag{R.12}$$

Rewriting equation R.12 gives:

$$V_m = \frac{B_T A_T}{B_m H_m}\left(H_T l_T - \frac{B_T A_T l_g}{\mu_0 A_g}\right) \tag{R.13}$$

The flux density in the rod is a function of the field in the rod:

$$B_T = B_T(H_T) \tag{R.14}$$

The required field in the rod is equal to the bias field:

$$H_T = H_b \tag{R.15}$$

Substitution of equation R.15 into equation R.14 gives the flux density in the rod in terms of the bias field:

$$B_T = B_T(H_b) \tag{R.16}$$

Substitution of equations R.15 and R.16 into equation R.13 gives:

$$V_m = \frac{B_T(H_b)A_T}{B_m H_m}\left(H_b l_T - \frac{B_T(H_b)A_T l_g}{\mu_0 A_g}\right) \tag{R.17}$$

# Appendix S
# Maximum coil power for electromagnetic field biasing

The coil current, in terms of the magnetic field, is given by (see equation 3.4.2.7):

$$I = \frac{l_T}{N} H \tag{S.1}$$

The coil voltage, in terms of the field, is given by (see equation 3.4.2.10):

$$V = \frac{l_T}{N} \sqrt{R_c^2 + \omega^2 L_0^2}\, H \tag{S.2}$$

The coil power is the product of the coil voltage and coil current:

$$P = VI \tag{S.3}$$

Substitution of equations S.1 and S.2 into equation S.3 gives the following equation for coil power in terms of magnetic field:

$$P = \left(\frac{l_T}{N}\right)^2 \sqrt{R_c^2 + \omega^2 L_0^2}\, H^2 \tag{S.4}$$

Parameters which are of particular importance in the analysis of the electromagnetic field biasing, are the maxima of the coil current, voltage and power. For excitation frequencies that are considerably lower than the coil $R_c/L_0$ ratio, the phase angle of the coil can be ignored. It can therefore be assumed that the maximum voltage and current coincide with the maximum field. By sustitution of $H = H_{\max}$ into equations S.1, S.2 and S.4, the maximum current, voltage and power are given by:

$$I_{\max} = \frac{l_T}{N} H_{\max} \tag{S.5a}$$

$$V_{\max} = \frac{l_T}{N} \sqrt{R_c^2 + \omega^2 L_0^2}\, H_{\max} \tag{S.5b}$$

$$P_{\max} = \left(\frac{l_T}{N}\right)^2 \sqrt{R_c^2 + \omega^2 L_0^2}\, H_{\max}^2 \tag{S.5c}$$

In equations S.5, the maximum field is the sum of the bias field $H_b$ and the amplitude $H_A$ of the AC component of the field:

$$H_{\max} = H_b + H_A \tag{S.6}$$

By substitution of equation S.6 into equations S.5, the maximum coil current, voltage and power are expressed as follows:

$$I_{\max} = \frac{l_T}{N}\left(H_b + H_A\right) \tag{S.7a}$$

$$V_{\max} = \frac{l_T}{N}\sqrt{R_c^2 + \omega^2 L_0^2}\left(H_b + H_A\right) \tag{S.7b}$$

$$P_{\max} = \left(\frac{l_T}{N}\right)^2 \sqrt{R_c^2 + \omega^2 L_0^2}\left(H_b + H_A\right)^2 \tag{S.7c}$$

# Appendix T
# Fundamental natural frequency of a simply-supported beam with a concentrated mass attached at the centre and which is subjected to a compressive axial force

The fundamental natural frequency of a beam with a concentrated mass at the centre, and which is subjected to an axial force acting at the beam ends, is analyzed in the following steps. The fundamental natural frequency of a simply-supported, uniform beam is first analyzed in the absence of any concentrated mass or axial force. The effect of the concentrated mass is then added. For the purpose of simplifying the analysis, the concentrated mass is expressed in terms of an equivalent density, which is added to the beam material density to give the total distributed beam density.

The next step will be to write the fundamental natural frequency of a uniform beam, which is subjected to an axial force. The frequency is then adjusted by replacing the beam material density with the total distributed density, to include the effect of the concentrated mass.

The fundamental angular natural frequency $\omega_1$ of a simply-supported uniform beam, in the absence of any concentrated mass, can be obtained from the following equation:

$$\omega_1^2 = \left(\frac{\pi}{l_T}\right)^4 \frac{EI}{\rho A_T} \qquad \textbf{(T.1)}$$

where $E$ is Young's modulus of the rods, $I$ is the second moment of area of the rod cross-section, $\rho$ is the density of the rod material, $A_T$ is the rod cross-sectional area and $l_T$ is the rod length.

The relationship between the natural frequency $f_1$ and the angular natural frequency $\omega_1$ is:

$$f_1 = \frac{1}{2\pi}\omega_1 \qquad \textbf{(T.2)}$$

By taking the square root of the terms on both sides of equation T.1, and substitution of the resulting equation into equation T.2, the fundamental natural frequency is obtained as:

$$f_1 = \frac{1}{2\pi}\left(\frac{\pi}{l_T}\right)^2 \sqrt{\frac{EI}{\rho A_T}} \qquad \textbf{(T.3)}$$

An equation of the same form as equation T.3, for the fundamental natural frequency of a beam with a concentrated mass attached at the centre, is required. This will facilitate inclusion of the effect of the axial force. To this end, the concentrated mass is first expressed in terms of an equivalent density. The equivalent density is then added to the beam material density to give the distributed density of the beam.

The equivalent density $\rho_{eq}$ is given by the following equation:

$$\rho_{eq} = \frac{2m_c}{A_T l_T} \tag{T.4}$$

where $m_c$ is the concentrated mass.

The distributed density $\rho_{distr}$ is the sum of the beam material density and the equivalent density:

$$\rho_{distr} = \rho + \rho_{eq} \tag{T.5}$$

Substitution of equation T.4 into equation T.5 gives the distributed density as follows in terms of the beam material density and concentrated mass:

$$\rho_{distr} = \rho\left(1 + \frac{2m_c}{\rho A_T l_T}\right) \tag{T.6}$$

The fundamental natural frequency of the beam with a mass attached at the centre, is expressed as follows in the form of equation T.3:

$$f_1 = \frac{1}{2\pi}\left(\frac{\pi}{l_T}\right)^2 \sqrt{\frac{EI}{\rho_{distr} A_T}} \tag{T.7}$$

where $\rho_{distr}$ is given by equation T.6.

Substitution of equation T.6 into equation T.7 gives the fundamental natural frequency of a simply-supported beam with a concentrated mass at the centre, as:

$$f_1 = \frac{1}{2\pi\sqrt{1 + 2\,m_c/(\rho A_T l_T)}}\left(\frac{\pi}{l_T}\right)^2 \sqrt{\frac{EI}{\rho A_T}} \tag{T.8}$$

It can be seen from equation T.8 that the addition of a concentrated mass at the beam centre lowers the fundamental natural frequency.

The effect of the axial force on the fundamental natural frequency of the beam can now be included. The fundamental natural frequency of a uniform, simply-supported beam subjected to an axial compressive force $F_b$ acting at the ends, can be obtained from the following equation [Tse et al, 1978]:

$$\omega_1^2 = \left(\frac{\pi}{l_T}\right)^4 \frac{EI}{\rho A_T} - \left(\frac{\pi}{l_T}\right)^2 \frac{F_b}{\rho A_T} \tag{T.9}$$

The first term on the right hand sents the natural frequency of the uniform beam, as given by equat n corrects for the axial force. Note that the second term is negative for a compressive force, implying that a compressive force lowers the beam natural frequency. By substitution of equation T.2 into equation T.9 and taking the square root on both sides of the resulting equation, the fundamental natural frequency of a uniform beam subjected to an axial force at the ends, is given by:

$$f_1 = \frac{1}{2\pi}\sqrt{\left(\frac{\pi}{l_T}\right)^4 \frac{EI}{\rho A_T} - \left(\frac{\pi}{l_T}\right)^2 \frac{F_b}{\rho A_T}} \qquad \textbf{(T.10)}$$

In order to include the effect of the concentrated mass on the natural frequency, the material density $\rho$ in equation T.10 is replaced with the distributed density $\rho_{distr}$:

$$f_1 = \frac{1}{2\pi}\sqrt{\left(\frac{\pi}{l_T}\right)^4 \frac{EI}{\rho_{distr} A_T} - \left(\frac{\pi}{l_T}\right)^2 \frac{F_b}{\rho_{distr} A_T}} \qquad \textbf{(T.11)}$$

Finally, by substitution of equation T.6 into equation T.11, the fundamental natural frequency of a simply-supported beam with a concentrated mass attached at the centre and which is subjected to compressive axial force, is given by:

$$f_1 = \frac{1}{2\pi}\sqrt{\left(\frac{\pi}{l_T}\right)^4 \frac{EI}{\rho(1+2m_c/\rho A_T l_T)A_T} - \left(\frac{\pi}{l_T}\right)^2 \frac{F_b}{\rho(1+2m_c/\rho A_T l_T)A_T}} \qquad \textbf{(T.12)}$$

# Appendix U
# Linear and nonlinear system identification models and techniques

## U.1 Linear system identification models and techniques

The objective of linear identification is to obtain a system in transfer function or state-space form from measured data. Different models have been developed for this purpose, such as the following: AR (Auto Regressive), MA (Moving Average), ARX (Auto Regressive with eXogenous inputs), ARMA (Auto Regressive Moving Average), ARMAX (Auto Regressive Moving Average with eXogenous inputs) and ARIMA (Auto Regressive Integrated Moving Average). In mechanical system identification terminology, "exogenous inputs" refers to measurement noise.

The ARMA model is widely used for discrete time-domain identification of linear systems. The model is a combination of the AR and MA models. Output at the current time step is expressed in terms of previous outputs, previous inputs and the current input, using the discrete delay element $z^{-1}$. The current output is given by:

$$Y(z) = Y(z)\sum_{k=1}^{N} a_k z^{-k} + U(z)\sum_{k=0}^{M} b_k z^{-k} \qquad \textbf{(U.1.1)}$$

where $Y(z)$ is the $z$-domain output, $U(z)$ is the $z$-domain input, $a_k$ is the $k$-th output delay gain and $b_k$ is the $k$-th input delay gain. $N$ is the number of output delay elements used in the model and $M$ is the number of input delays. The $z$-domain $TF$ is given by:

$$G(z) = \frac{Y(z)}{U(z)} = \frac{\sum_{k=0}^{M} b_k z^{-k}}{1 - \sum_{k=1}^{N} a_k z^{-k}} \qquad \textbf{(U.1.2)}$$

Regression methods are used to determine the gains. Regression methods will be discussed in short later.

### Time-domain model from free-decay system response

The method used for obtaining system parameters from free-decay response is known as the complex exponential method. The output is written as a linear series of exponentially decaying functions in complex conjugate pairs. Each function is represented by a modal amplitude and an eigenvalue. A number of methods for determining the amplitudes and eigenvalues exist, such as the Prony and Ibrahim time-domain (ITD) methods [Ewins, 1991]. The Prony method is limited in its application by the fact that the number of poles contained in the response data must be known in advance and the data must be noise-free. Many techniques have been developed to improve the performance of the method, two of which are based on singular value decomposition (SVD) and oversized eigenmatrix methods.

## Identification models for time-varying systems

Various model types may be used to represent characteristics and behaviour of time-dependent systems, such a discrete-time and state-space models. In both model types, characteristics vary with time. In discrete-time models, the $a_k$'s and $b_k$'s in equation U.1.2 are functions of time. Identification of time-varying systems is described in more detail by Bittanti et al [1992] and Kashyap & Rao [1976]. The difference between time-invariant and time-dependent state-space models was discussed in short in section 2.5 (see equations 2.5.1.1 to 2.5.1.3). In linear time-dependent state-space systems, state and output matrices are of the form $A = A(t)$, $B = B(t)$, $C = C(t)$ and $D = D(t)$. If a discrete-time model of the system is known, state and output matrices can be obtained from the coefficients $a_k$ and $b_k$.

## Regression techniques

Regression techniques are used to determine system model coefficients. Least-squares (LS) models are generally used for off-line identification of parameters. This method of identification may however be time-consuming.

In order to speed up the process, real-time identification tools, such as exponentially-weighted recursive least-squares (RLS) algorithms, have been developed. RLS identification is described by, inter alia, Goodwin & Sin [1984], Kim [1997] and Schoukens & Pintelon [1991]. The least-square error is given by Cowan & Grant [1985] as:

$$E_{n+1} = \sum_{i=1}^{n+1} w^{n+1-i} \left| \hat{y} - y \right|^2 \qquad \textbf{(U.1.3)}$$

where $E$ is the identification model error and $w$ is an exponential weighting function of time, such that $0 \leq w \leq 1$. $\hat{y}$ is the modelled output and $y$ is the measured output. $E$ is a function of the coefficient, or parameter vector, $C$:

$$E = E(C) \qquad \textbf{(U.1.4)}$$

where $C = \{a_1, a_2, \ldots, a_N \quad b_0, b_1, \ldots, b_M\}^T$. The parameter vector is determined in real-time.

For off-line identification, the weighting function is unity. The parameter vector is obtained by setting the partial derivatives of $E$ with respect to each of the parameters, equal to zero:

$$\frac{\partial E}{\partial C_l} = 0, \quad l = 1, 2, \cdots, N + M + 1 \qquad \textbf{(U.1.5)}$$

where $C_l$ the $l$-th element of the coefficient vector.

For linear-in-the-parameters models, the solution of equation U.1.5 can be obtained using orthogonal, linear LS solution techniques. For nonlinear-in-the-parameters models, the

Gauss-Newton and Newton-Raphson methods are generally used. The Gauss-Newton method is described in appendix V.

## Laplace- and frequency domain *TF* models from discrete time-domain models

The complex Laplace-domain *TF* of a system whose time-domain *TF* is known, is obtained by substitution of $z$ with $e^{sT}$ in equation U.1.2:

$$z = e^{sT} \tag{U.1.6}$$

where $s$ is the complex Laplace-domain differential operator and $T$ is sample time. The transfer function $G(s)$ can be written in the form:

$$G(s) = \frac{\sum_{k=0}^{M} p_k s^k}{\sum_{l=0}^{N} q_l s^l} \tag{U.1.7}$$

where the $p_k$'s and $q_l$'s are the numerator and denominator polynomial coefficients respectively.

The complex $\omega$-domain *TF* of a system whose time-domain *TF* is known, is obtained by substitution of $z$ with $e^{j\omega T}$ in equation U.1.2:

$$z = e^{j\omega T} \tag{U.1.8}$$

The transfer function $G(j\omega)$ can be written in the following form:

$$G(j\omega) = \frac{\sum_{k=0}^{M} p_k (j\omega)^k}{\sum_{l=0}^{N} q_l (j\omega)^l} \tag{U.1.9}$$

where the $p_k$'s and $q_l$'s are the numerator and denominator polynomial coefficients respectively, which are equal to those in equation U.1.7.

The polynomial coefficients can be determined if the $a_k$'s and $b_k$'s in equation U.1.2 are known. If not, the *TF* model must be available in some other form, such as measured spectra.

## Frequency-domain models from measured *TF* spectra

The objective is to obtain system *TF* spectra that match the experimentally measured spectra as closely as possible. A vast number of $\omega$ domain identification techniques exist. The technique used will mainly depend on system characteristics, e.g. linearity and number of degrees of freedom. Linear frequency-domain identification techniques can broadly be classified as SDOF and MDOF identification techniques.

Frequency-domain identification of an SDOF system can be done by means of the peak-amplitude method, circle fit method and the so-called inverse method [Ewins, 1991]. Receptance properties are used in the peak amplitude and circle fit methods to determine system characteristics, while inverse receptance properties are used in the "inverse method".

The receptance curve (*X/F*) of an SDOF system displays, inter alia, a peak amplitude and two frequencies where the amplitudes are 70,7% of the peak amplitude. The frequency where the peak occurs, is the natural frequency $f_n$. The two frequencies where the amplitudes are 70,7% of the peak amplitude, are the half-power points. The half-power bandwidth is denoted by $\Delta f$. The dimensionless damping factor $\zeta$ is given by the equation $\zeta = 2\Delta f / f_n$. This identification method is known as the peak amplitude method. Stiffness and mass are respectively given by:

$$k = \left[ (X/F)\big|_{f=0} \right]^{-1} \qquad \textbf{(U.1.10a)}$$

$$m = k/(2\pi f_n)^2 \qquad \textbf{(U.1.10b)}$$

The Nyquist plot of the receptance of an SDOF system is a circle in the complex plane. This circle is known as the modal circle. Natural frequency, damping factor and modal amplitude can be calculated from the circle properties. The procedure is not given here, but is described in full by Ewins [1991]. This method is known as the circle-fit method and is widely used for frequency-domain identification of SDOF systems.

An alternative to the circle-fit method, is the "inverse" method. In the complex plane, the inverse receptance curve (*F/X*) produces a horizontal straight line. The maximum real value of *F/X* is *k*, the spring constant. The intercept of the line with the imaginary axis gives the damping $c\omega$ directly. The frequency at the origin of the graph, i.e. where the real and imaginary axes cross, is the natural frequency.

Three types of MDOF frequency-domain identification techniques are discussed here. The first type is the circle-fit method, which is an extension of the SDOF circle-fit method. The method is described by Ewins [1991]. The method cannot be used if the modes are closely-coupled or if damping is extremely light. (Closely coupled modes occur in systems where the natural frequencies are closely-spaced or where damping is high, or both).

A more general approach to multi-mode curve-fitting is an LS data fit to measured *TF* frequency spectra in complex form. Depending on reliability of measured data and system characteristics, more accurate data fits are generally obtained than with the circle fit method. One disadvantage of the method is that the LS problem is nonlinear, which requires iterative solution techniques, such as the Newton-Raphson and Gauss-Newton methods. As is the

case with all iterative techniques, starting values in the range of convergence of the numerical system, are required. Furthermore, poles of the fitted *TF* may be unstable, even for globally stable plants. The LS method for frequency-domain identification is discussed in short by Ewins [1991].

The third method is identification using overdetermined systems, as described by Braun & Ram [1987]. Model order is assumed higher than that of the physical system. The method was developed to overcome the problem of specifying model order in the presence of noise. Singular value decomposition is used to solve the LS data fitting problem.

## State-space identification of linear systems

State-space identification techniques can broadly be classified as direct and indirect techniques. Indirect techniques are applied to convert existing time-, frequency- or Laplace-domain models to state-space models. Direct models are used to obtain state-space models from measured spectra without intermediate steps.

Conversion of *s*-domain models to state-space models is described by Schwarzenbach & Gill [1986]. The *TF* (*Y*/*U*) is written as the product of two functions in *s*:

$$\frac{Y(s)}{U(s)} = \frac{Y(s)}{V(s)} \frac{V(s)}{U(s)} \qquad \textbf{(U.1.11)}$$

where $Y(s)/V(s)$ is the numerator, divided by the highest power of *s*, and $V(s)/U(s)$ is the denominator, divided by the highest power of *s*. *V*/*U* is written as a linear DE and expressed in canonical state-space form. The output is expressed in terms of the state vector and input, in the form of equation 2.5.1.3b.

A similar technique can be used to convert discrete-time models to discrete state-space form if the $a_k$ and $b_k$ coefficients in equation U.1.2 are known. The state and output equations of a linear discrete system are:

$$x(k+1) = \Phi x(k) + \Gamma u(k) \qquad \textbf{(U.1.12a)}$$

$$y(k) = Hx(k) + Ju(k) \qquad \textbf{(U.1.12b)}$$

where $x(k)$, $u(k)$ and $y(k)$ are the *k*-th state vector, input and output respectively. $\Phi$, $\Gamma$, *H* and *J* are the coefficient-, driving-, output- and transmission matrix, respectively.

The discrete state and output matrices are related to their respective continuous equivalents by means of the following equations [Franklin et al, 1990] and [Liu & Miller, 1995]:

$$\Phi = e^{AT} \tag{U.1.13a}$$

$$\Gamma = \int_0^T e^{A\eta} B d\eta \tag{U.1.13b}$$

$$H = C \tag{U.1.13c}$$

$$J = D \tag{U.1.13d}$$

where $T$ is the sample period and $\eta$ is an integration variable.

State-space models can be directly obtained from measured spectra, using, for instance, the Frequency domain Observability Range Space Extraction (FORSE) algorithm. The algorithm is explained in detail by Liu et al [1996]. It uses proper state-space parameterization and Singular Value Decomposition (SVD) to ensure good numerical properties for multivariable and high dimensional structural systems. It achieves high accuracy in the frequency domain by overparameterizing the model. The FORSE algorithm is an extension of the ORSE time-domain identification algorithm [Liu & Miller, 1995].

## U.2 Nonlinear system identification models and techniques

Techniques for determining the parameters of nonlinear systems from measured data can broadly be classified as time-domain techniques, frequency-domain techniques, force-state component identification and identification using neural networks.

### Time-domain identification techniques for nonlinear systems

Similar models to the linear time-invariant models have been developed for time-domain identification of nonlinear systems. Two of the most popular models are as the NARX (Nonlinear Auto Regressive with eXogenous inputs) and NARMAX (Nonlinear Auto Regressive Moving Average with eXogenous inputs) models. The NARX model is a special case of the NARMAX model. The NARMAX model is described by Chen et al [1989] and Worden et al [1994]. Othogonal LS data fit techniques, such as the classical Gram-Schmidt (CGS) and modified Gram-Schmidt (MGS) schemes, Householder transformation and Givens method can be used to determine model parameters [Chen et al, 1989].

## Force-state component identification

Force-state component identification is done to obtain the restoring force $f$ in a component or structure in terms of the state vector $x$ and its derivative with respect to time, $\dot{x}$.

The equation of motion is written in the following form:

$$m\ddot{x} + f(x,\dot{x}) = p(t) \qquad \textbf{(U.2.1)}$$

where $p(t)$ is the load vector.

$f$ can be determined for a large variety of nonlinearities, e.g. nonlinear spring and nonlinear damping characteristics, nonlinearities with memory and combinations of linear and nonlinear stiffness and damping.

Characteristics may be represented mathematically, i.e. by $f(x,\dot{x})$, or graphically, by a 3-dimensional force-state map. Force-state component identification is described in more detail by Masters et al [1996], Worden & Tomlinson [1988] and Wright & Al Haddid [1991].

## Frequency-domain identification of nonlinear systems

Nonlinear frequency-domain identification can broadly be classified as SDOF identification, modal analysis (for MDOF systems), and identification using time-domain inputs. The SDOF and modal analysis identification techniques are, in essence, extensions of linear system identification methods. Two SDOF identification techniques are the circle fit method, as described by Ewins [1991] and the use of response-surface plots, as explained by Dimas & Pardoen [1988].

Modal analysis identification methods for MDOF systems include the Hilbert transform method, the use of functional series (Volterra method) and range-dependent linear identification. The Hilbert transform method is a well-known linearization technique in the fields of numerical signal processing of filters, acoustics and physics. It is extended to MDOF mechanical system identification by Vinh et al [1984] and Simon & Tomlinson [1984]. The frequency response function (*FRF*) of an MDOF system, for a sinusoidal input, is expressed in terms of an equivalent linear *TF*. The method can be applied to systems with strong nonlinearities and no a priori assumption of the nonlinearities is required. The disadvantage, however, is that the method is more difficult to apply to identification procedures where random excitation is used.

The Volterra system model consists of two parts, i.e. a linear system model and a nonlinear extension to the model, using higher order terms. In the $\omega$-domain, the linear term is expressed by a classical Fourier transform of the *TF*. The nonlinear terms are written as multiple convolutions, using Volterra kernels. The $\omega$-domain representation of the nonlinear part is obtained by taking the multi-dimensional Fourier transform of the higher order terms. Two difficulties associated with the method are the number of terms required for accurate

modelling and efficient methods of computing multi-dimensional Fourier transforms (MDFT's). The Volterra method is explained in more detail by Tomlinson [1986].

A third method is range-dependent linearization. The system is assumed linear for a given input energy level. Linear identification is done for each input energy level, using linear MDOF techniques. The effects of nonlinearities on the $\omega$-domain *FRF* for a constant input energy level are ignored. This method is applicable if the system is weakly nonlinear or if the nonlinearity only has a significant influence outside the frequency band of interest. The disadvantage is that characterization tests must be done for each input energy level in order to determine the effect of the nonlinearity on the *FRF*.

Nonlinear frequency-domain identification is often done from measured time-domain inputs and responses, using methods such as the NARMAX method. Application of the NARMAX method to nonlinear frequency response estimation is described by Billings et al [1988]. The NARMAX method is a convenient method of expressing inputs and outputs as higher order series. The model is validated in the time domain and transformed to the frequency-domain. The procedure is as follows: The input is first assumed to be harmonic. The input is substituted in the NARMAX model and the output amplitude at the given frequency is calculated, using harmonic balance. A second harmonic is added to the input. The output amplitude is calculated as a function of the two input frequencies. The procedure is repeated until the amplitudes of all the desired frequencies have been obtained.

## Identification using neural networks

Neural network identification makes use of parallel distributed processing to identify the internal forces of structure-unknown nonlinear dynamic systems typically encountered in the field of applied mechanics [Masri et al, 1992]. Identification of the restoring force of an SDOF system is described by Masri et al [1993]. The restoring force $g(y,\dot{y})$ is written in terms of the measured input $u(t)$, acceleration $\ddot{y}(t)$ and mass $m$ as:

$$g(y,\dot{y}) = u(t) - m\ddot{y}(t) \qquad \textbf{(U.2.2)}$$

Measured signals are discretized and fed into the neural network. Network output is an approximate restoring force $\hat{g}(y,\dot{y})$. The identification procedure consists of two phases, i.e. the network learning phase and the evaluation phase. The procedure is described in detail by Masri et al [1993].

# Appendix V
# Gauss-Newton method applied to LS identification in the frequency domain

The difference between the modelled *TF* and experimentally-determined *TF* is known as the estimation error and is given by:

$$e = G - \hat{G} \tag{V.1}$$

where $e$ is the error, $\hat{G}$ is the modelled *TF* and $G$ is the experimentally-determined *TF*. $G$ is known at discrete frequencies, thus the error can only be evaluated at these frequencies. The error $e_r$ at the $r$-th frequency is:

$$e_r = G_r - \hat{G}_r \tag{V.2}$$

where $G_r$ and $\hat{G}_r$ are the measured *TF* and approximate *TF* at the $r$-th frequency, given by:

$$G_r = G(j\omega_r) \tag{V.3a}$$
$$\hat{G}_r = \hat{G}(j\omega_r) \tag{V.3b}$$

It can be seen from equations V.2 and V.3 that the error varies with frequency. As a globally accurate model is required, the error squared is summed and minimized over the frequency band. The global error is given by:

$$E = \sum_{r=1}^{R} e_r^2 \tag{V.4}$$

where $E$ is the global error and of the model and $R$ is the number of discrete frequencies.

Both $G$ and $\hat{G}$ are complex (see equations V.3). The global error can therefore be expressed as the sum of the error of the real term squared, plus the error of the imaginary term squared [Schoukens & Pintelon, 1991]:

$$E = \sum_{r=1}^{R}\left[\left(\mathrm{Re}\{G_r\} - \mathrm{Re}\{\hat{G}_r\}\right)^2 + \left(\mathrm{Im}\{G_r\} - \mathrm{Im}\{\hat{G}_r\}\right)^2\right] \tag{V.5}$$

$E$ is a nonlinear function of the polynomial coefficient vector $C$:

$$E = E(C) \tag{V.6}$$

$C$ is given as follows in terms of the $TF$ numerator and denominator polynomial coefficients:

$$C = \{p_0, p_1, \cdots, p_M, \quad q_0, q_1, \cdots, q_N\}^T \tag{V.7}$$

where $M$ and $N$ are the numerator and denominator polynomial orders respectively.

From equation V.4, $E$ can be expressed in matrix notation as:

$$E = e^T e \tag{V.8}$$

Substitution of equation V.1 into equation V.8 gives:

$$E = \left(G - \hat{G}\right)^T \left(G - \hat{G}\right) \tag{V.9}$$

where $G$ and $\hat{G}$ are $R$ x 1 vectors and $E$ is a 1 x 1 scalar.

The objective of LS identification is to determine the parameter vector $C$, which minimizes $E$. $C$ is obtained by setting the partial derivatives of $E$ with respect to each of the parameters $C_l$, equal to zero and by solving for $C_l$:

$$\frac{\partial E}{\partial C_l} = 0, \quad l = 1, 2, \cdots, N + M + 2 \tag{V.10}$$

where $C_l$ is the $l$-th element of the coefficient vector.

The solution of equation V.10 is determined iteratively. An initial estimate of $C$ is made, which will not necessarily satisfy equation V.10. The initial estimate is known as the starting value. Using the estimated $C$, the error gradient $\partial E/\partial C$ is calculated, from which the change $\Delta C$ in the parameter vector is obtained. $C$ is added to $\Delta C$ to obtain an updated parameter vector. The updated $C$ is subsequently used to calculate $\partial E/\partial C$. If the error gradient is sufficiently close to zero, the procedure is stopped. This condition is known as the stopping criterion. If the stopping criterion is not met, $\Delta C$, $C$ and $\partial E/\partial C$ are updated and the procedure is repeated until the stopping criterion is met.

The starting value must be selected within a limited range, known as the system range of convergence. If the starting value is selected outside this range, the method will diverge. If the starting value is selected inside the range of convergence, the method will either converge to a local minimum, or to the global minimum. The selection of starting values of a system with unknown coefficients is generally difficult. The method suggested by Schoukens & Pintelon [1991] is to linearize equation V.4, in order to obtain the linear solution to equation V.10 and to use this solution as a starting value. With a known starting value, $\Delta C$ can be calculated, using the procedure set out below.

For a small increment $\Delta C$ in equation V.6, the estimation error can be written as follows, using a Taylor series expansion:

$$E(C+\Delta C)=E(C)+(\Delta C)^T\frac{\partial E}{\partial C}+\frac{1}{2}(\Delta C)^T\frac{\partial^2 E}{\partial C^2}\Delta C+\cdots+ \qquad \textbf{(V.11)}$$

where $C$ and $\partial E/\partial C$ are ($N$+$M$+2) x 1 vectors. $\partial^2 E/\partial C^2$ is an ($N$+$M$+2) x ($N$+$M$+2) matrix.

The partial derivative of equation V.11 with respect to $\Delta C$ is:

$$\frac{\partial E(C+\Delta C)}{\partial \Delta C}=\frac{\partial E(C)}{\partial \Delta C}+\frac{\partial E}{\partial C}+\frac{\partial^2 E}{\partial C^2}\Delta C+\cdots+ \qquad \textbf{(V.12)}$$

For $E$ to be a minimum, the partial derivative of $E(C+\Delta C)$ with respect to $\Delta$C must be zero:

$$\frac{\partial E(C+\Delta C)}{\partial \Delta C}=0 \qquad \textbf{(V.13)}$$

The first term on the right hand side of equation V.11 is constant, therefore:

$$\frac{\partial E(C)}{\partial \Delta C}=0 \qquad \textbf{(V.14)}$$

Substitution of equations V.13 and V.14 into equation V.12 gives:

$$\frac{\partial E}{\partial C}=-\frac{\partial^2 E}{\partial C^2}\Delta C \qquad \textbf{(V.15)}$$

$\Delta C$ is obtained from equation V.15 as:

$$\Delta C=-\left(\frac{\partial^2 E}{\partial C^2}\right)^{-1}\frac{\partial E}{\partial C} \qquad \textbf{(V.16)}$$

It can be seen from equation V.16 that $\Delta C$ depends on both 1st order and 2nd order derivatives of $E$ with respect to $C$. It is however more convenient to express $\Delta C$ in terms of the 1st order derivative only. This is done with the aid of equation V.9.

The 1st order partial derivative of $E$ with respect to $C$, from equation V.9, is given by:

$$\frac{\partial E}{\partial C}=-2\left(\frac{\partial \hat{G}}{\partial C}\right)^T\left(G-\hat{G}\right) \qquad \textbf{(V.17)}$$

where $\partial\hat{G}/\partial C$ is an $R$ x ($N$+$M$+2) matrix.

$\partial^2 E/\partial C^2$ is obtained by partial differentiation of equation V.17 with respect to $C$. For a small error, $\partial^2 E/\partial C^2$ is given by:

$$\frac{\partial^2 E}{\partial C^2} = 2\left(\frac{\partial \hat{G}}{\partial C}\right)^T\left(\frac{\partial \hat{G}}{\partial C}\right) \qquad \textbf{(V.18)}$$

Substitution of equationsV.17 and V.18 into equation V.16 gives:

$$\Delta C = \left[\left(\frac{\partial \hat{G}}{\partial C}\right)^T\left(\frac{\partial \hat{G}}{\partial C}\right)\right]^{-1}\left(\frac{\partial \hat{G}}{\partial C}\right)^T\left(G - \hat{G}\right) \qquad \textbf{(V.19)}$$

Methods of determining the stopping criterion are explained by Schoukens & Pintelon [1991]. For the purpose of this study, the stopping criterion can either be a relatively small change in $E$, or a negligible increment $\Delta C$ in the parameter vector. The former stopping criterion may be mathematically expressed as:

$$\frac{E(C + \Delta C)}{E(C)} \leq \alpha \qquad \textbf{(V.20)}$$

where $\alpha$ is an arbitrarily selected factor, e.g. 0,1%.

If system sensitivity to parameter variations is low, equation V.20 will not necessarily guarantee a negligible $\Delta C$. For systems of this type, the following stopping criterion is recommended:

$$\frac{\Delta C_l}{C_l} \leq \alpha \qquad \textbf{(V.21)}$$

The stopping criterion given in equation V.21 is generally stricter than that in equation V.20, since the latter may give a parameter vector whose elements do not satisfy equation V.21.

# Appendix W
# Derivation of system transmissibility and two-input model

System transmissibility (*TR*) can be expressed in terms of transfer functions such as the input force to output force *TF*, base angular displacement to output angular displacement *TF* ($\theta/\theta_b$), base angular velocity to output angular velocity *TF* ($\dot{\theta}/\dot{\theta}_b$) and base angular acceleration to output angular acceleration *TF* ($\ddot{\theta}/\ddot{\theta}_b$). The most appropriate transfer function is mainly determined by the sensors used for system characterization and control.

Accelerometers were used for dynamic system characterization in chapter 4. The measured vertical accelerations were subsequently used to calculate the base and output angular accelerations (see section 4.5.1). Accelerometers will also be used as sensors during testing of the control system. It is therefore appropriate to express the *TR* as the transfer function between base angular acceleration and output angular acceleration ($\ddot{\theta}/\ddot{\theta}_b$).

The transmissibility is required in terms of system characteristics, such as state and output parameters, natural frequencies, damping factors and normal mode shapes. A derivation of the *TR* follows below. In order to simplify the derivation, an assumption is made that the *TR* is independent of sensor dynamics. The consequence of this assumption is that the transfer functions, $\theta/\theta_b$, $\dot{\theta}/\dot{\theta}_b$ and $\ddot{\theta}/\ddot{\theta}_b$, are equal over a wide frequency bandwidth. This makes it possible to derive the transfer function $\theta/\theta_b$ and set it equal to $\ddot{\theta}/\ddot{\theta}_b$:

$$TR = \frac{\ddot{\theta}}{\ddot{\theta}_b} = \frac{-\omega^2\theta}{-\omega^2\theta_b} = \frac{\theta}{\theta_b} \qquad \textbf{(W.1)}$$

Consider figure 5.5.1. The displacement of the moving base is denoted by $y_b$. The base mass, stiffness and excitation force, are respectively denoted by $k_b$, $m_b$ and $F_b$.

In this derivation, $y_b$ is a known signal, i.e. the disturbance signal. For a known base displacement, the system displacement vector is given by:

$$y = \left\{ \{y_{a1}\} \quad w_s(x) \quad \{y_{a2}\} \right\}^T \qquad \textbf{(W.2)}$$

The equation of motion of actuator II, for a base *translational* displacement input $y_b$, is:

$$\begin{bmatrix} m_{a21} & 0 \\ 0 & m_{a22} \end{bmatrix} \begin{Bmatrix} \ddot{y}_{a21} \\ \ddot{y}_{a22} \end{Bmatrix} + \begin{bmatrix} k_{211}+k_{212} & -k_{212} \\ -k_{212} & k_{212}+k_{222} \end{bmatrix} \begin{Bmatrix} y_{a21} \\ y_{a22} \end{Bmatrix} = \begin{Bmatrix} k_{211} \\ k_{222} \end{Bmatrix} y_b \qquad \textbf{(W.3)}$$

The equation of motion, for a base *angular* displacement input $\theta_b$, is:

$$\begin{bmatrix} m_{a21} & 0 \\ 0 & m_{a22} \end{bmatrix} \begin{Bmatrix} \ddot{y}_{a21} \\ \ddot{y}_{a22} \end{Bmatrix} + \begin{bmatrix} k_{211}+k_{212} & -k_{212} \\ -k_{212} & k_{212}+k_{222} \end{bmatrix} \begin{Bmatrix} y_{a21} \\ y_{a22} \end{Bmatrix} = l \begin{Bmatrix} k_{211} \\ k_{222} \end{Bmatrix} \theta_b \qquad \textbf{(W.4)}$$

where $l$ is the horizontal distance between the two actuators.

The equation of motion of motion of actuator II, in modal coordinates, is:

$$M_{a1} \begin{Bmatrix} \ddot{q}_{a21} \\ \ddot{q}_{a22} \end{Bmatrix} + K_{a1} \begin{Bmatrix} q_{a21} \\ q_{a22} \end{Bmatrix} = \{F_{a2}\} \qquad \textbf{(W.5)}$$

where $\{F_{a2}\}$ is the modal excitation force vector, given by:

$$\{F_{a2}\} = l \psi_{a2}^T \begin{Bmatrix} k_{211} \\ k_{222} \end{Bmatrix} \theta_b \qquad \textbf{(W.6)}$$

The system equation of motion, in component modal coordinates, is:

$$M\ddot{q} + Kq = F \qquad \textbf{(W.7)}$$

where $F$ is the modal base excitation force.

$M$, $K$, $q$ and $F$ are respectively given by:

$$M = \begin{bmatrix} [M_{a1}] & & \\ & [M_s] & \\ & & [M_{a2}] \end{bmatrix} \qquad \textbf{(W.8a)}$$

$$K = \begin{bmatrix} [K_{a1}] & & \\ & [K_s] & \\ & & [K_{a2}] \end{bmatrix} \qquad \textbf{(W.8b)}$$

$$q = \begin{Bmatrix} \{q_{a1}\} \\ \{q_s\} \\ \{q_{a2}\} \end{Bmatrix} \qquad \textbf{(W.8c)}$$

$$F = \begin{Bmatrix} \{0\} \\ \{0\} \\ \{F_{a2}\} \end{Bmatrix} \qquad \textbf{(W.8d)}$$

The sizes of $M$ and $K$ are 14 x 14 each, while those of $q$ and $F$ are 14 x 1 each.

The equations of motion of the actuators and structure are currently uncoupled. Coupling is done by means of the modal coupling equation:

$$q = Cq_r \tag{W.9}$$

where $q_r$ is the coupled modal displacement vector and $C$ is the coupling matrix, given by:

$$C = \begin{bmatrix} 1 & \{0\} & 0 \\ 1 & -\{\psi_s(0)\} & 0 \\ \{0\} & [I] & \{0\} \\ 0 & \{0\} & 1 \\ 0 & -\{\psi_s(l)\} & 1 \end{bmatrix} \tag{W.10}$$

The sizes of $C$ and $q_r$ are 14 x 12 and is 12 x 1 respectively. The coupling matrix given above, is the $C$-matrix given in equation 5.5.38, whose last row and last column are deleted.

The coupled system modal equation of motion is:

$$M_r\ddot{q}_r + K_r q_r = F_r \tag{W.11}$$

where $M_r$ and $K_r$ are given by equations 5.5.41 and $F_r$ is given by:

$$F_r = C^T F \tag{W.12}$$

The reduced coordinate vector $q_r$ is written as follows in terms of the eigenvector $U$ and the normal mode displacement vector $q_n$ (see equation 5.5.42):

$$q_r = Uq_n \tag{W.13}$$

The sizes of $U$ and $q_n$ are 12 x 12 and 12 x 1 respectively.

Substitution of equation W.13 into equation W.11 and premultiplication of the resulting equation with $U^T$, gives:

$$M^*\ddot{q}_n + K^* q_n = Q \tag{W.14}$$

where $M^*$ and $K^*$ are the normal mode mass and stiffness matrices respectively, as given by equations 5.5.48. $Q$ is the modal excitation force vector, given by:

$$Q = U^T C^T F \tag{W.15}$$

Premultiplication of equation W.14 with $M^{*-1}$ gives the normal mode equation of motion in the following form:

$$\ddot{q}_n + \Omega^2 q_n = M^{*-1} Q \tag{W.16}$$

where $\Omega$ is the diagonal natural frequency matrix.

Adding modal damping terms to equation W.16 gives:

$$\ddot{q}_n + 2Z\Omega\dot{q}_n + \Omega^2 q_n = M^{*-1}Q \qquad \textbf{(W.17)}$$

The modal state and output equations can be written as follows:

$$\dot{x} = A_h x + B_h \theta_h \qquad \textbf{(W.18a)}$$
$$\theta = C_h x + D_h \theta_h \qquad \textbf{(W.18b)}$$

The state vector $x$ is:

$$x = \begin{Bmatrix} q_n \\ \dot{q}_n \end{Bmatrix} \qquad \textbf{(W.19)}$$

$A_h$, $B_h$, $C_h$ and $D_h$ are respectively given by:

$$A_h = \begin{bmatrix} 0 & I \\ -\Omega^2 & -2Z\Omega \end{bmatrix} \qquad \textbf{(W.20a)}$$

$$B_h = \begin{Bmatrix} \{0\} \\ M^{*-1}U^T C^T \begin{Bmatrix} \{0\} \\ \{0\} \\ l\psi_{a2}^T \begin{Bmatrix} k_{211} \\ k_{222} \end{Bmatrix} \end{Bmatrix} \end{Bmatrix} \qquad \textbf{(W.20b)}$$

$$C_h = \begin{Bmatrix} \dfrac{\Phi_s(x_2) - \Phi_s(x_1)}{x_2 - x_1} & \{0\} \end{Bmatrix} \qquad \textbf{(W.20c)}$$

$$D_h = 0 \qquad \textbf{(W.20d)}$$

The sizes of $A_h$, $B_h$, $C_h$ and $D_h$ are 24 x 24, 24 x 1, 1 x 24 and 1 x 1 respectively.

Combining equations W.18 to W.20 gives:

$$\begin{Bmatrix} \dot{q}_n \\ \ddot{q}_n \end{Bmatrix} = \begin{bmatrix} 0 & I \\ -\Omega^2 & -2Z\Omega \end{bmatrix} \begin{Bmatrix} q_n \\ \dot{q}_n \end{Bmatrix} + \begin{Bmatrix} \{0\} \\ M^{*-1} U^T C^T \begin{Bmatrix} \{0\} \\ \{0\} \\ l\psi_{a2}^T \begin{Bmatrix} k_{211} \\ k_{222} \end{Bmatrix} \end{Bmatrix} \end{Bmatrix} \theta_b \qquad \textbf{(W.21a)}$$

$$\theta = \begin{bmatrix} \dfrac{\Phi_s(x_2) - \Phi_s(x_1)}{x_2 - x_1} & \{0\} \end{bmatrix} \begin{Bmatrix} q_n \\ \dot{q}_n \end{Bmatrix} \qquad \textbf{(W.21b)}$$

The system transmissibility is the *TF* between $\theta_b$ and $\theta$ is given by:

$$\frac{\theta}{\theta_b} = C_b [sI - A_b]^{-1} B_b \qquad \textbf{(W.22)}$$

By application of equation W.1, the *TR*, i.e. the *TF* between $\ddot{\theta}_b$ and $\ddot{\theta}$, is given by:

$$\frac{\ddot{\theta}}{\ddot{\theta}_b} = C_b [sI - A_b]^{-1} B_b \qquad \textbf{(W.23)}$$

The number of state equations, for the selected number of actuator and optical instrument assumed modes, is 24. The system as described by equations W.21 has 24 eigenvalues in complex conjugate pairs. However, many of the eigenvalues occur at high frequencies, well above the bandwidth, and have no significant effect on system performance inside the band. States corresponding with these frequencies, can therefore be eliminated. This was also done for the coil voltage input, where, apart from the three coil states, only the first ten mechanical subsystem states were retained. For the base input, the 5$^{th}$ and 10$^{th}$ states (corresponding with the 5$^{th}$ normal mode) are eliminated, while the 1$^{st}$ to 4$^{th}$ and 6$^{th}$ to 9$^{th}$ states (corresponding with the first four normal modes) are retained.

The transmissibility magnitude and phase spectra, for a frequency bandwidth of 0 to 500 Hz, are shown in figure W.1.

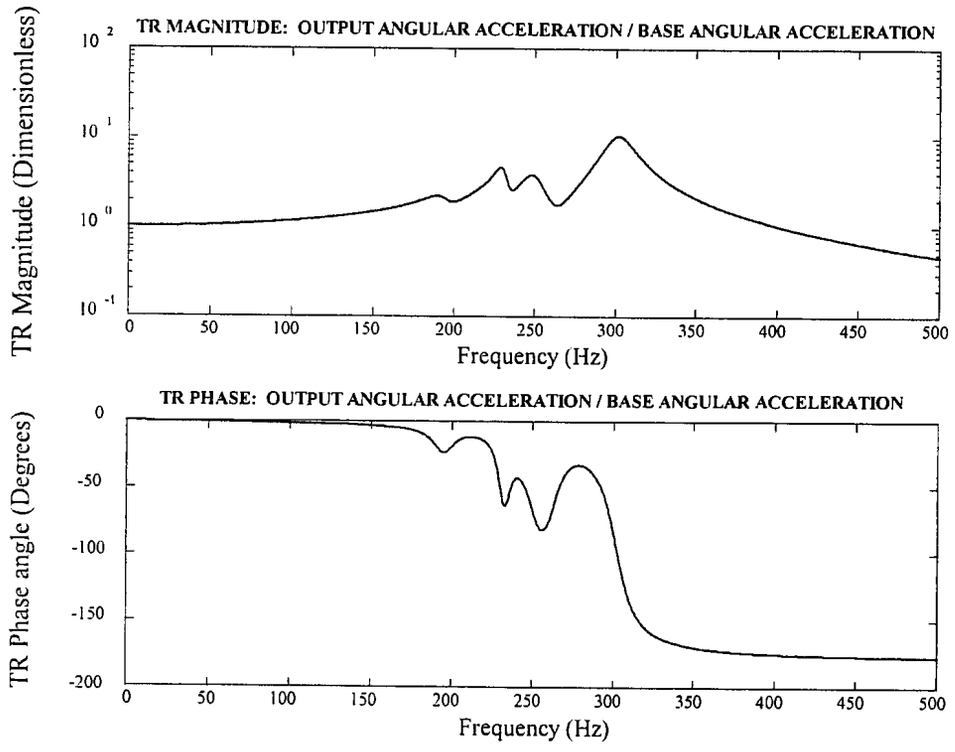


**Figure W.1: System base to output transmissibility spectra**

## Two-input state-space model for control system analysis and design purposes

The state-space model of the system currently consists of two separate state models, one for the coil voltage input, given by equations 5.6.6 to 5.6.9, and one for the base angular acceleration input, given by equations W.18 to W.23. For the purpose of analyzing and designing the control system, it is convenient to combine the two state models into a single state model, with two simultaneous inputs, i.e. coil voltage and base angular acceleration. The coil voltage is the controllable input, while the base motion is the disturbance. The state and output equations, for these two inputs, are:

$$\dot{x} = Ax + B\begin{Bmatrix} V \\ \ddot{\theta}_b \end{Bmatrix} \qquad \textbf{(W.24a)}$$

$$\ddot{\theta} = Cx + D\begin{Bmatrix} V \\ \ddot{\theta}_b \end{Bmatrix} \qquad \textbf{(W.24b)}$$

The state vector, from equation 5.6.6, is:

$$x = \begin{Bmatrix} q_n \\ \dot{q}_n \\ x_c \end{Bmatrix} \qquad \textbf{(W.25)}$$

$A$ is the system coefficient matrix, given in equation 5.6.9a:

$$A = \begin{bmatrix} [0] & [I] & [0] \\ -\Omega^2 & -2Z\Omega & M^{*-1}\Phi_s^T F_l C_c \\ [0] & [0] & A_c \end{bmatrix} \qquad \textbf{(W.26)}$$

The first ten rows and columns of $A$ correspond with $A_h$ in equation equation W.20a.

$B$ is a matrix with two vector columns:

$$B = [B_V \quad B_{\ddot{\theta}h}] \qquad \textbf{(W.27)}$$

$B_V$ is given by equation 5.6.9b:

$$B_V = \begin{Bmatrix} \{0\} \\ \{0\} \\ B_c \end{Bmatrix} \qquad \textbf{(W.28a)}$$

For the first four normal modes, $B_{\ddot{\theta}h}$ is given by:

$$B_{\ddot{\theta}h} = \begin{Bmatrix} \{B_h\}_{rows\,1-4} \\ 0 \\ \{B_h\}_{rows\,13-16} \\ 0 \\ \begin{Bmatrix} 0 \\ 0 \\ 0 \end{Bmatrix} \end{Bmatrix} \qquad \textbf{(W.28b)}$$

$C$ is the output matrix given in equation 5.6.9c:

$$C = \frac{\Phi_s(x_2) - \Phi_s(x_1)}{x_2 - x_1}\left[-\Omega^2 \quad -2Z\Omega \quad M^{*-1}\Phi_s^T F_l C_c\right] \qquad \textbf{(W.29)}$$

$D$ is a row vector with two zero elements:

$$D = \{0 \quad 0\} \qquad \textbf{(W.30)}$$

Note that the $C$-matrix in equation W.29 corresponds with the $C$-matrix in equation 5.6.9c. However, this $C$-matrix does not correspond with $C_h$ in equation W.20c. In order to obtain a $C$-matrix, which is valid for both inputs, the elements of $B_{\ddot{\theta}h}$ are modified as explained next.

The procedure is as follows: Equations W.21 are written in canonical form, whereby uncoupled state and output equations for each normal mode are obtained. Each modal state equation is then written as follows in *TF* form, using equation W.1:

$$\left(\frac{\ddot{\theta}}{\ddot{\theta}_h}\right)_i = \left(\frac{\theta}{\theta_h}\right)_i = C_i\left[sI - A_i\right]^{-1} B_i \qquad \textbf{(W.31)}$$

where the subscript $i$ denotes the $i$-th normal mode. The sizes of $A_i$, $B_i$, $C_i$ and $D_i$ are respectively 2 x 2, 2 x 1, 1 x 2 and 1 x 1.

Equation W.31 is written as follows for the $i$-th mode:

$$\left(\frac{\ddot{\theta}}{\ddot{\theta}_h}\right)_i = \{C_1 \quad C_2\}_i \begin{bmatrix} \dfrac{s - A_{22}}{s^2 - (A_{11} + A_{22})s + A_{11}A_{22} - A_{21}A_{12}} & \dfrac{A_{12}}{s^2 - (A_{11} + A_{22})s + A_{11}A_{22} - A_{21}A_{12}} \\ \dfrac{A_{21}}{s^2 - (A_{11} + A_{22})s + A_{11}A_{22} - A_{21}A_{12}} & \dfrac{s - A_{11}}{s^2 - (A_{11} + A_{22})s + A_{11}A_{22} - A_{21}A_{12}} \end{bmatrix}_i \begin{Bmatrix} B_1 \\ B_2 \end{Bmatrix}_i$$

**(W.32)**

Expanding equation W.32 gives:

$$\left(\frac{\ddot{\theta}}{\ddot{\theta}_h}\right)_i = \left(\frac{p_1 s + p_0}{s^2 + q_1 s + q_0}\right)_i \qquad \textbf{(W.33)}$$

where:

$$p_{0i} = \left(-A_{11}B_2C_2 + A_{12}B_2C_1 + A_{21}B_1C_2 - A_{22}B_1C_1\right)_i \qquad \textbf{(W.34a)}$$

$$p_{1i} = \left(B_1C_1 + B_2C_2\right)_i \qquad \textbf{(W.34b)}$$

$$q_{0i} = \left(A_{11}A_{22} - A_{12}A_{21}\right)_i \qquad \textbf{(W.34c)}$$

$$q_{1i} = \left(-A_{11} - A_{22}\right)_i \qquad \textbf{(W.34d)}$$

The input voltage to angular acceleration *TF* is subsequently written in canonical form to obtain an uncoupled state and output equation for each of the first four normal modes. The modal state equation for the $i$-th mode is then written as follows, in the *TF* form of equation W.33:

$$\left(\frac{\ddot{\theta}}{V}\right)_i = C_i\left[sI - A_i\right]^{-1} B_i \qquad \textbf{(W.35)}$$

Equations W.34a and W.34b are written in matrix form as:

$$\begin{bmatrix} C_1 & C_2 \\ A_{21}C_2 - A_{22}C_1 & A_{12}C_1 - A_{11}C_2 \end{bmatrix}_i \begin{Bmatrix} B_1 \\ B_2 \end{Bmatrix}_i = \begin{Bmatrix} p_1 \\ p_0 \end{Bmatrix}_i \qquad \textbf{(W.36)}$$

where $C_{1i}$ and $C_{2i}$ are the elements of $C_i$ in equation W.35. From equation W.36, $B_{1i}$ and $B_{2i}$ are determined as follows:

$$\begin{Bmatrix} B_1 \\ B_2 \end{Bmatrix}_i = \begin{bmatrix} C_1 & C_2 \\ A_{21}C_2 - A_{22}C_1 & A_{12}C_1 - A_{11}C_2 \end{bmatrix}_i^{-1} \begin{Bmatrix} p_1 \\ p_0 \end{Bmatrix}_i \qquad \textbf{(W.37)}$$

The resulting $B_{\ddot{\theta}h}$ -vector, is:

$$B_{\ddot{\theta}h} = \{(B_1)_{i=1} \quad (B_1)_{i=2} \quad (B_1)_{i=3} \quad (B_1)_{i=4} \quad 0 \quad (B_2)_{i=1} \quad (B_2)_{i=2} \quad (B_2)_{i=3} \quad (B_2)_{i=4} \quad 0 \quad 0 \quad 0 \quad 0\}^T \qquad \textbf{(W.38)}$$

Equations W.24 therefore become:

$$\begin{Bmatrix} \dot{q}_n \\ \ddot{q}_n \\ \dot{x}_c \end{Bmatrix} = \begin{bmatrix} [0] & [I] & [0] \\ -\Omega^2 & -2Z\Omega & M^{*-1}\Phi_s^T F_l C_c \\ [0] & [0] & A_c \end{bmatrix} \begin{Bmatrix} q_n \\ \dot{q}_n \\ x_c \end{Bmatrix} + \begin{bmatrix} B_V & B_{\ddot{\theta}h} \end{bmatrix} \begin{Bmatrix} V \\ \ddot{\theta}_h \end{Bmatrix} \qquad \textbf{(W.39a)}$$

$$\ddot{\theta} = \frac{\Phi_s(x_2) - \Phi_s(x_1)}{x_2 - x_1} \begin{bmatrix} -\Omega^2 & -2Z\Omega & M^{*-1}\Phi_s^T F_l C_c \end{bmatrix} \begin{Bmatrix} q_n \\ \dot{q}_n \\ x_c \end{Bmatrix} \qquad \textbf{(W.39b)}$$

# Appendix X
# General control system requirements

General controller requirements are normally expresessed in terms of performance factors such as accuracy, stability, sensitivity, reaction speed, control effort, robustness, observability and controllability. These factors are discussed in short below, together with methods to meet the requirements.

## X.1 Accuracy

Control accuracy is influenced by parameters such as transient overshoot, settling time, DC error, tracking error and disturbance attenuation over a given bandwidth. Excessive transient overshoot may damage the plant and must therefore be reduced to within a safe range. Two simple methods of transient overshoot control, are rate feedback and PID-control [Schwarzenbach & Gill, 1986]. Differentiation of the error signal, by means of a differentiator (D) element, in parallel with the P and I elements, will lower the overshoot peak. The higher the D-element gain, the lower the overshoot. However, the higher the D-element gain, the longer the transient rise time.

Rate feedback is accomplished by placing a differentiator in parallel with the output feedback elements. A disadvantage of rate feedback is that it may drive the plant unstable if control is non-collocated.

Settling time is the time it takes the system output to reach and stay within 5% of the steady-state value, during step excitation [Schwarzenbach & Gill, 1986]. The settling time $T$ of a system with distinct, complex poles, can be obtained from the following approximate equation:

$$T \approx \frac{5}{\zeta_1 \omega_1} \qquad \textbf{(X.1.1)}$$

where $\omega_1$ is the lowest angular natural frequency and $\zeta_1$ is the corresponding damping factor.

DC error is the deviation of the system output from the setpoint, after the settling time has elapsed. A simple method of eliminating DC error is to integrate the error signal, by means of an integrator element, placed in parallel with the proportional element. The disadvantage of this measure is that it will lower the damping required to limit transient overshoot [Schwarzenbach & Gill, 1986].

Tracking error is the relative error between the reference signal and output. It is, as the name indicates, only applicable to tracking controllers. Tracking error may depend on a variety of factors, such as the transient phenomena discussed above, system frequency bandwidth, nonlinearities, measurement noise, control hardware throughput delay, as well as sensor range, resolution and bandwidth. All of these factors must necesssarily be addressed during the design of a tracking controller. This is, however, beyond the scope of this study.

Disturbance attenuation, on the other hand, is important in this study. The plant must provide the necessary filtering characteristics to reject the base disturbance, in order to obtain a sufficiently low output angular acceleration. Due to noise and unmodelled plant characteristics, such as nonlinearities, it will be extremely difficult to totally reject the disturbance. Instead, the remaining output must be minimized. The ratio of the remaining output to the base disturbance, is known as the attenuation factor. This factor is a measure of determining the performance of the system. The attenuation factor was discussed in more detail in section 6.3.1.

Control accuracy may also be affected by the control system type. It may for instance be attractive, from a cost point of view, to use an analogue controller, instead of a digital controller. Simple analogue controllers, although outdated, do not require digital signal processing equipment, analogue-to-digital (A/D) and digital-to-analogue (D/A) converters.

The limitation of an analogue controller, however, is that the required feedforward and feedback characteristics may be difficult to obtain. If the controller does not perform as originally anticipated during the design, certain parameters may have to be changed. Whereas this is easily accomplished with digital controllers, it may be extremely difficult with analogue controllers. The reason is that analogue equipment such as resistors, capacitors and inductors, may not have the required range of adjustment. While rheostats have been around for a long time, adjustable capacitances are currently only available in capacitors with relatively small capacitances.

## X.2 Stability

Stability, together with accuracy, is probably the most important requirement of a control system. Stability of a linear time invariant (LTI) system is determined by the real parts of its eigenvalues: An LTI system is unconditionally stable if the real parts of all its eigenvalues are negative.

This statement must, however, be qualified for a *linearized* system. Linear systems analysis applied to a nonlinear system, may only be accurate over a limited working range. This phenomenon was discussed in detail in section 2.7. The equivalent linear range will depend on the nature of the nonlinearity. A weakly nonlinear system may have a fairly large linear range of operation and may therefore be accurately represented by a linear model. Linear stability (gain and phase) margins of the linearized system will closely approximate those of the nonlinear system. This system type can be relatively easily stabilized by a linear controller.

On the other hand, a strongly nonlinear system may have relatively small linear ranges of operation, also known as regions of local stability. If the system is operated inside any of these regions, it will be stable. If operated outside these regions, it will be unstable. Such a system is globally unstable. Local and global stability are discussed in more detail by Slotine & Li [1991].

Nonlinear systems may be accurately controlled and stabilized by nonlinear controllers. The design and implementation of nonlinear controllers is however beyond the scope of this study.

Alternatively, a nonlinear plant may be controlled by a linear controller, with sufficient robustness to compensate for changes in characteristics (e.g. DC gains, natural frequencies and damping factors), without sacrificing other important performance parameters (e.g. accuracy). Techniques of improving system robustness will be discussed in section X.6.

## X.3 Sensitivity

Sensitivity of a control system depends on two factors, i.e. parameter sensitivity and sensor sensitivity. Parameter sensitivity can be described as the "inverse phenomenon" of robustness, i.e. a more robust system is less sensitive to a change in the value of a specific parameter. Robustness will be discussed in short in section X.6. More detailed discussions on the subject are provided by D'Azzo & Houpis [1986], Maciejowski [1989], Skogestad & Postlethwaite [1997], Slotine & Li [1991] and Tsui [1996].

Sensor sensitivity mainly depends on sensor resolution and sensor calibration factor. Sensor resolution is the smallest increment in a measured signal to which a sensor will respond [Cooper & Helfrick, 1985]. The smaller the increment, the better the resolution. Sensor resolution is an important parameter in vibration isolation applications. The objective of vibration isolation is to obtain output signals with low magnitudes, in comparison with the disturbances. In order to measure and control accurately, sensors must be able to respond to small changes in outputs.

Calibration factor is the ratio of the sensor output signal to the measured variable [Cooper & Helfrick, 1985]. The calibration factor of an accelerometer, for instance, is the ratio of the output voltage to the measured acceleration, and is normally expressed in mV/g. The most suitable calibration factor is determined by the full-scale range of the data acquisition equipment. It is preferable that this range correspond to the output range of the sensor, as it will eliminate the need for unduly high control signal gains. (In section 4.3.3, for example, it was mentioned that the coil voltage exceeded the signal analyzer range, and had to be scaled by means of a voltage divider, before it could be measured).

## X.4 Reaction speed

Reaction speed is determined by two main factors, i.e. controller frequency bandwidth and throughput lag. The required frequency bandwidth can be obtained during the design phase, by calculation of the controller feedforward and feedback parameters. Optimal and pole-placement design techniques are often used for this purpose. The cutoff frequency of the controlled system can be verified by comparing it with the required cutoff-frequency.

Throughput lag is the time it takes to execute the A/D conversion of sensor signals, apply digital control (e.g. by feedforward and feedback compensation, digital filtering, frequency shaping, addition, subtraction, gaining and clipping of signals) and convert the signals back to analogue form. The lag is often also expressed in terms of data buffer length or number of samples.

The lag depends, inter alia, on the control hardware configuration. If the controller runs on its own processor (DSP), the DSP does the A/D and D/A conversion, as well as the control calculations. The processor must be specifically programmed for this purpose. Programming is normally done externally, in languages like Assembler, C, Pascal, Quick Basic, or Visual Basic, whereafter the program is compiled and loaded onto the processor. Some processors may be programmed and compiled from graphic environments like Simulink (see section 4.4). Processing speed mainly depends on the DSP clock speed. Compiling of the program necessarily improves throughput speed.

## X.5 Control effort

Control effort is the input required to drive the plant to its desirable output. In the case of the magnetostrictive LOS stabilization system, coil voltage is the input, and the optical instrument angular acceleration is the output. The objective is to minimize the output. While this is an important goal, it must be achieved with as little control effort as possible. Both the output and control effort must therefore be minimized. This process is known as optimization. A type of controller which simultaneously minimizes output and control input, is an optimal regulator.

The optimal feedforward and feedback control parameters are determined mathematically, by application of methods such as variational optimization and linear quadratic optimal regulator (LQR) design. In order to obtain a criterion which can be used to evaluate system optimality, and which can be expressed in terms of a single numerical value, an objective function is defined. This function, also known as the cost function, must be minimized to obtain the optimal control parameters.

The linear quadratic (LQ) optimal cost function for the regulator problem under discussion, is:

$$J = \int_{t=0}^{t=T} \left[ y^2(t) + u^2(t) \right] dt \qquad \textbf{(X.5.1)}$$

where $J$ is the cost function.

In equation X.5.1, the output and control are equally weighed. The output and control can be separately weighed, as follows:

$$J = \int_{t=0}^{t=T} \left[ Q_y y^2(t) + R u^2(t) \right] dt \qquad \textbf{(X.5.2)}$$

where $Q_y$ and $R$ are the output and control weights, respectively.

The cost function is more conveniently expressed in matrix form, where $y$ and $u$ are vectors:

$$J = y^T Q_y y + u^T R u \qquad \textbf{(X.5.3)}$$

The cost function can be extended to include a term which contains the product of the input and output:

$$J = \int_{t=0}^{t=T} \left[ Q_y y^2(t) + Ru^2(t) + Ny(t)u(t) \right] dt \qquad \textbf{(X.5.4)}$$

where $N$ is the weight of the product $yu$. Inclusion of this term may result in a cost function which cannot strictly be termed "linear quadratic", as $yu$ will only be positive for all $t$ if $u$ and $y$ are in phase. This is however not the case with the magnetostrictive active vibration isolation system (see figure 4.5.2.3). For this reason, the $yu$-term will henceforth not be included in the cost function.

Optimization can either be unconstrained or constrained. Unconstrained optimization means that neither $y$ nor $u$ is bounded. An example of an unconstrained optimization equation is given by equation X.5.2. The equation does not supply sufficient information to minimize $J$, since there is no relationship between $u$ and $y$. The required relationship is supplied by the state and output equations, which are the constraint equations for the LQR state regulation problem under discussion:

$$\dot{x} = Ax + B_u u + B_d d \qquad \textbf{(X.5.5a)}$$

$$y = Cx \qquad \textbf{(X.5.5b)}$$

Equations X.5.5 may not necessarily be the only constraint equations. Constraints can be added to suit the problem. Although the input is accounted for in the cost function, it may exceed the available supply. To avoid this, an additional constraint, i.e. available source voltage (+28 V for the magnetostrictive active isolation system) can be added. Another constraint, which can be added in the interest of robustness, is minimum damping.

A relationship between the states and control, which satisfies equations X.5.3 and X.5.5 above, is required. In a state-controlled linear system, the control is a linear combination of the states:

$$u = -Kx \qquad \textbf{(X.5.6)}$$

where $K$ is the optimal state feedback gain, or "state feedback control law". A necessary condition for equation X.5.6 is that all the states be known from measured outputs. This property, which is known as observability, will be discussed later.

The elements of $K$ can be determined in a number of ways, e.g. by variational optimization methods and by solving the algebraic Riccati equation (ARE). The Riccati equation, in its steady state form, is:

$$Q_x + A^T S_{ss} + S_{ss} A - S_{ss} B_u R^{-1} B_u^T S_{ss} = 0 \qquad \textbf{(X.5.7)}$$

where $S_{ss}$ is the steady-state Riccati matrix and $Q_x$ is the state weight, related to $Q_y$ by:

$$Q_x = C^T Q_y C \qquad \textbf{(X.5.8)}$$

Equation X.5.7 must be solved to obtain the steady-state Riccati matrix. A solution method often used, is Hamiltonian eigenvector decomposition, which is described in detail by Meirovitch [1990].

The optimal feedback gain matrix $K$ is given in terms of the Riccati matrix as:

$$K = R^{-1} B_u^T S_{ss} \qquad \textbf{(X.5.9)}$$

The closed-loop state and output equations are obtained by substitution of equation X.5.6 into equation X.5.5:

$$\dot{x} = (A - B_u K)x + B_d d \qquad \textbf{(X.5.10a)}$$

$$y = Cx \qquad \textbf{(X.5.10b)}$$

It can be seen from equation X.5.10a that the only input to the closed-loop regulator, is the disturbance $d$.

The closed-loop eigenvalues are the values of $s$ for which:

$$\left| sI - (A - B_u K) \right| = 0 \qquad \textbf{(X.5.11)}$$

The block diagram of the plant and state feedback regulator, with state and control equations given by equations X.5.5 and X.5.6 respectively, is shown in figure X.5.1.

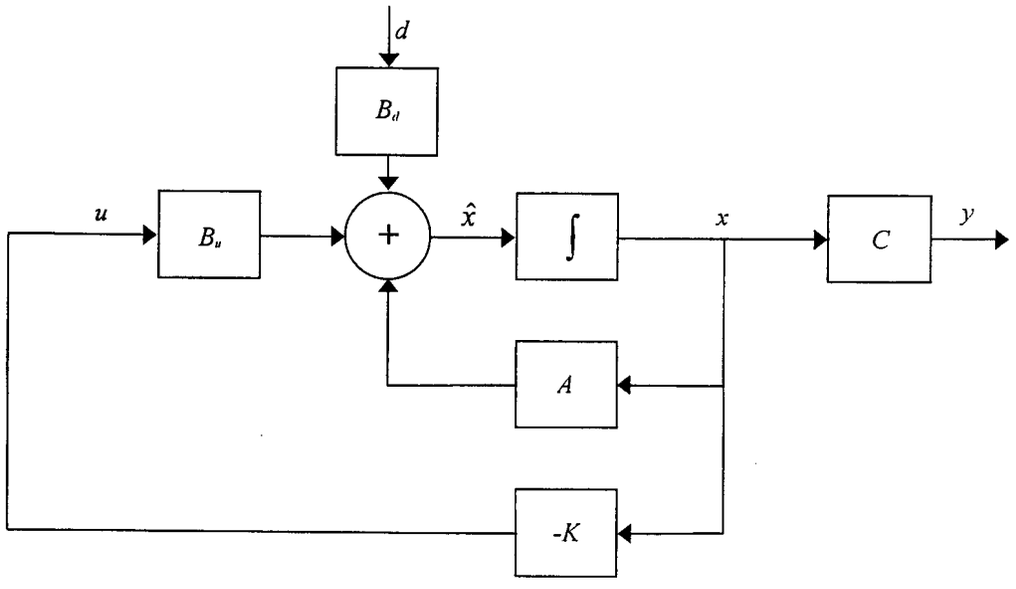


**Figure X.5.1: State feedback regulator block diagram**

More thorough discussions on optimal control can be found in Anderson & Moore [1989], Brogan [1985], D'Azzo & Houpis [1986], Kirk [1970], Kuo [1982] and Meirovitch [1990].

## X.6 Robustness

The ability of a controller to meet its performance criteria in the presence of plant, input, disturbance and measurement noise uncertainties, is known as robustness. An example of a plant uncertainty is a nonlinearity, which may cause the plant to display different characteristics at different excitation levels. Depending on the nature of the nonlinearity, a robust controller will partly or fully compensate for the changes in characteristics.

Examples of input and disturbance uncertainties are DC offsets, which may be attributed to unmodelled sensor characteristics. A typical example is the DC characteristic of an accelerometer. Theoretically, an accelerometer has a zero DC output, but practically, the output voltage may contain a DC component. Resistive accelerometers, in particular, display this characteristic. Noise uncertainties may include input and output sensor noise, noise generated by measurement equipment, such as amplifiers, and electromagnetic noise in unscreened cables.

Linear quadratic (LQ) optimal state feedback controllers are seldom robust [Kuo, 1982]. The reason is that these controllers often operate on the principle of pole-zero cancellation, i.e. the frequency and damping factor of a *TF* pole coincide with those of a *TF* zero. When the plant is excited at the design drive level, the zero will exactly cancel the pole. If, however, the drive level is slightly altered, phenomena such as nonlinear plant behaviour may cause the frequency and damping factor of the pole to shift, to such an extent that it may no longer coincide with those of the zero. The pole may not be cancelled at all, with the result that transmissibility of the closed-loop system may be worse than that of a system without vibration isolation.

A number of solutions exist to improve robustness, three of which are as follows: Firstly, pole damping may be increased, using pole-placement techniques. If the pole shifts within a narrow frequency band, it will still be partly cancelled by the zero. Although performance, in terms of attenuation, will not match that of the LQ optimal controller, robustness will improve.

Secondly, the optimality constraints (see equations X.5.5) may be expanded to include minimum closed-loop damping factors. Although this measure may complicate the solution of the Riccati equation, the optimal feedback gain may be obtained by application of alternative optimization methods, such as variational methods.

Thirdly, a solution suggested by Kuo [1982], is to place an output integrator, with gain $H_I$, in parallel with the state feedback matrix, as shown in figure X.6.1. The effect of this method on improving the robustness of an absolute motion controller was discussed in section 6.3.8.5.

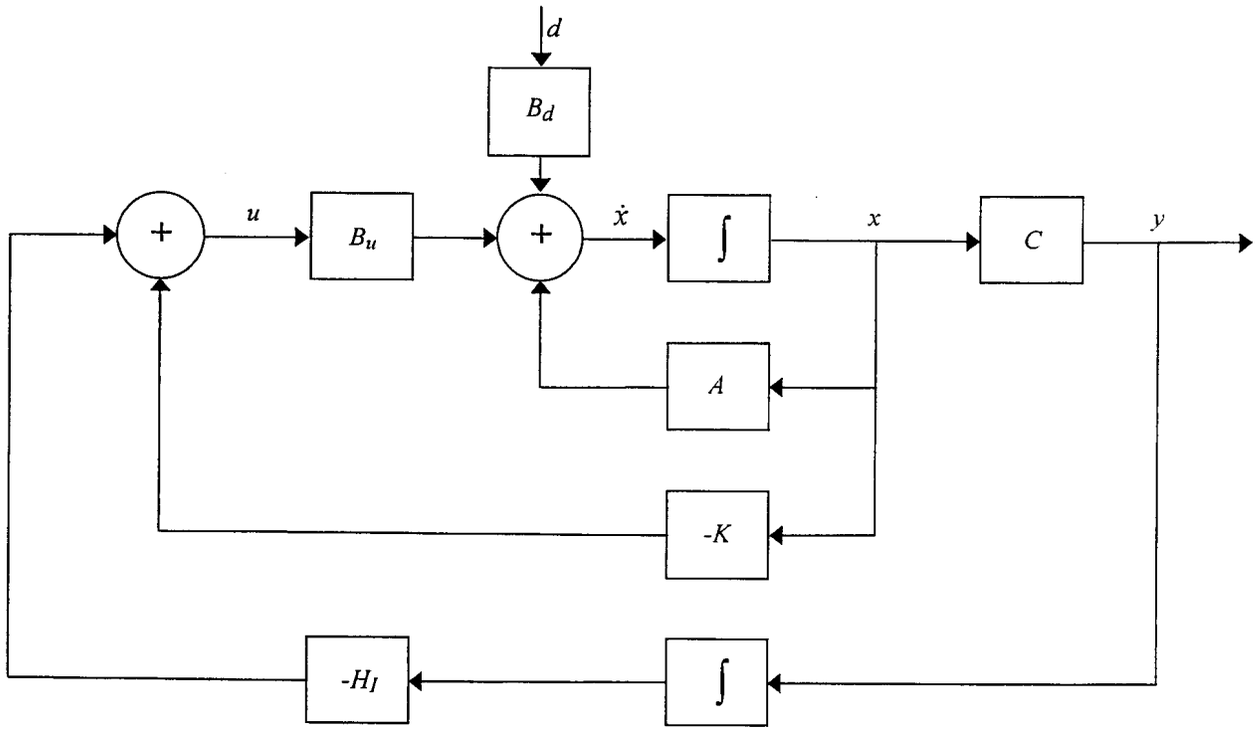


**Figure X.6.1: State plus output integral feedback regulator block diagram**

The control law is of the following form:

$$u = -Kx - H_I \int y dt \qquad \textbf{(X.6.1)}$$

Differentiation of equation X.6.1 with respect to time, gives:

$$\dot{u} = -K\dot{x} - H_I y \qquad \textbf{(X.6.2)}$$

Substitution of equations X.5.5 into equation X.6.2 and simplification of the resulting equation gives:

$$\dot{u} = -\left(KA + H_I C\right)x - KB_u u - KB_d d \qquad \textbf{(X.6.3)}$$

Equation X.6.3 is the controller state equation. The term $KA + H_I C$ couples the plant and controller state equations.

Combination of the plant and controller state and output equations X.5.5 and X.6.3 gives the closed-loop system state-space equations as follows:

$$\dot{x}_{cl} = A_{cl}x_{cl} + B_{cl}d \qquad \textbf{(X.6.4a)}$$

$$y_{cl} = C_{cl}x_{cl} \qquad \textbf{(X.6.4b)}$$

where $x_{cl}$ is the closed-loop state vector, given by:

$$x_{cl} = \begin{Bmatrix} x \\ u \end{Bmatrix} \qquad \textbf{(X.6.5)}$$

$A_{cl}$, $B_{cl}$ and $C_{cl}$ are the closed-loop coefficient, driving and output matrices, respectively given by:

$$A_{cl} = \begin{bmatrix} A & B_u \\ -(KA + H_f C) & -KB_u \end{bmatrix} \qquad \textbf{(X.6.6a)}$$

$$B_{cl} = \begin{bmatrix} B_d \\ -KB_d \end{bmatrix} \qquad \textbf{(X.6.6b)}$$

$$C_{cl} = \begin{bmatrix} C & 0 \end{bmatrix} \qquad \textbf{(X.6.6c)}$$

The eigenvalues of the closed-loop system are the values of $s$ for which:

$$|sI - A_{cl}| = 0 \qquad \textbf{(X.6.7)}$$

The integrator raises the DC and low-frequency content of the control signal, thereby making the system more sensitive to feedback at low frequencies and less sensitive at high frequencies. A typical application is DC disturbance rejection in electric motor control, as explained by Kuo [1982].

The method can also be applied to improve low-frequency behaviour of the magnetostrictive LOS stabilization system, which is the topic of this study. All but one of the plant poles are well in excess of the disturbance band (see table 5.3.2), therefore an integrator will make the system less sensitive to feedback at most of the plant natural frequencies.

However, a disadvantage of this method, is that an integrator in the feedback loop may drive the control to infinity, although the output may be bounded. A cure to the problem is to high-pass filter the control signal. If the filter cutoff frequency is sufficiently low, the DC component will be eliminated, but the desirable low-frequency characteristics will be retained.

More sophisticated robust control methods include loop transfer recovery (LTR), as discussed by Maciejowski [1989], Skogestad & Postlethwaite [1997] and Tsui [1996].

## X.7 Observability

State feedback is a powerful control method, especially for high-order systems. A condition for state control is that the states be observable from output measurements. If all the states can be reconstructed from the output, a system is said to be completely observable, or simply, observable.

Mathematically, the *n*-th order LTI system, whose state and output equations are given by

$$\dot{x} = Ax + Bu \qquad \textbf{(X.7.1a)}$$

$$y = Cx \qquad \textbf{(X.7.1b)}$$

is observable if and only if the matrix

$$\left[C^T \;\vdots\; A^TC^T \;\vdots\; \left(A^T\right)^2C^T \;\vdots\; \cdots \;\vdots\; \left(A^T\right)^{n-1}C^T\right] \qquad \textbf{(X.7.2)}$$

has rank *n* [Kirk, 1970].

Observability makes it possible to observe the states by means of a state observer, or estimator. State observer dynamics can be described by means of observer state and output equations. The inputs to the observer depend on the controller configuration. For an absolute motion controller, i.e. for pure output feedback (see section 6.3.8.2), the observer input is the plant output. For a relative motion controller and an absolute plus base motion controller (see sections 6.3.8.1 and 6.3.8.4), the observer inputs are the plant output and disturbance.

The observer state-space equations, for an absolute plus base motion controller, are:

$$\dot{\hat{x}} = A\hat{x} + B_u u + B_d d + L\left(y - \hat{y}\right) \qquad \textbf{(X.7.3a)}$$

$$\hat{y} = C\hat{x} \qquad \textbf{(X.7.3b)}$$

where $\hat{x}$ is the observed state vector, which differs from the true plant state vector, $A$ is the plant coefficient matrix, $B_u$ is the plant driving matrix for the controllable input $u$, $B_d$ is the plant driving matrix for the disturbance input, $y$ is the plant output, $\hat{y}$ is the observed output and $L$ is the observer driving matrix. The observer state equation for a pure output feedback controller is given by equation X.7.3a, with a zero disturbance driving matrix $B_d$.

For full-state feedback control, the control is a linear combination of the observed states:

$$u = -K\hat{x} \qquad \textbf{(X.7.4)}$$

where $K$ is the state feedback gain matrix.

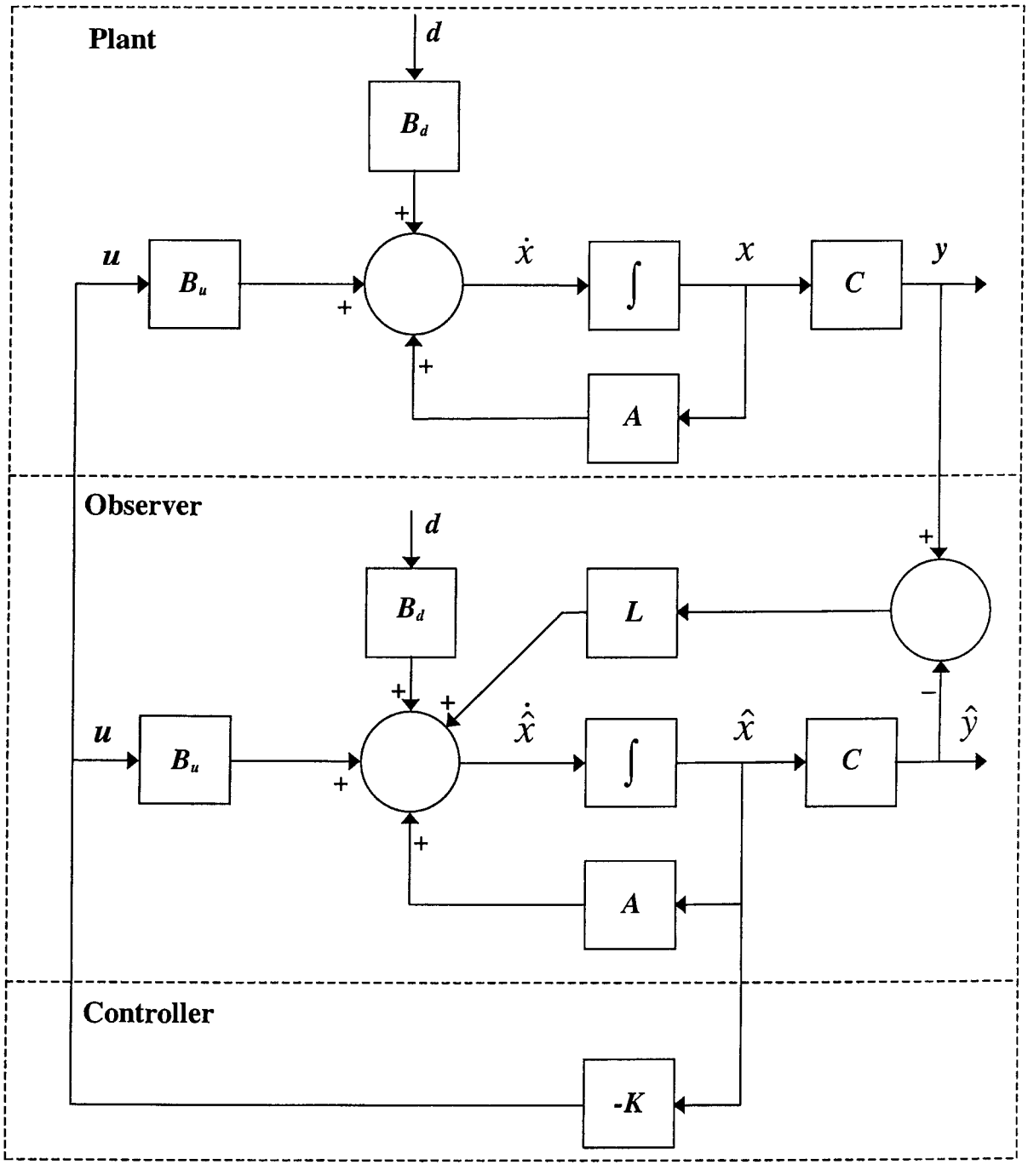


**Figure X.7.1: Block diagram of plant, state observer and state feedback controller**

To conclude, if the system is non-observable, the observable states may still be estimated, by means of a reduced-order observer. Reduced-order observers are described in more detail by Anderson & Moore [1989], Franklin et al [1990] and Kwakernaak & Sivan [1972].

## X.8 Controllability

A system is said to be completely controllable if every state variable can be controlled to reach a certain objective in finite time by some unconstrained control $u$ [Kuo, 1982]. The physical interpretation of controllability is that, if any one of the state variables is independent of the control $u$, driving this particular state to a desired state in finite time by means of $u$ will be impossible. This state is said to be uncontrollable, which means that the system is not completely controllable, or simply uncontrollable [Kuo, 1982].

Controllability can be expressed as follows in terms of the plant state matrices $A$ and $B$. Mathematically, the $n$-th order LTI system, whose state and output equations are given by

$$\dot{x} = Ax + Bu \qquad \textbf{(X.8.1a)}$$

$$y = Cx \qquad \textbf{(X.8.1b)}$$

is controllable if and only if the matrix

$$\left[B \;\vdots\; AB \;\vdots\; A^2B \;\vdots\; \cdots \;\vdots\; A^{n-1}B\right] \qquad \textbf{(X.8.2)}$$

has rank $n$ [Kirk, 1970].

Alternative practical methods of testing controllability of a system are discussed by Kuo [1982].